

A Role for RUNX3 in Balanced Myeloid-Erythroid Differentiation

Peter Balogh
Merrimack, NH

Master of Science, Pharmaceutical Biotechnology
Northeastern University, 2012

A dissertation presented to the graduate faculty
of the University of Virginia in candidacy for the
degree of Doctor of Philosophy

Department of Experimental Pathology

University of Virginia
April, 2019

“Enter
by this gateway
and seek
the way of honor,
the light of truth,
and the will to work for men.”

Edwin Anderson Alderman

Abstract

Hematopoiesis is the life-long process of blood cell production that undergoes dynamic changes with ontogeny. In the embryo, primitive endothelial cells in the yolk sac undergo a cell-fate alteration to produce progenitor blood islands that generate primitive erythroid cells to aid in delivering oxygen to the growing organism. Blood island progenitors gradually gain lineage potency to produce other cells of the hematopoietic system. Multipotent progenitors start to arise from specialized zones in the circulatory system that allows them to travel to the fetal liver where the bulk of blood cell production occurs for the remainder of embryogenesis. Fetal liver progenitors develop the capability to generate all cells of the hematopoietic system, at which point they are designated *bona fide* hematopoietic stem cells. After birth, hematopoietic stem cells travel once again to seed the bone marrow, where they will reside for the duration of the life-span.

As hematopoietic stem cells age, they experience a gradual decline in function characterized by imbalanced lineage output, increased self-renewal, poor engraftment, and increased cytokine responsiveness. These changes manifest from cell-intrinsic shifts in cell cycle, gene expression, metabolism, as well as changes in the bone marrow microenvironment. Functional decline of aged hematopoietic stem cells leads to an increased risk of developing hematological malignancies. This connection is evident due to the fact that many molecular components that are perturbed in normal aging are key drivers of bone marrow disorders. Current approaches to understand the mechanisms of aging rely on global metrics of mutational burden, epigenetic drift, gene expression perturbations, and metabolic

shifts. As such, there is a lack of clearly defined molecular mechanisms by which hematopoietic stem cell aging occurs.

In this study, we identified the transcription factor RUNX3 to be down-regulated in aged hematopoietic stem and progenitor cells, and describe a novel role for this factor in regulating myeloid lineage balance. Human and mouse RUNX3 transcript levels were diminished in aged hematopoietic stem and progenitor cells, and were correlated with diminished protein levels in aged human bone marrow specimens. The deregulation of RUNX3 appeared to be related to epigenetic alterations at the RUNX3 locus characterized in human cells by loss of activating histone acetylation marks at the enhancer and promoter, and in mouse cells by hypermethylation of the promoter. A functional defect in myeloid differentiation was demonstrated *in vitro* using colony formation assays and suspension culture, wherein erythroid and megakaryocyte differentiation was blocked, but granulocyte differentiation was spared. Committed erythroid progenitors also displayed defective maturation as evidenced by surface antigen expression and failure to express globin genes. RUNX3-deficient stem and progenitor cells grown in erythroid cell culture conditions experienced a significantly myeloid-skewed distribution of progenitor subtypes at the expense of erythroid and megakaryocyte progenitors. Changes in gene expression in RUNX3-deficient progenitors indicated a regulatory role for RUNX3 upstream of key erythroid factors GATA1 and KLF1. Due to the highly robust erythroid phenotype, individuals with unexplained anemia of the elderly were interrogated for RUNX3 expression and functional defects. RUNX3 transcripts were found to be significantly lower than healthy age-matched controls

and erythroid colony formation was impaired at the bi-potent erythroid-megakaryocyte progenitor stage, suggesting that RUNX3 deficiency may contribute to bone marrow pathogenesis.

Table of Contents

Abstract	iii
Table of Contents	vi
List of Figures	vii
List of Abbreviations	viii
I. Introduction	1
A. Hematopoiesis	1
B. Hematopoietic Stem Cell Assays	3
C. Progenitor Hierarchy	7
D. Aging Defects	11
E. Mechanisms of Aging Defects	12
1. DNA Damage	12
2. Epigenetic Alterations	13
3. Gene Expression Perturbations	16
4. ROS/Metabolism	17
5. Bone Marrow Niche	19
F. RUNX Transcription Factors	21
1. RUNX overview	22
2. RUNX1 during development	23
3. RUNX1 in bone marrow disorders	25
4. RUNX3 overview	26
5. Evidence for a role for RUNX3 in hematopoiesis and aging	27
II. RUNX3 levels in human hematopoietic progenitors are regulated by aging and dictate erythroid-myeloid balance.....	30
A. Abstract	31
B. Introduction	31
C. Results	33
D. Discussion	55
E. Methods	63
III. Discussion and Future Directions.....	73
A. Discrepancies between <i>in vivo</i> and <i>in vitro</i> models of RUNX3 deficiency...74	
B. Potential RUNX factor compensation	80
C. Identification of direct RUNX3 targets	83
D. Mechanism and implication of RUNX3's sub-cellular localization	87
E. Regulation of RUNX3 Expression	89
F. Does RUNX3 deficiency drive aging?	91
IV. References	93

List of Figures

Figure 1. Schematic of the human hematopoietic hierarchy	10
Figure 2.1. HSPC <i>RUNX3</i> Levels Decline With Aging	35
Figure 2.2. HSPC <i>RUNX3</i> Levels Decline With Aging	36
Figure 3.1. <i>RUNX3</i> Participates in Erythroid but Not Granulocytic Differentiation of Human Progenitors	39
Figure 3.2. <i>RUNX3</i> Participates in Human Erythroid and Megakaryocyte Differentiation	41
Figure 3.3. Cellular localization of <i>RUNX3</i> in primary cells	43
Figure 3.4. Cellular localization of <i>RUNX3</i> in HUDEP-2 cell line	44
Figure 4.1. <i>RUNX3</i> Levels Influence Progenitor Lineage Output Balance	47
Figure 4.2. <i>RUNX3</i> Levels Influence Progenitor Lineage Output Balance	49
Figure 5. <i>RUNX3</i> Deficiency Causes Perturbations in Erythroid Transcriptional Program	52
Figure 6. Decreased <i>RUNX3</i> Expression and Impaired Erythropoiesis in Unexplained Anemia of the Elderly	54
Table 1. Populations in erythroid culture identified by CyTOF to be significantly affected by <i>RUNX3</i> deficiency.....	58
Supplementary Figure 1. Megakaryocyte and erythroid phenotypes with CBF β and <i>RUNX1</i> inhibition	86

List of Abbreviations

5' UTR: 5' untranslated region

5-FU: 5-fluorouracil

ALL: acute lymphoblastic leukemia

AML: acute myelogenous leukemia

B/NK: B and NK cell progenitor

BFU-E: burst forming unit erythroid

BSO: buthionine sulfoximine

CFU: colony forming unit

CFU-E: colony forming unit erythroid

CFU-GEMM: colony forming unit granulocyte erythroid macrophage megakaryocyte

CFU-GM: colony forming unit granulocyte monocyte

CLP: common lymphoid progenitor

CMP: common myeloid progenitor

DCF-DA: 2'-7'-dichlorofluoroscein diacetate

EPO: erythropoietin

FDR: false discovery rate

FLT3L: FMS-like tyrosine kinase 3 ligand

G-CSF: granulocyte-colony stimulating factor

GFP: green fluorescent protein

GM-CSF: granulocyte/macrophage-colony stimulating factor

GMP: granulocyte/monocyte progenitor

GO: gene ontology

H3K4me2: histone 3 lysine 4 di-methylation

H3K4me3: histone 3 lysine 4 tri-methylation

H3K27me3: histone 3 lysine 27 tri-methylation

HAT: histone acetyltransferase

HDAC: histone deacetylase

HSC: hematopoietic stem cell

HSPC: hematopoietic stem and progenitor cell

IL-3: interleukin-3

IL-6: interleukin-6

iPSC: induced pluripotent stem cell

LAK cell: lymphokine-activated killer cell

LMPP: lymphoid-primed multipotent progenitor

LSK: Lin⁻ Sca-1⁺ c-Kit⁺

LT-HSC: long term hematopoietic stem cell

MEP: megakaryocyte/erythroid progenitor

MDP: monocyte and dendritic cell progenitor

MDS: myelodysplastic syndrome

MLP: multi-lymphoid progenitor

MPP: multipotent progenitor

MST: minimum spanning tree

NAC: N-acetyl-L-cysteine

Poly I:C: polyinosinic:polycytidylic acid

ROS: reactive oxygen species

SCF: stem cell factor

SCID: severe combined immunodeficiency

SDF-1: stromal derived factor 1

SP: side population

ST-HSC: short term hematopoietic stem cell

TGF β : transforming growth factor beta

TPO: thrombopoietin

UAE: unexplained anemia of the elderly

I. INTRODUCTION

A. Hematopoiesis

Hematopoiesis is the process by which an array of specialized progenitors and lineage-terminal blood cells is created. Blood cells are first needed when the developing embryo becomes too large for oxygen to fully diffuse through¹⁻³. At this point, the first phase of hematopoiesis, termed primitive hematopoiesis, begins when cells from the extra-embryonic mesoderm of the yolk sac differentiate into blood islands⁴⁻⁶. The appearance of these islands precedes the formation of a bona fide circulatory system, but the cells within express cell surface markers that are used to define endothelial cells in the adult organism^{2,4,7}. Despite these markers, cells in the blood islands have the capacity to differentiate into primitive erythrocytes as well as macrophages and megakaryocytes, although at a much lower frequency^{2,6,8}. Primitive erythrocytes are characterized by their large size and expression of embryonic globin genes, while macrophages and megakaryocytes are relatively similar to their adult counterparts^{1,5,8}. Models wherein blood islands arise from single or multiple cells have been proposed to explain the dual endothelial and blood precursor phenotype, but the exact origin of these cells remains unknown^{1,4}.

After the establishment of the early circulatory system, a wave of transient erythro-myeloid progenitors arise from the hemogenic endothelium, a specialized region of the aortic-gonad-mesonephros structure^{6,7,9}. This marks the onset of the second phase of hematopoiesis, called definitive hematopoiesis. Erythro-myeloid progenitors are thought to be the first progenitors that are multipotent, although they are initially restricted from lymphoid differentiation until CD45 is expressed^{2,3}. Erythrocytes that are formed during this phase are definitive erythrocytes, with

smaller cellular mass and shifted expression of globin genes to the adult forms⁵⁻⁷. The macrophages generated during this phase differ from the primitive wave of hematopoiesis in that they become the tissue resident macrophages of the brain, lung, and liver^{1,2,8}. Lastly, these initial erythro-myeloid progenitors also have the capacity to form most granulocytic myeloid lineages^{3,5,8}.

As definitive hematopoiesis progresses, lymphoid progenitors arise in both the yolk sac and aortic-gonad-mesonephros. These lymphoid precursors can generate B and T cells, but are restricted in B cell potential and can only form long lived B1 and marginal zone B cells^{1,3}. It is only after the lymphoid progenitors are formed that the appearance of the first hematopoietic stem cells (HSCs) is observed. In contrast to the erythro-myeloid progenitors, HSCs arise from the aorta, the vitelline vessels, as well as the yolk sac, and become the long-lived, true multipotent progenitors that will eventually seed the organism for the remaining lifespan^{1,3,9}. Initially, the fetal liver is colonized by HSCs and lymphoid progenitors and is the predominant site of hematopoiesis^{1,2,5}. It remains unclear if the lymphoid progenitors arise from HSCs or if they originate from the prior wave of hematopoiesis³. Lastly, HSCs colonize the bone marrow where they reside in a specialized niche where they are relatively quiescent and can efficiently self-renew⁷.

B. Hematopoietic Stem Cell Assays

The hematopoietic stem cell field was born out of the search for a medical intervention to treat exposure to radiation. The bone marrow was promptly identified as the tissue that is uniquely sensitive to radiation, and bone marrow

transplantation as a potentially curative therapeutic modality was subsequently pursued¹⁰. In principle, animals could be irradiated to a point where their bone marrow was ablated, and donor marrow could be engrafted as a functional replacement. The first transplants were indeed capable of rescuing a lethally irradiated animal, but another critical observation was made: donor cells were capable of forming mixed blood lineage colonies in the spleens of the recipients¹¹. Through limiting cell dilutions and tracking chromosomal abnormalities from irradiated donor cells, it was concluded that the colonies were spawned by individual cells with multi-lineage potential^{12,13}. The observation of delayed colony formation in secondary transplant recipients that displayed robust chimerism indicated that a multipotent progenitor with reduced proliferative status existed as a subset of spleen-colonizing bone marrow cells¹⁴. Indeed, treatment of bone marrow with 5-fluorouracil (5-FU), a reagent that selectively kills rapidly dividing cells, significantly reduced the colony forming capacity of the donor cells, but did not affect long-term repopulation of the recipient marrow¹⁴. This led to the realization that there exists a rare, more primitive progenitor – the hematopoietic stem cell (HSC).

Two main varieties of *in vitro* assays were devised to characterize, enumerate, and partially purify HSCs from the bone marrow cellular milieu. The first modality was based on the concept of limiting dilution, and involved serial replating of 5-FU-treated bone marrow cells to generate small colonies that exhibited reduced proliferative capacity, but increased self-renewal. Lineage potential could be discerned as a function of colony size, with small colonies representing blast-like

progenitors with indeterminate lineage potential^{15,16}. Large colonies were comprised of erythroid, megakaryocyte, and granulocyte progenitors as well as rare cells that were found at a frequency of roughly 2 in 10^5 and were able to generate other large mixed-lineage colonies upon re-plating¹⁷. The second modality was based on two-phase co-culture systems in which enhanced expansion of the progenitors was supported by primary or immortalized stromal cells and followed by re-plating into semi-solid medium for lineage colony formation. These assays were able to detect colony forming units of mixed granulocyte, erythroid, macrophage, and megakaryocyte potential (CFU-GEMM), granulocyte-macrophage potential (CFU-GM), and burst-forming unit erythroid potential (BFU-E). The two varieties of this assay, Cobblestone-area Forming Cell Assay and Long Term Culture Initiating Cell Assay, were able to enrich for long term colony-forming progenitors 10 to 20-fold over serial re-plating assays, and estimated their frequency to be about one percent of the CD34+ bone marrow population^{17,18}.

While *in vitro* assays were helpful in estimating progenitor frequencies and understanding the hierarchical organization of the hematopoietic compartment, *in vivo* assays were required to determine if those progenitors had true HSC function – namely, long-term bone marrow reconstitution with multilineage potential. Syngeneic murine bone marrow transplantation became widely used after the discrimination of CD45 isoforms (CD45.1 and CD45.2) became possible through flow cytometric analysis. This simple strategy involves transplantation of donor cells taken from an animal with an isoform of CD45 that differs from the recipient animal. Because the mice are syngeneic, there are reduced immunological

complications after transplantation, and donor cells can be traced over time using the corresponding CD45 allele. For these reasons, transplant-based HSC assays have become the standard for investigating HSC function. Human xenograft assays were possible once immune-compromised mouse strains were engineered, as to avoid graft rejection by the recipient animal. The generation of these animals involved crossing animals with various genetic backgrounds that inhibited aspects of the immune system, including beige (impaired T cell differentiation), nude (T and NK cell dysfunction), and X-linked immunodeficiency (impaired LAK and B cell function) as in the bnx strain, or by inhibiting B and T cell function through a mutation of the critical VDJ recombination machinery as in the SCID strain¹⁹⁻²². Both bnx and SCID animals needed to be further crossed with NOD/Lt animals to inhibit macrophage activity which could still compromise the engraftment of the xenotransplant²³.

Early transplant studies relied on purification of prospective stem cell populations so that lineage contribution could be scrutinized in the recipient. These types of experiments delineated most subsets of known bone marrow HSPCs which were classified according restricted surface antigen expression that correlated to their varying degrees of lineage potential and engraftment durability. A lineage roadmap or progenitor hierarchy was derived from these studies and is described below. New technologies have allowed for the description of HSC progenitor and lineage output without the need for transplantation. By labeling HSCs using random transposon tagging or fluorescent tagging, the native contribution of HSCs to the downstream progenitor pool and ultimately the terminal lineage cells in the

circulation can be assessed. These studies found long-term HSCs (LT-HSCs) to generate very few progeny, with short-term HSCs (ST-HSCs) generating the vast majority of cells during homeostatic hematopoiesis²⁴. Perturbation of native hematopoiesis via 5-FU treatment or transplantation showed HSC labeling frequencies and numbers to be markedly different than controls indicating that native hematopoiesis cannot be accurately reiterated in models that introduce high proliferative demand on HSCs and progenitors²⁵.

C. Progenitor Hierarchy

In adult hematopoiesis, the HSC is able to give rise to every myeloid and lymphoid blood lineage in the circulation. Data from both *in vitro* and *in vivo* assays indicated that HSC differentiation is achieved through the step-wise commitment of HSC daughter cells to a given lineage by way of a series of intermediary progenitors with increasingly restricted lineage potential. Human HSCs have been defined according to various groupings of cell surface antigens including Lin- CD34+ HLA-DR-, Lin- ALDH^{hi} CD133+, CD34+ CD133+, Lin- CD34+ CD38- Rho-123^{lo}, and CD34+ CD38- c-kit+ CD33- Rho-123-²⁶. Intriguingly, these antigen groupings isolate cells with similar function, albeit varying purity, suggesting heterogeneity even within the HSC compartment. Only more recently was this heterogeneity appreciated from a cell phenotype standpoint. Indeed, the expression of CD90 can prospectively isolate HSCs with long-term repopulating ability in transplant assays (Lin- CD34+ CD38- CD90+) ²⁶⁻²⁸. HSC isolation was further refined to include CD45RA- Rho123^{lo} CD49f+^{27,28}. Mouse HSCs immune-phenotypes are quite distinct from their human

counterparts. The general HSPC population is typically defined as Lin⁻ Sca-1⁺ c-kit⁺ (LSK)²⁹. More stringent HSC definitions include the use of Hoechst stain efflux (side population, SP), CD34^{lo}, CD38⁺, Flt3, and CD244⁻, although current HSC definitions usually include LSK CD48⁻ CD150⁺ and LSK CD34⁻ Flk2^{-29,30}.

HSCs generate multipotent progenitors (MPPs) which have a high proliferative capacity, have only short-term repopulating ability, and contribute the bulk of day to day blood production^{28,29}. In the classical model of the hematopoietic hierarchy, progenitors then become restricted to myeloid or lymphoid differentiation in the common myeloid progenitor (CMP) or common lymphoid progenitor (CLP) populations respectively. In humans, CMP are CD34⁺ CD38⁺ CD45RA⁻ CD123⁺, while CLPs are CD34⁺ CD38⁺ CD10⁺ CD19⁻^{26,31}. Alternate definitions include CD135⁺ for CMP and CD7 for CLP²⁷. In mice, CLPs are LSK Il7ra⁺ while CMP are LSK Ilr7a⁻²⁹. CLPs differentiate into NK, dendritic, T-cell, and B-cell lineages; however, CMPs further specialize into either granulocyte-macrophage progenitors (GMPs) or erythroid-megakaryocyte progenitors (MEPs). The classical definition for human GMPs is CD34⁺ CD38⁺ CD45RA⁺ CD123⁺ and for MEPs is CD34⁺ CD38⁺ CD45RA⁻ CD123⁻^{26,31}. These definitions, especially for MEPs, have been refined more recently to include CD38^{mid}, CD135, and CD110 antigens³². Terminal blood lineages formed from GMPs include mast cells, basophils, eosinophils, neutrophils, and macrophages.

The current perspective of the hematopoietic hierarchy considers lineage commitment to be a continuum of intermediate progenitor stages undergoing gradual changes in lineage programming rather than abrupt changes that lead to

discrete cell populations with fixed lineage potential. Figure 1³³⁻³⁹ illustrates the hematopoietic hierarchy including increased mixed lineage potential between myeloid and lymphoid compared to the classical model. In this model, the lymphoid-primed multipotent progenitor (LMPP) resides down-stream of the MPP, and represents a lymphoid-biased progenitor with the capacity to generate GMP-like progeny separate from the CMP route³⁶. The LMPP then yields the CLP, also designated the multi-lymphoid progenitor (MLP) to appreciate its previously unrecognized ability to generate some myeloid cells via the monocyte and dendritic cell progenitor (MDP) route^{33,37}. Thus, the new model views the lymphoid branch as becoming increasingly restricted to lymphoid potential by losing myeloid potential.

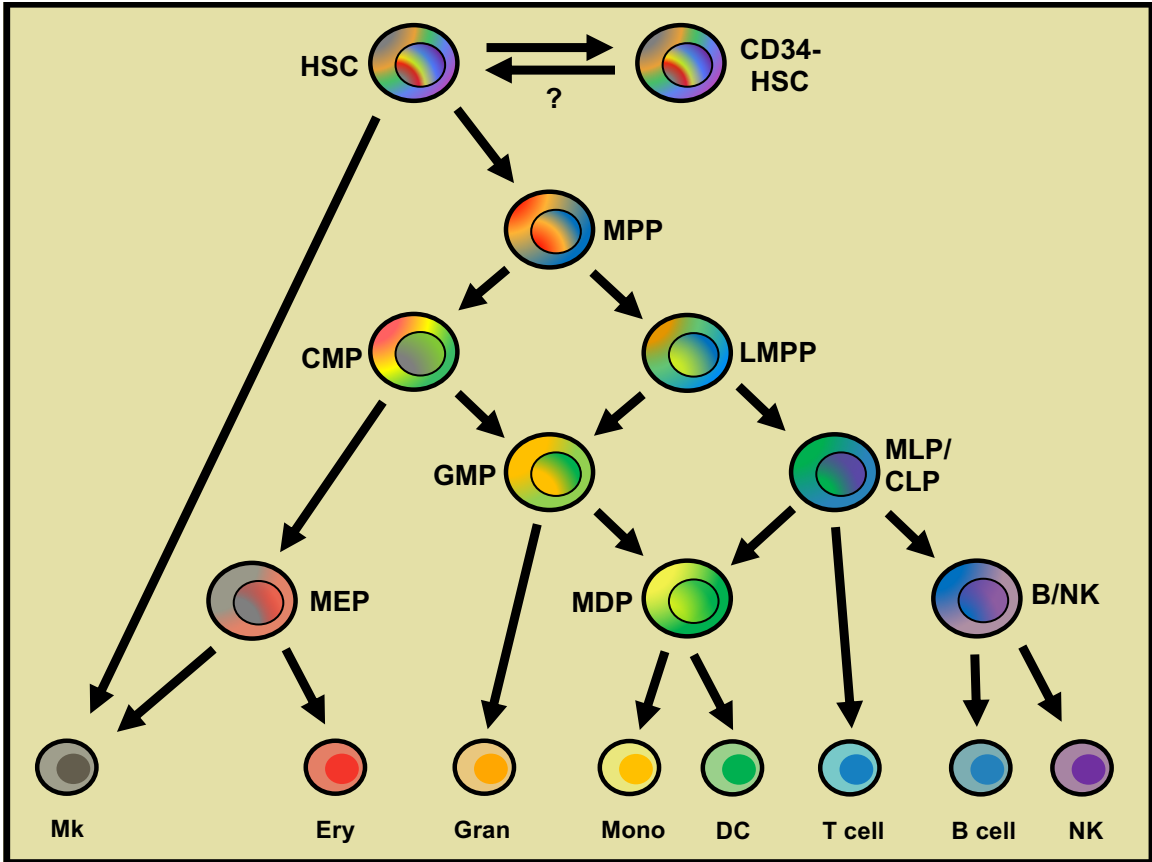


Figure 1. Schematic of the human hematopoietic hierarchy.

HSC: hematopoietic stem cell; MPP: multipotent progenitor; CMP: common myeloid progenitor; LMPP: lymphoid-primed multipotent progenitor; GMP: granulocyte-monocyte progenitor; MLP: multi-lymphoid progenitor; CLP: common lymphoid progenitor; MEP: megakaryocyte-erythroid progenitor; MDP: monocyte-dendritic cell progenitor; B/NK: B and NK cell progenitor; Mk: megakaryocyte; Ery: erythroid; Gran: granulocyte; Mono: monocyte; DC: dendritic cell; NK: natural killer cell.

D. Aging Defects

In the developing organism, progenitors progressively gain lineage potency, starting from dedicated erythroid progenitors and eventually culminating in the HSC. As a counterpoint to this development, HSCs gradually lose function with age. A hallmark of stem cell aging is myeloid skewing⁴⁰⁻⁴⁵. This phenotype is characterized as a perturbation in the frequencies of peripheral blood cells and bone marrow progenitors. Peripheral blood counts of lymphocytes and erythrocytes are often diminished in aged individuals compared to young, while granulocytic monocytes are augmented⁴⁶. These changes are accompanied by alterations in the frequencies of corresponding progenitors cells in the bone marrow. A critical implication of these changes is the functional decline of HSCs. Indeed, transplantation of aged marrow has a significantly reduced capacity to home to the bone marrow niche and engraft young recipients compared to young marrow, and the cells that manage to engraft exhibit myeloid skewing or impaired lymphoid and erythroid reconstitution^{40,45,47}. Paradoxically, aged individuals have a greatly expanded pool of HSCs, despite having a reduced capacity for long-term repopulating^{40,43}. In line with their expansion, aged HSCs exhibit alterations of proliferative capacity characterized by slow yet continuous cell cycle progression as compared to their quiescent counterparts^{48,49}. Also counterintuitive is the aged HSC's increased sensitivity to G-CSF, resulting in enhanced mobilization into the peripheral circulation⁵⁰. A recent study showed that in young animals, G-CSF selectively mobilizes dormant HSCs; however, it is unknown whether in aged animals the increased mobilization is due to increased HSC numbers or a functional

perturbation⁵¹. These age-associated changes render individuals more likely to develop bone marrow disorders, many of which exhibit exaggerated aging phenotypes.

E. Mechanisms of Aging Defects

1. DNA Damage

Because transplantation of aged stem cells into young recipients does not rescue HSC functional capacity, several cell-intrinsic mechanisms have been proposed to contribute to aging. The most prevalent model for stem cell aging is that a genetic perturbations including both DNA damage and gene expression alterations cause the dysfunction of aged HSCs. It has long been known that chromosomes erode with aging, and that telomeres, chromosomal end-caps consisting of non-coding DNA, serve as a buffer to protect against this phenomenon⁵². In mice, it has been shown that telomerase, the enzyme that rebuilds telomeres, is required for normal HSC function, as telomerase deficient cells have reduced capability to undergo serial transplantation⁵³. This finding was corroborated in an experiment that subjected telomerase-deficient animals to six generations of breeding after which point HSC attrition was observed both *in vivo* and in *in vitro* colony assays⁵⁴. Interestingly, myeloid skewing was observed in those animals prior to HSC exhaustion⁵⁴. It remains unclear whether restoration of telomeres restores HSC function despite alleviating telomere shortening⁵⁵⁻⁵⁸. By contrast, a separate study showed that wild type marrow behaved like aged marrow

when transplanted into telomerase-deficient animals, indicating a requisite function for telomerase in bone marrow micro-environment rather than HSCs themselves⁵⁹.

DNA damage can be accumulated anywhere across the chromatin, not just the telomere. It has been shown that wild type aging HSCs accumulated gamma-H2AX foci, histone marks that are associated with damaged DNA, preferentially on non-telomere sites and have up to 40% more DNA damage than young cells as evidenced by comet tail assay^{60,61}. Quiescent aged cells were impaired in their ability to resolve new radiation-induced DNA damage, suggesting that DNA damage repair mechanisms are compromised with age⁶². Indeed, aged HSCs exhibit reduced expression of several DNA damage repair pathways; however, when induced to proliferate, these pathways were shown to become upregulated and the cells were able to efficiently resolve DNA damage^{60,61}. In line with these findings, replicative stress, as in the collapse of DNA replication forks, has been shown to cause sustained gamma-H2AX foci, but were not linked to DNA damage or even alterations in the kinetics of DNA damage repair⁶¹. This was further supported by a recent study that failed to identify major changes in DNA repair fitness or susceptibility to irradiation between young and old HSCs, although an approximate 2-fold increase in mutational burden across the genome was observed in aged cells⁶³. Thus, it remains unclear to what extent DNA damage influences HSC aging phenotypes.

2. Epigenetic Alterations

Another genetic feature implicated in stem cell aging is the deregulation of gene expression through epigenetic alterations. Epigenetic modifications include all

non-sequence-based changes in the genome such as histone modifications and changes in DNA methylation and physical configuration. Because aging is most commonly studied in healthy organisms with no known or common genetic mutations, epigenetic and transcriptional changes are interrogated on a global genomic scale, rather than at the loci of putative target genes. The notion that epigenetic drift contributes to HSC aging was illustrated via transplantation of aged HSPC-derived iPSCs, which are induced pluripotent stem cells engineered by overexpression of master regulators of a variety of global epigenetic modifications⁶⁴. These iPSCs were found to have several features of HSCs aging corrected, presumably through epigenetic alterations. Although that study did not characterize which modifications were changed, it was an elegant demonstration that strongly implicated epigenetic drift as a contributor to HSC aging.

DNA methylation is the direct methylation of cytosine residues across the chromatin, with nearly all occurrences targeted to CpG dinucleotides in somatic cells^{65,66}. While hypermethylation of a given locus is typically associated with the diminished expression of its genes, most down-stream effects of alterations of methylation status appear to be context dependent. Interrogation of the bone marrow HSC methylome revealed significant differences in methylation profile of aged HSCs compared to fetal liver or young bone marrow HSCs, with an increase in overall methylation. Changes include hypermethylation (repressive) of gene loci required for erythroid and lymphoid differentiation, and hypomethylation (activating) of myeloid genes^{66,67}. Two critical families of enzymes responsible for global maintenance of the methylome, TETs and DNMTs, are downmodulated with

aging^{67,68}. Genetic deletion of these factors recapitulate aging phenotypes including myeloid skewing, HSC expansion, and poor engraftment after transplantation^{66,69}.

Intriguingly, forcing young HSCs into the cell cycle with 5-FU treatment causes changes in the methylome and transplantation fitness that closely resemble that of aged HSCs⁶⁷. Furthermore, many loci that harbor changes in methylation status do not exhibit altered gene expression, which suggests that targets become dysregulated in HSC progeny. This is supported by the fact that the methylation of lineage-specific loci is perturbed in HSCs, but lineage skewing only manifests after several rounds of cell division in the context of more mature progenitors⁶⁷.

Histones, the structures responsible for organizing higher order chromatin configurations, are also capable of influencing gene expression. This is generally achieved through various histone modifications including methylation, acetylation, ubiquitination that have unique signaling capabilities that can orchestrate chromatin accessibility and recruitment of regulatory factors. The histone mark H3K4me2 that is responsible for maintaining chromatin in an open, active configuration was among the first epigenetic marks observed in high levels in HSCs^{65,70,71}. The proposed model that came from this finding is that loci that harbor this mark were shown to be lineage-specific zones that are poised for expression in the HSC, and that only loci needed for a given lineage is maintained during differentiation. Of similar function to H3K4me2 is H3K4me3, an activating mark that protects promoter regions of genes from becoming methylated and thus inactivated⁶⁶. Changes with age include loss of clear promoter localization, especially in genes that promote HSC self-renewal and inhibit differentiation. In

contrast, H3K27me3 is a repressive histone mark that also impacts HSC behavior and is also dysregulated with aging in the same manner as H3K4me3⁷². Gain of H3K27me3 has not been directly linked to HSC aging phenotypes; however, manipulation of critical regulators of this mark, such as PRC2 constituents EZH2 and EED, modulate self-renewal and compromise HSC fitness in the context of transplantation, respectively^{65,67}.

3. Gene Expression Perturbations

Direct gene expression analysis through sequencing and quantitating transcript levels has been a key complement to epigenetic analysis which is typically indirect and only correlative to changes in the transcriptome. Gene expression in aged HSCs has been assessed using microarray and RNA-sequencing platforms and have revealed gene signatures indicative of myeloid bias, diminished lymphoid potential, and gross signaling perturbations⁷³. One study showed that up to 19% of transcripts that are altered with age correspond to the TGF β signaling pathway⁶⁸. This is significant considering myeloid and lymphoid lineages have variable responses to TGF β including induction of lineage-specific gene expression⁷⁴. Critical epigenetic regulators including Ezh2 and Tet2 were also dysregulated in aged HSCs⁶⁸.

The use of single-cell RNA-seq in conjunction with data clustering tools has unveiled greater heterogeneity in the HSC compartment than was previously appreciated through surface antigen phenotyping. Changes with aging that are found in HSC are generally concordant between studies. Two major shifts in gene

expression are associated with stem cell aging: cell cycle status and lineage bias. These have been described in a series of studies in which discrete subsets of LT-HSCs are reported to: 1) have a decreased tendency to reside in the G1/S cell cycle phase compared to ST-HSCs and MPPs, suggestive of increased self-renewal and decreased differentiation potential⁷⁵; 2) exhibit increased JAK/STAT signaling that drives the cells to megakaryocyte bias and partial functional exhaustion in a p53-dependent manner⁷⁶; 3) express high levels of von Willebrand factor and become functionally platelet biased⁷⁷; and 4) express high levels of CD61 and become myeloid-biased under inflammatory conditions in a manner dependent on Stat3, Klf5, and Ikzf1⁷⁸.

4. ROS/Metabolism

Reactive oxygen species (ROS) have also been implicated in the functional decline of HSCs. In a triple knock-out mouse model targeting FoxO1, 3, and 4, LSK HSCs showed increased levels of ROS which was associated with impaired HSC function. FoxO-deficient animals had increased peripheral white blood count and splenomegaly with enhanced expansion of myeloid elements in the tissue⁷⁹. HSCs from these animals produced fewer colonies in *in vitro* assays, with changes in frequencies of colony types favoring myeloid differentiation by approximately 7-fold more than their wild type counter-parts. Loss of FoxO also significantly impaired long-term repopulation in bone marrow transplantation assays which was associated with increased cell cycle entry of HSCs but not myeloid progenitors. Treatment of animals with N-acetyl-L-cysteine (NAC) after FoxO deletion reduced

ROS levels to near wild-type levels and restored HSC numbers and cell cycling to normal⁷⁹.

In *Atm*-deficient animals, severe bone marrow failure arises in association with increased ROS. *Atm*-deficient HSCs generate fewer colonies regardless of lineage type, and exhibit a markedly diminished capacity for long term reconstitution after transplantation. This phenotype is reversible with administration of NAC before and after transplant, indicating that an accumulation of ROS after loss of *Atm* is causative⁸⁰. Accordingly, p16 and p19 are upregulated in *Atm*-null HSCs, and a follow-up study using buthionine sulfoximine (BSO) to induce ROS confirmed that the upregulation of these factors is specific to ROS rather than loss of *Atm*. Furthermore, p38 MAPK was found to be the critical signaling node in the cellular response to ROS, and its inhibition rescues long-term HSC repopulating ability as well as increases engraftment efficiency in serial transplantation assays⁸¹.

Importantly, the effects of ROS in unperturbed cells have also been characterized. Using 2'-7'-dichlorofluorescein diacetate (DCF-DA), a molecule that becomes fluorescent when oxidized in the presence of ROS, viable CD45+ bone marrow cells could be grouped according to high or low ROS content. In young animals, ROS-high cells were myeloid-skewed in their colony formation and bone marrow reconstitution abilities, and long-term bone marrow reconstitution and serial transplantation were significantly impaired. An intriguing additional phenotype observed in ROS-high cells was the reduced expression of a cohort of osteoblastic niche factors, and a diminished ability to adhere to niche components such as collagen I⁸². This suggests that HSCs may be mis-localized from the ROS-

protective hypoxic niche over time, although this has not yet been tested.

Treatment with NAC or inhibition of p38 MAPK or mTOR could all modulate the behavior of ROS-high cells to match that of ROS-low cells. Importantly, the relative frequencies of ROS-high and ROS-low cells change with over time; specifically, the ROS-low population is diminished by approximately 25% in aged animals⁸².

Other metabolic perturbations have also been implicated in HSC aging. Approximately 33% of aged HSCs have been reported to exhibit reduced autophagic activity and increased metabolic functions indicated by elevated ATP and NADH levels. Accordingly, loss of critical autophagy factor Atg12 causes accelerated aging effects with many of the aforementioned phenotypes, and correlates with increased mitochondrial mass⁸³. SIRT7 has also been shown to mediate mitochondrial activity, and is expressed at a lower level in aged HSC compared to young. Deletion of SIRT7 in young HSC recapitulates the myeloid skewing phenotype, and also leads to a modest impairment in engraftment at both short and long time-points. Over-expression of SIRT7 in aged HSCs leads to more robust engraftment and ameliorates myeloid skewing⁸⁴.

5. Bone Marrow Niche

Another critical facet of HSC aging is the interaction of HSCs with the bone marrow stroma and localization within the bone marrow niche. Osteoblastic, perivascular, and endothelial cells all have roles in regulating HSC maintenance and localization through secretion of various growth factors⁸⁵. With respect to aging, increased fat content observed in aged bone marrow is correlated with diminished

CD45+ hematopoietic cellularity. HSPCs taken from fatty marrow of young mice exhibits poor engraftment and colony output on a per cell basis. HSC function of aged cells is restored in bone marrow progenitors taken from genetically engineered fatless mice or mice treated with a PPAR- γ inhibitor that blocks bone marrow adipocyte formation⁸⁶.

Reduced numbers of mesenchymal progenitors have been reported within the endosteal region of the bone marrow, which is the deepest, most hypoxic zone in the stroma and is thought to house HSCs⁸⁷. Correlated with this is a dramatic shift in localization of aged HSCs away from the endosteal region, and toward the central and sinusoidal zones where progenitors and mature cells tend to reside⁸⁸. Whether the loss of mesenchymal progenitors directly affects HSC localization has not been determined; however, changes in HSC localization have been shown to affect myeloid and lymphoid differentiation bias⁸⁹. Aged HSCs also exhibited perturbed cytoskeletal polarization and reduced adhesion in the extra-endosteal region, which may contribute to increased mobilization in response to G-CSF stimulation⁸⁸.

In the context of transplantation, there are significant differences in lineage potential and over-all engraftment between young and old recipients regardless of donor age. Both young and aged donor cells transplanted into aged recipients show inferior engraftment and myeloid-shifted distribution of donor cells⁹⁰. Aged bone marrow featured reduced levels of a host of interleukins, SDF-1, GM-CSF and MCP1 cytokines compared to young counterparts, but had increased levels of interferon-gamma and Ccl5^{90,91}. Intriguingly, Ccl5 was exclusively expressed in stromal cells, and its enforced expression generated long-term myeloid skewing post-

transplantation. By contrast, *Ccl5*-deficient animals had increased peripheral white blood cell counts and reduced numbers of myeloid progenitors in the bone marrow⁹⁰.

F. RUNX transcription factors

From a molecular standpoint, there is a vast and interconnected network of transcription factors required for embryonic establishment of HSCs through to adult HSC maintenance and function. Because HSC progenitors are very rare and hard to isolate by distinct cell surface antigens, the proteins that govern HSC formation have primarily been studied through various models of genetic manipulation. *SCL*, *LMO2*, and *GATA2* are three of the most critical transcription factors in early embryogenesis. Deletion of each of these factors completely blocks primitive hematopoiesis and halts hematopoietic progression^{92,93}. *LYL1*, *ERG*, *FLI1*, and *CEBP/B* factors also have various roles in generating circulatory architecture and lineage programming of progenitors during early hematopoiesis⁹⁴. *RUNX1* is dispensable during primitive hematopoiesis, but has a requisite role in establishing definitive hematopoiesis and generating the early HSCs that go on to seed the fetal liver⁹⁵⁻⁹⁷. Mechanistically, *RUNX1* orchestrates the chromatin occupancy of several other critical transcription factors and remodels the epigenetic landscape of key targets⁹⁸. Further, *RUNX1* also has a myriad of roles in stem cell maintenance and lineage specification and maturation which is why it is among the most studied transcription factors in HSC biology.

1. RUNX Overview

The RUNX family is comprised of RUNX1, RUNX2, RUNX3, and a common binding partner, CBF β . The proteins are highly homologous, all containing activating and inactivating domains, as well as the critical Runt domain that is responsible for chromatin interaction⁹⁹. RUNX proteins recognize a cognate DNA binding motif that is generally defined as PyGPyGGTPy; however, this interaction is very weak in biochemical assays unless CBF β is present^{100,101}. Degenerate or variant DNA binding motifs have also been identified, which may be indicative of functional diversity¹⁰². Structural analysis of RUNX1 indicated that heterodimerization with CBF β causes a change in its conformation that makes the Runt domain fully accessible to chromatin^{103,104}. It is generally accepted that RUNX factors function by dimerizing with CBF β and binding to the RUNX DNA-binding motif, although CBF β -independent functions have been described as well as instances of RUNX factors associated with non-RUNX binding motifs¹⁰⁵.

All RUNX proteins undergo several forms of post-translational modification which can modulate their stability and/or their function. RUNX interaction with their co-repressor Sin3A is thought to be dependent on ERK mediated phosphorylation, and the binding of RUNX2 to CBF β is dependent on its phosphorylation by factors downstream of TGF β /BMP signaling^{99,106}. CBF β binding has been shown to be critical for RUNX protein stability¹⁰⁷. Cyclin dependent kinases also target RUNX proteins and regulate their stability at different stages of the cell cycle. RUNX1 has been shown to undergo methylation by PRMT1, which is also thought to block Sin3A binding⁹⁹. All RUNX proteins are acetylated by p300,

and are also targeted by various HDACs and histone transferases to modulate their function by altering DNA-binding, transactivation, or stability^{99,106}. RUNX proteins function via interaction with their various partners. Some of these partners are Wnt and Hippo signaling factors, DNA damage repair factors, and chromatin organizing factors⁹⁹. RUNX proteins also bind other transcription factors such as Smads and STATs which can affect their sub-cellular localization as well as their chromatin occupancy¹⁰⁸⁻¹¹⁰.

Each of the RUNX factors is critical for the survival of the organism. Germline deletion of RUNX2 in mice results in an inability to generate ossified skeletal tissue due to a blockade in osteoblast maturation and is lethal due to respiratory failure shortly after birth^{111,112}. Germline deletion of RUNX3 is lethal due to gastric or neuronal defects, depending on the strain of mouse that was used^{113,114}. As mentioned previously, loss of RUNX1 results in a failure to establish definitive hematopoiesis. CBF β -null mice also die from an inability to establish definitive hematopoiesis¹¹⁵. While all RUNX protein functions are perturbed in the absence of CBF β , the RUNX1 phenotype is lethal earliest during embryogenesis. This is likely why germline deletion of CBF β recapitulates the RUNX1 phenotype rather than that of RUNX2 or RUNX3, although this has not been experimentally validated.

2. RUNX1 During Development

In the context of hematopoiesis, RUNX1 has been extensively studied. During embryogenesis, the expression of RUNX1 in blood island progenitors is partially required for the generation of primitive erythrocytes through down-stream

upregulation of Gata1 and EKLF⁹⁵. In ESC differentiation models, RUNX1 was shown to coordinate localization of several key transcription factors to new gene regulatory elements and to reconfigure the epigenetic landscape of hematopoietic loci⁹⁸. RUNX1 is critical for the generation of the next wave of hematopoietic progenitors derived from the hemogenic endothelium in the aortic-gonad-mesonephros structure. RUNX1 deficiency at all stages prior to fetal liver colonization by hematopoietic progenitors blocks the formation of full-fledged HSCs that eventually seed the bone marrow^{96,97,116}.

During adult hematopoiesis, RUNX1 deficiency in the hematopoietic compartment leads to an expansion of LSK+ HSPCs, granulocytes, and myeloid precursors, accompanied by a blockade in lymphoid differentiation of B- and T-cells¹¹⁷. Transplantation of RUNX1-deficient cells results in efficient bone marrow chimerism but reduced terminal blood cell output as evidenced by reduced peripheral chimerism¹¹⁸. Intriguingly, the disruption of a single RUNX1 allele leads to nearly the opposite phenotype - reduced HSC numbers, and enhanced bone marrow engraftment generating normal numbers of most terminal blood cells compared to wild type animals, with the exceptions being reduced T-cells and platelets¹¹⁹. RUNX1 also has a demonstrated role in the immune cell compartment, specifically the differentiation and maturation of CLPs, dendritic cells, and regulatory and helper T cell subsets¹¹⁷.

3. RUNX1 in Bone Marrow Disorders

In accordance with its many roles in hematopoiesis, RUNX1 perturbations are frequently observed in bone marrow disorders that harbor differentiation defects and generally involve loss of function mutations and chromosomal aberrations. In AML, RUNX1 is involved in t(8;21) and chromosomal rearrangement which results in the dominant-negative AML-ETO fusion protein¹²⁰. In AMLs with the inv(16) rearrangement, RUNX1 is indirectly inactivated through sequestration via the inv(16) product, CBF β -SMMHC¹²¹. A functionally defective RUNX1 allele is also found in ALLs with the t(12;21)(p13;q22) rearrangement that produces the ETV6-RUNX1 fusion protein¹²¹. Other non-chromosomal rearranging mutations also target RUNX1; however, while most of these inactivate RUNX1, there is almost always an intact or amplified wild-type RUNX1 allele, suggesting RUNX1 also confers a growth or survival advantage in diseased cells^{121,122}.

High throughput screenings of small molecule drugs led to the identification of the RUNX1 inhibitor Ro5-3335 (Ro5) and the development of the CBF β inhibitor AI-14-91 (AI). The mechanism of action for Ro5-3335 is not fully understood; however, there is evidence indicating that the molecule may actually inhibit the SWI/SNF complex, which has been shown to associate with RUNX1^{123,124}. In a zebrafish model of AML1-ETO leukemia, Ro5 rescued defective blood cell production from blood islands in the developing embryo¹²³. In mice, administration of the drug *in vivo* showed effective elimination of HSPCs that ectopically express the CBF β -MYH11 fusion, and an overall diminished burden of disease¹²³. In contrast to Ro5, AI-14-91 underwent rigorous structural analysis to confirm its binding to

the Runt domain of RUNX1. AI-14-91 was shown to block known functions of RUNX1 including embryonic HSPC formation in zebrafish, proliferation of leukemic cell lines and murine bone marrow progenitors, and expression of genes that regulate lipid and ribosomal biogenesis¹²⁵.

4. RUNX3 Overview

RUNX3 is expressed in the mouse embryo after RUNX1 and the establishment of definitive hematopoiesis and does not appear to contribute to the formation of early hematopoietic progenitors¹²⁶. In adult animals, RUNX3 is predominantly expressed in lymphoid cells where it has been studied extensively, but is also expressed in other hematopoietic cell types as well as neuronal cells. In B-cells, RUNX3 contributes to proliferation and immunoglobulin class switching¹²⁷. Its expression is induced by TGF β , and it also binds to Smad3 and propagates TGF β signaling^{99,109,110,127}. Interestingly, loss of RUNX3 results in a lack of Langerhans cells in the epidermis, a phenotype that also arises in the context of TGF β deficiency^{128,129}. In T-cells, RUNX3 regulates differentiation to the CD8 single-positive state by binding repressive elements of the CD4 locus as well as binding to the enhancer of the CD8 locus¹³⁰. RUNX3 also has a role in CD8+ T-cell function, as its deletion results in defective antigen recognition via T-cell receptor¹³¹. A similar role has been demonstrated in Th1 subsets, where Th1 cytokine production was activated by RUNX3, while Th2 cytokine production was repressed¹³⁰. Furthermore, Th17 cells, regulatory T-cells, and NK cells all require RUNX3 to varying degrees for normal differentiation and/or function¹³⁰. In addition to its roles in lymphoid and

epidermal cells, RUNX3 is also expressed in TrkC+ proprioceptive neurons in the cranial and dorsal root ganglion where it regulates neurotrophin response and axonal guidance^{113,132}.

5. Evidence for a role for RUNX3 in Hematopoiesis and Aging

Several lines of evidence implicate RUNX3 in myeloid hematopoiesis and aging. Loss of RUNX3 during zebrafish embryogenesis blocks progenitor formation and subsequent production of circulating cells, and disrupts expression of other critical transcription factors RUNX1, myb, and Spi1¹³³. All phenotypes were rescued by injection of RUNX3 mRNA. RUNX3 was further implicated in myeloid differentiation in a study that used a predictive algorithm to identify RUNX3 as an essential node in transcription factor networks that regulate adult erythropoiesis¹³⁴. A partial erythroid phenotype was indeed observed in mice with hematopoietic deletion of RUNX3. In young adult mice, RUNX3 deficiency rendered bone marrow HSPCs hyper-sensitive to G-SCF-induced mobilization and enhanced their colony forming capacity in serial re-plating assays, but produced no gross hematopoietic defects. As the animals aged, the bone marrow progenitor distribution shifted toward a higher frequency of myeloid progenitors at the expense of erythroid progenitors, and the animals developed a myeloproliferative disorder characterized by leukocytosis¹³⁵. Co-deletion of RUNX1 and RUNX3 produced a synthetic phenotype involving the development of either bone marrow failure or myeloproliferative disorder accompanied by severe cytopenias including anemia. Using this model, a DNA damage response requiring both RUNX1 and RUNX3 was

also identified, supporting the notion that RUNX1 and RUNX3 could have overlapping and potentially compensatory functions¹⁰⁵.

RUNX3 was further implicated in aging and disease states. Promoter hyper-methylation of RUNX3 was observed in both neoplastic and non-neoplastic gastric epithelial cells and was correlated with diminished protein levels as a function of age rather than tumorigenesis^{136,137}. RUNX3 hyper-methylation was also detected in bladder tumors and in cells of the frontal cortex with a strong positive correlation between methylation status and age^{138,139}. Diminished RUNX3 transcripts were also associated with RUNX3 hyper-methylation in CD8+ T-cells¹⁴⁰. Hematopoietic malignancies including AML, ALL, and MDS also harbor hyper-methylated RUNX3 loci at high frequencies in human samples. Retrospective analysis of patient survival indicates higher relapse-free survival with lower RUNX3 methylation. Of note, myeloid cells had a significantly higher frequency of RUNX3 methylation than lymphoid cells. Methylation of RUNX1 and RUNX2 loci was not observed in these cases¹⁴¹.

Despite these findings, a clear role for RUNX3 in myeloid hematopoiesis has not yet been demonstrated, and it remains unknown whether RUNX3 has overlapping roles with RUNX1. In the context of aging and disease, this is especially important given the frequency with which RUNX1 perturbations are observed. A major hallmark of normal aging and age-associated hematologic malignancies is the skewing of lineage output. Diminished expression of RUNX3 has already been shown in many age-associated disease states including myeloid malignancies such as AML; however, these observations remain correlative, as specific roles for RUNX3

in these conditions have not been identified. This study aimed to determine whether RUNX3 has a role in normal myeloid hematopoiesis using an *in vitro* setting wherein a discrete population of primary human cells could be rigorously interrogated with respect to multi-lineage differentiation. Further, a role for RUNX3 in hematopoietic aging was examined.

II. RUNX3 Levels In Human Hematopoietic Progenitors Are Regulated By Aging And Dictate Erythroid-Myeloid Balance

Modified from "RUNX3 Levels In Human Hematopoietic Progenitors Are Regulated By Aging And Dictate Erythroid-Myeloid Balance" (*Haematologica* 2019).

Peter Balogh, Emmalee R. Adelman, John V. Pluinage, Brian J. Capaldo, Katie C. Freeman, Sandeep Singh, Kamaleldin E. Elagib, Yukio Nakamura, Ryo Kurita, Goro Sashida, Eli R. Zunder, Hui Li, Alejandro A. Gru, Elizabeth A. Price, Stanley L. Schrier, Irving L. Weissman, Maria E. Figueroa, Wendy W. Pang, and Adam N. Goldfarb.

A. Abstract

Healthy bone marrow progenitors yield a coordinated balance of hematopoietic lineages. This balance shifts with aging toward enhanced granulopoiesis with diminished erythropoiesis and lymphopoiesis, changes which likely contribute to the development of bone marrow disorders in the elderly. In this study, RUNX3 was identified as a hematopoietic stem and progenitor cell factor whose levels decline with aging in humans and mice. This decline is exaggerated in hematopoietic stem and progenitor cells from subjects diagnosed with unexplained anemia of the elderly. Hematopoietic stem cells from elderly unexplained anemia patients had diminished erythroid but unaffected granulocytic colony forming potential. Knockdown studies revealed human hematopoietic stem and progenitor cells to be strongly influenced by RUNX3 levels, with modest deficiencies abrogating erythroid differentiation at multiple steps while retaining capacity for granulopoiesis. Transcriptome profiling indicated control by RUNX3 of key erythroid transcription factors, including *KLF1* and *GATA1*. These findings thus implicate RUNX3 as a participant in HSPC aging, and a key determinant of erythroid-myeloid lineage balance.

B. Introduction

Hematopoietic stem and progenitor cells (HSPCs) execute tightly coordinated self-renewal and lineage commitment programs that generate a balanced output of peripheral blood cell types. With aging, these programs undergo perturbation resulting in increased numbers and decreased function within the stem cell

compartment as well as a shift in the balance of cell types produced – namely, an increased proportion of granulocytes at the expense of erythroid and lymphoid lineages^{40,68,142,143}. Thus normal aged mice have diminished peripheral red blood cells and lymphocytes, increased circulating neutrophils and monocytes, and increased sensitivity to G-CSF-induced leukocytosis and HSPC mobilization^{50,67}. The transplantability of age-related HSPC changes highlights the importance of cell-intrinsic determinants, although micro-environmental factors also exert a critical influence^{43,144,145}.

The transcription factor RUNX3 has been characterized as a participant in neural and lymphocyte development, TGF β signaling, and solid tumor suppression^{128,132,146–148}. Several studies have also demonstrated its repression in aged normal as well as tumor tissues, with the principal mechanism of inactivation being epigenetic alterations, particularly DNA methylation^{138–140,149}. Emerging data suggest a role in hematopoiesis, with zebrafish and murine loss of function studies revealing progenitor perturbations, although the extent of its role has remained unclear due to redundancy with Runx1^{105,117,133}. Most notably, induction of hematopoietic *Runx3* deletion in mice elicited marrow changes similar to those reported with normal aging: increased marrow colony forming units (CFU) and increased peripheral blood mobilization of CFU by G-CSF treatment^{135,150}.

This study shows *RUNX3* to be expressed in murine and human HSPC, where it undergoes repression and epigenetic modification during normal aging. HSPC levels of RUNX3 were found to determine developmental potential, with deficiency restricting erythropoiesis at commitment and subsequent stages while fully

permitting granulopoiesis. HSPC purified from patients with unexplained anemia of aging manifested *RUNX3* deficiency and similar developmental alterations. Changes in HSPC transcriptome due to *RUNX3* deficiency suggest a role upstream of the erythroid master regulatory transcription factors KLF1 and GATA1.

C. Results

HSC *RUNX3* Levels Decline With Aging

Prior reports have shown marrow-specific *Runx3* knock-out to elicit aspects of the aging phenotype and to exaggerate the myeloid skewing associated with aging^{135,150}. We therefore assessed *RUNX3* expression in rigorously purified human and murine hematopoietic stem cells. In humans, RNA-seq has been conducted on Lin- CD34+ CD38- marrow cells from healthy young (18-30 years old) and aged (65-75) subjects (GSE104406). In mice, side population (SP) Lin- Sca+ Kit+ CD150+ marrow cells from young (4 months old) and aged (24 months) animals have undergone RNA-seq⁶⁸ (GSE47819). Both datasets demonstrated HSC expression of *RUNX3* with significant decreases associated with aging [Figure 2.1 A-B]. Human CD34+ CD38+ later stage progenitors also showed diminished *RUNX3* expression with aging, indicating that the changes are not HSC-restricted [Figure 2.2A]. Evidence for an aging-associated decline in progenitor protein levels was seen in human marrow samples immunostained for *RUNX3* [Figure 2.2B]. Analysis of murine bone marrow single-cell RNA-seq datasets¹⁵¹ (GSE89754) from animals with or without Epo treatment confirmed that the signals for *Runx3* expression came from multipotent and early committed erythroid progenitors rather than

contaminant lymphocytes. Discrimination of HSC versus MPP compartments is not possible by this approach [Figure 2.2C].

Because epigenetic changes occur with HSC aging and participate in regulation of *RUNX3*^{64,136,152}, we investigated the effect of aging on DNA and histone modifications within the murine and human loci. Analysis of comprehensive DNA methylation mapping by whole genome bisulfite sequencing⁶⁸ (GSE47819) revealed significant increases in P2 promoter methylation in aged murine HSC [Figure 2.1 C-D]. Datasets for H3K27ac in young versus aged murine HSC are not currently available. The human *RUNX3* locus showed aging-associated decreases in H3K27ac within the P2 promoter, as well as the super-enhancer region located approximately 97 kilobases upstream of the P2 promoter¹⁵³ (GSE104406) [Figure 2.1 E-G].

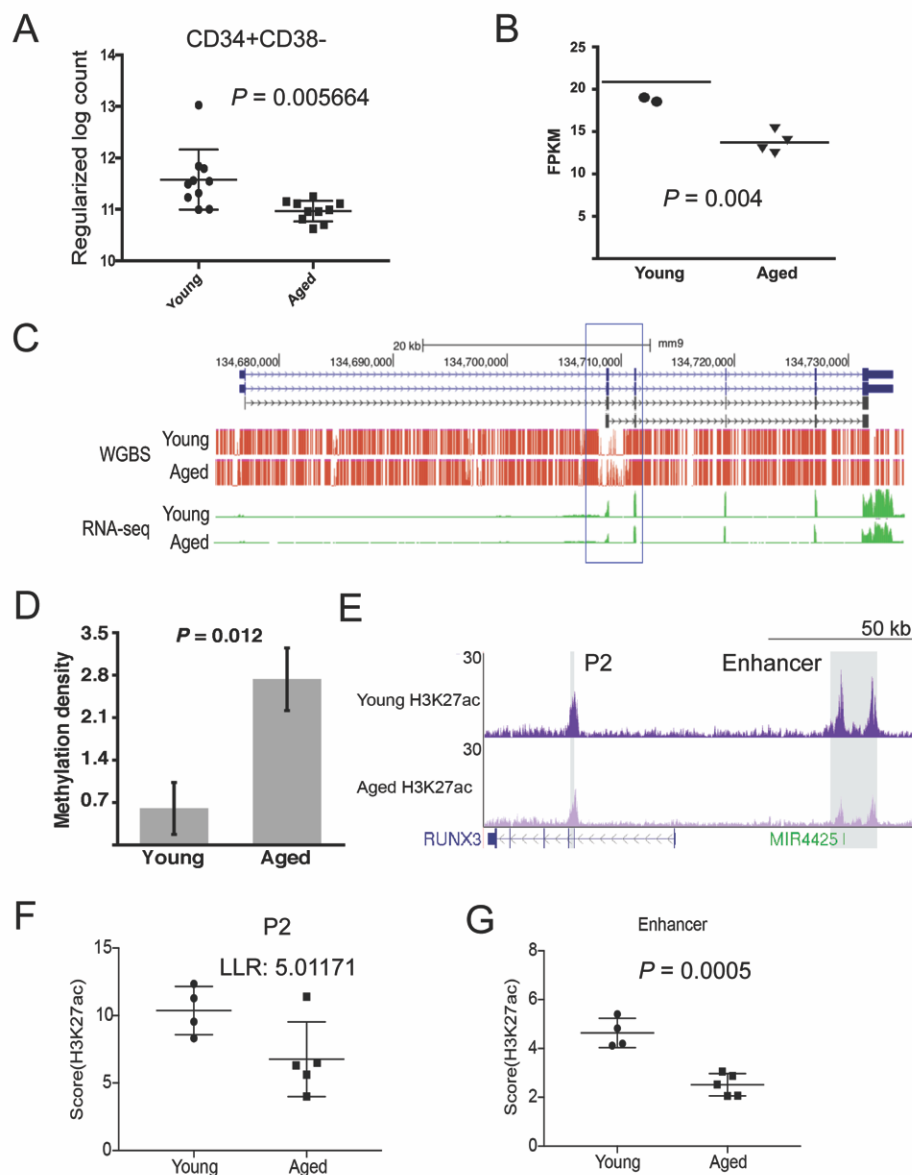


Figure 2.1. HSPC *RUNX3* Levels Decline With Aging

(A) Human *RUNX3* mRNA levels in Lin-CD34+CD38⁻ bone marrow HSPC obtained from healthy young and aged individuals. N = 10/group. (B) Mouse *Runx3* mRNA levels in side population, Lin-Sca1+Kit+CD150⁺ bone marrow HSC obtained from healthy young and aged animals (GSE47819; Sun et al., 2014). N = 4/group. (C-D) Tracks for DNA methylation by whole genome bisulfite sequencing (WGBS, red) and RNA-seq read counts (green) within the mouse *Runx3* locus in HSC from healthy young and aged animals (GSE47819; Sun et al., 2014). The blue box highlights the DNA methylation trough associated with the P2 promoter. Graph in D depicts mean methylation density (% of CpG reads with methylation) within trough, N = 5-6/group. (E-G) Histone H3K27 acetylation by ChIP-seq within the human locus in HSPC from healthy young and aged individuals. Gray shading highlights peaks within the P2 promoter and upstream super-enhancer. Graph in F depicts H3K27ac score for the P2 promoter peak, and the sum of peak scores across the enhancer is depicted in G. N = 4-5/group. All statistics two-tailed Student t test, except in F: log likelihood ratio (LLR). Error bars +/- SEM.

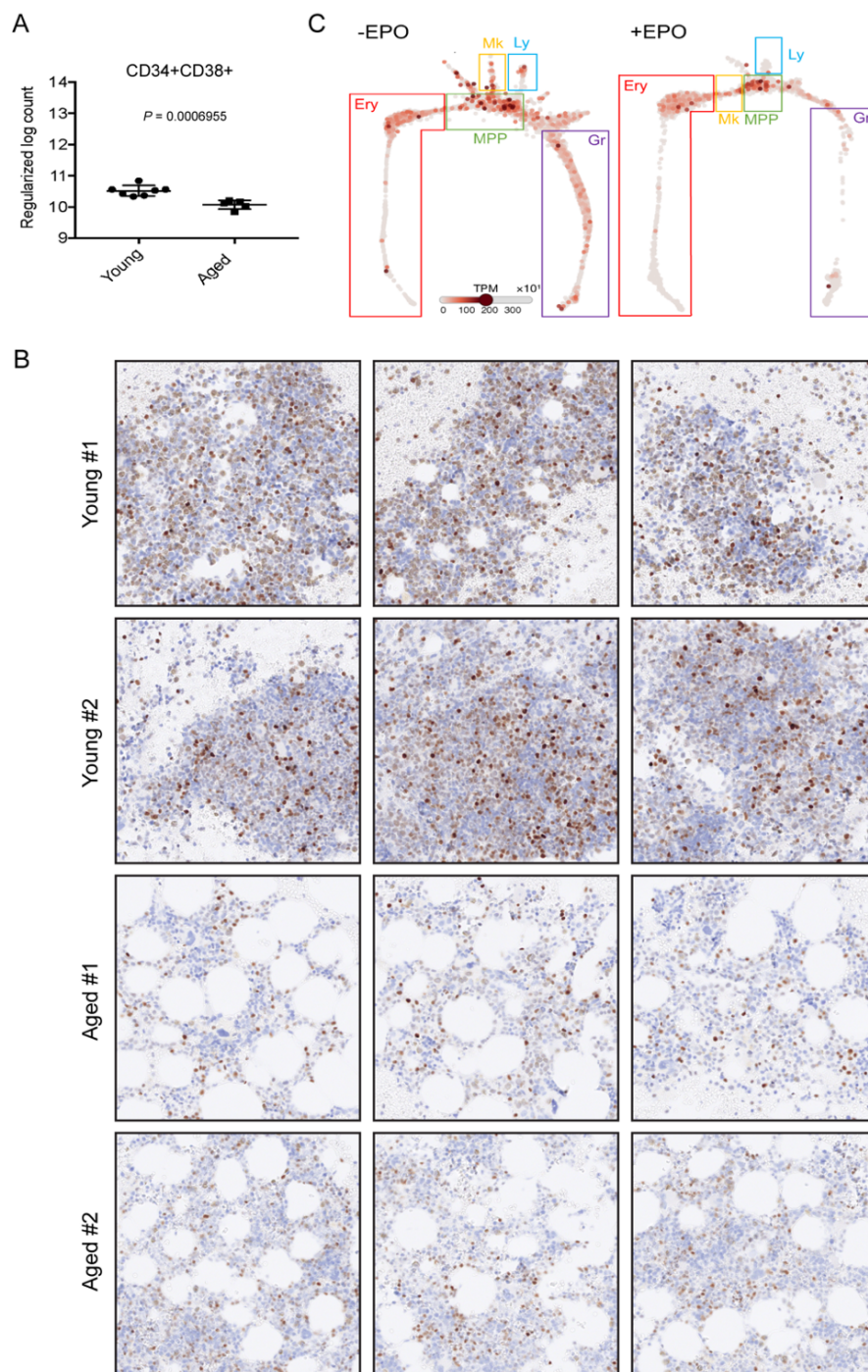


Figure 2.2. HSPC *RUNX3* Levels Decline With Aging

(A) Human *RUNX3* mRNA levels from RNA-seq analysis of Lin-CD34+CD38+ bone marrow HSC obtained from healthy young and aged individuals. (B) Immunostaining of *RUNX3* protein in bone marrow clots of two young (<10 years) and two aged (60-70) subjects shown at 20X magnification. (C) Mouse *Runx3* mRNA expression heat-map overlaid on a multi-lineage hematopoietic SPRING plot derived from single cell RNA-seq on Kit+ marrow cells (Ery: erythroid; MPP: multipotent progenitor; Mk: megakaryocyte; Ly: Lymphoid; Gr: granulocyte. Gene visualizer from Tusi et al. 2018 is available at https://kleintools.hms.harvard.edu/paper_websites/tusi_et_al/).

RUNX3 in Human HSPC Participates in Erythroid Programming

The decline in HSC *RUNX3* levels with aging illustrated in Figure 2A raised questions about potential roles in human hematopoietic differentiation. Human CD34+ HSPC cultures were used to examine protein expression and function. By immunoblot, the initial undifferentiated population displayed relatively high *RUNX3* levels, with gradual decline occurring during erythroid differentiation [Figure 3.2A]. Immunofluorescent staining revealed predominantly cytoplasmic localization in the undifferentiated cells and enhanced nuclear localization associated with erythroid differentiation [Figures 3.3 and 3.4]. Transduction of HSPC with empty or *RUNX3*-targeting lentiviral shRNA vectors did not alter the localization of *RUNX3* in erythroid differentiated cells. Both nuclear and cytoplasmic patterns of *RUNX3* localization have been observed in prior studies, and may reflect SMAD or STAT activation status as previously described^{108,154,155}.

Partial knockdown of *RUNX3* with three independent lentiviral short RNA hairpins blocked erythroid differentiation of CD34+ progenitors, preventing expression of glycophorin A (CD235a) [Figure 3.1A and 3.2B]. Subsequent experiments employed short hairpin #4 due to robust knockdown (~60% protein loss) with no significant cross-inhibition of other *RUNX* proteins [Figure 3.2C]. As additional controls, CD34+ progenitors also underwent transduction with shRNA vectors targeting GFP, which had no effect on erythroid differentiation, and *RUNX1*, which slightly enhanced erythroid differentiation as described¹⁵⁶ [Figure 3.2 D-E]. *RUNX3* deficiency in CD34+ HSPCs also blocked erythroid colony formation in semi-solid medium, with no significant impact on monocyte or mixed granulocyte-

monocyte colonies [Figure 3.1B]. As with the colony assays, RUNX3 deficiency caused minimal changes in granulocyte differentiation (CD15) after eight days of suspension culture [Figure 3.1C]. When maintained in uni-lineage, serum-free erythroid medium containing erythropoietin (Epo) and stem cell factor (SCF), RUNX3-deficient progenitors showed time-dependent declines in proliferation and viability [Figure 3.1 D-E]. By contrast, RUNX3-deficient progenitors cultured in expansion medium with SCF, IL-3, thrombopoietin (TPO), and Flt3-ligand retained normal proliferation and near-normal viability [Figure 3.1 D-E]. However, RUNX3 knockdown did prevent HSPC upregulation of CD41 in megakaryocytic cultures, suggesting an influence at the level of erythro-megakaryocytic progenitors [Figure 3.2F].

To determine contributions to post-commitment human erythropoiesis, we knocked down RUNX3 in sorted CD36⁺ CD235a⁻ early erythroid progenitors. RUNX3 deficiency in these cells impaired their progression to the more mature CD36⁺ CD235a⁺ stage, indicating involvement in post-commitment differentiation [Figure 3.1F]. Knockdown of RUNX3 in the human HUDEP-2 pro-erythroblast line shifted the cells to a less mature phenotype, characterized by increased CD71 and diminished CD235a expression, and blocked induction of hemoglobinization [Figure 3.1G and Figure 3.2 G-I]. Conversely, retroviral overexpression of RUNX3 in HUDEP-2 pro-erythroblasts enhanced their hemoglobinization [Figure 3.1H and Figure 3.2I].

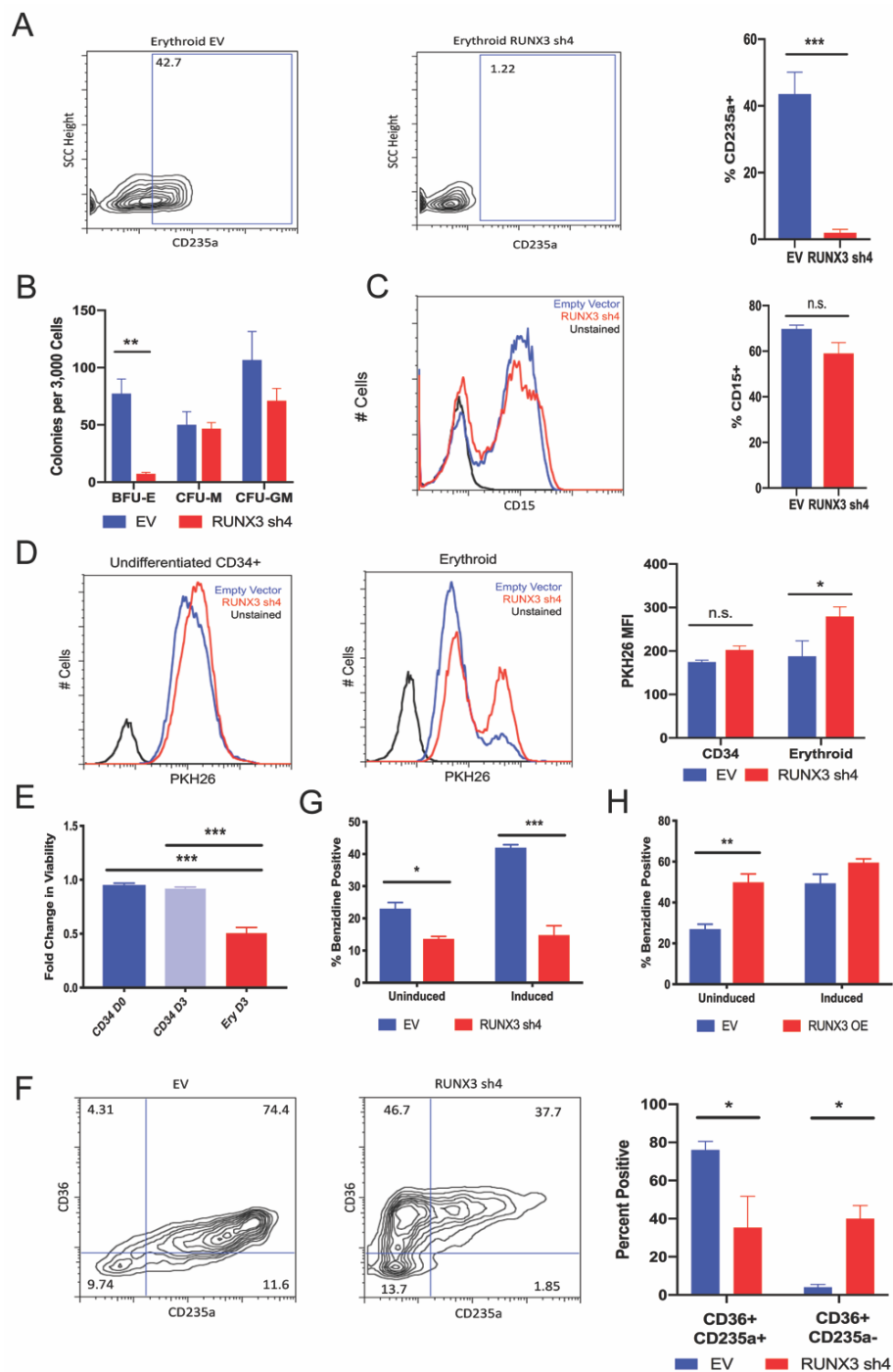


Figure 3.1. RUNX3 Participates in Erythroid but Not Granulocytic Differentiation of Human Progenitors

(A) Flow cytometry plots for erythroid differentiation of CD34+ cells transduced with empty vector (EV) or RUNX3-targeting (RUNX3 sh4) lentiviral shRNA constructs and subjected to unilineage erythroid culture for 3 days. Graph summarizes the quantitation of erythroid differentiation from 3 independent experiments. (B) Summary of colony formation assays on CD34+ cells transduced as in A. (C) Flow cytometry histogram overlays for granulocyte differentiation of CD34+ cells transduced as in A and subjected to unilineage granulocytic

culture for 8 days. Representative results from 3 independent experiments. (D) Flow cytometry histogram overlays for cell proliferation by dye dilution. Transduced CD34⁺ cells were stained with PKH26 followed by 3 days of culture in expansion medium (CD34) or erythroid medium. Graph summarizes mean fluorescence intensity due to dye retention from 3 independent experiments. (E) Summary of viability as assessed by flow cytometry on CD34⁺ cells transduced as in A and cultured in expansion or erythroid medium for indicated days. (F) Flow cytometry plots for erythroid differentiation of CD36⁺ CD235a⁻ early committed erythroid progenitors transduced as in A and cultured in erythroid medium for 3 days. Graph summarizes quantitation of erythroid differentiation from 3 independent experiments. (G-H) Summary of hemoglobinization, i.e. percent cells positive for benzidine staining, in HUDEP-2 cells transduced with control vectors (EV), *RUNX3*-knockdown lentivirus (sh4), or *RUNX3*-overexpression retrovirus (OE). Cells were cultured 48 hours in HUDEP-2 expansion (Uninduced) or differentiation (Induced) medium. N = 3. A and C: two-tailed Student t test. B, D, and F-H: two-way ANOVA with Bonferroni's test. E: one-way ANOVA with Tukey's test. * $P \leq 0.05$, ** $P \leq 0.01$, *** $P \leq 0.005$. Error bars +/- SEM.

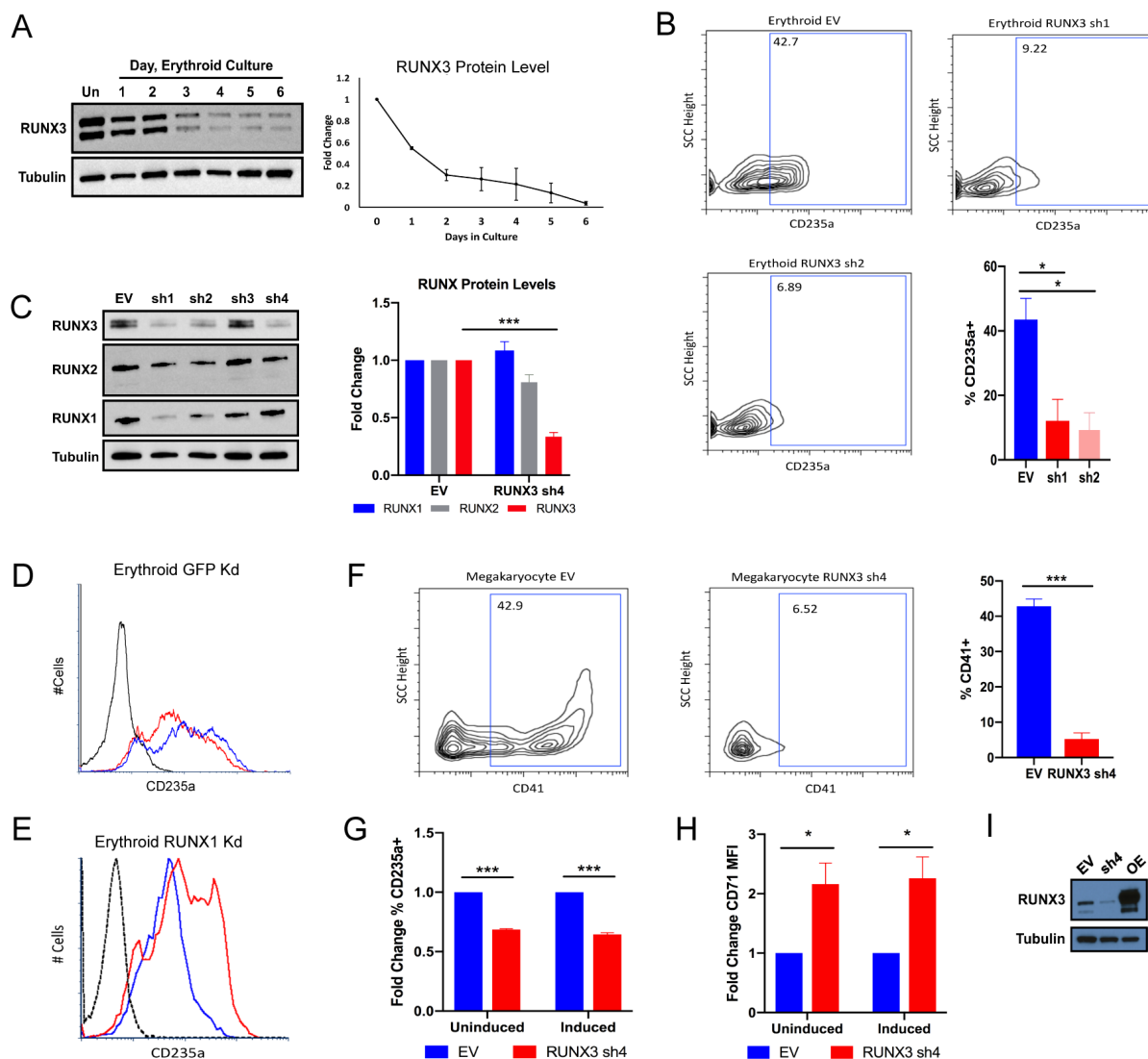


Figure 3.2. RUNX3 Participates in Human Erythroid and Megakaryocyte Differentiation
 (A) RUNX3 protein levels by immunoblot in CD34+ HSPC, undifferentiated and at indicated durations of erythroid culture. Representative immunoblot of whole cell lysates from 3 independent experiments. (B) Flow cytometry plots for erythroid differentiation of CD34+ cells transduced with empty vector (EV) or RUNX3-targeting (RUNX3 sh1 and sh2) lentiviral shRNA constructs and subjected to unilineage erythroid culture for 3 days. Graph summarizes the quantitation of erythroid differentiation from 3 independent experiments. (C) RUNX family protein expression by immunoblot in CD34+ cells transduced with lentiviral empty vector (EV) or shRNA expression constructs targeting *RUNX3*. Graph summarizes mean fold change in tubulin-normalized protein levels associated with RUNX3 knockdown. N=3. (D) Histogram overlay for erythroid differentiation of un-transduced CD34+ cells (blue), CD34+ cells transduced with a GFP-targeting lentiviral shRNA construct (red), and unstained cells (black). (E) Histogram overlay for erythroid differentiation of CD34+ cells transduced with empty vector (blue), CD34+ cells transduced with a RUNX1-targeting lentiviral shRNA construct (red), and unstained cells (black). (F) Flow cytometry plots for megakaryocyte differentiation of CD34+ cells transduced with empty vector (EV) or RUNX3-targeting (RUNX3 sh4) lentiviral shRNA constructs and subjected to unilineage megakaryocytic culture for 3 days. Graph summarizes

the quantitation of megakaryocyte differentiation from 3 independent experiments. (G-I) Summary of differentiation status by flow cytometry on transduced HUDEP-2 cells +/- differentiation induction, and immunoblot of RUNX3. Graphs show mean fold changes in CD235a+ percentage or CD71 mean fluorescence intensity associated with RUNX3 knockdown. N = 3. B: one-way ANOVA with Tukey's post hoc test. C, F, and G: Two-way ANOVA with Bonferroni's test. E: two-tailed Student t test. * $P \leq 0.05$, ** $P \leq 0.01$, *** $P \leq 0.005$. Error bars: +/- SEM.

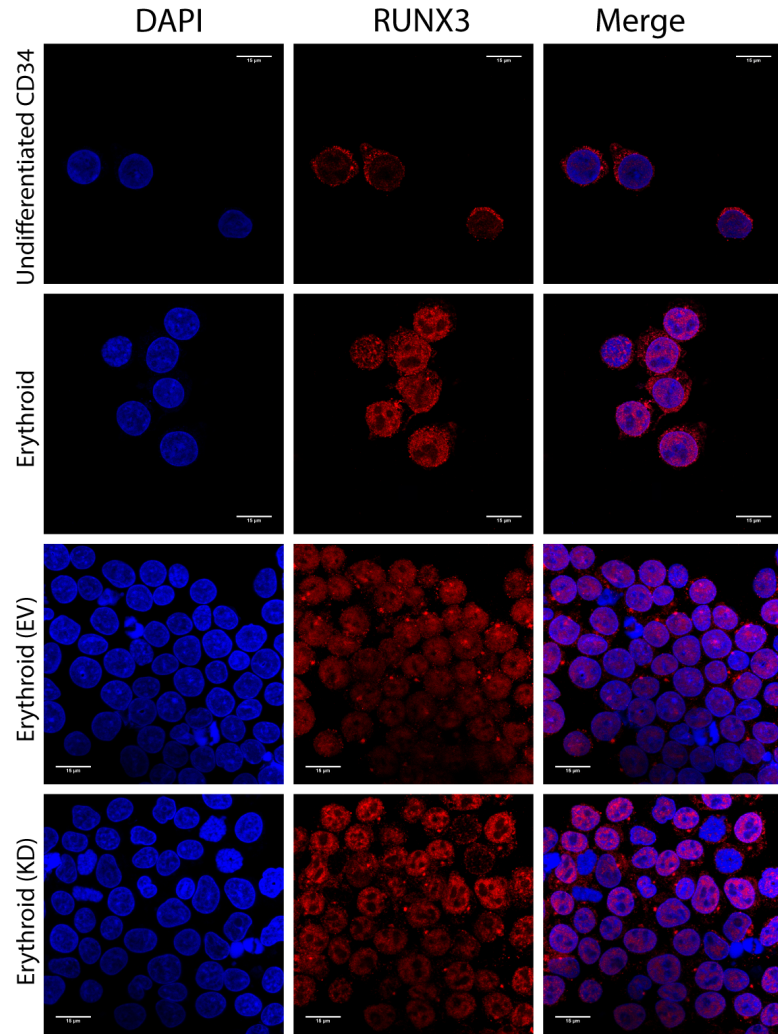


Figure 3.3. Cellular localization of RUNX3 in primary cells

Immunofluorescent detection of RUNX3 in untransduced, empty vector transduced, and RUNX3 sh4 transduced CD34+ HSPC. HSPC were analyzed undifferentiated and at day 3 of erythroid culture.

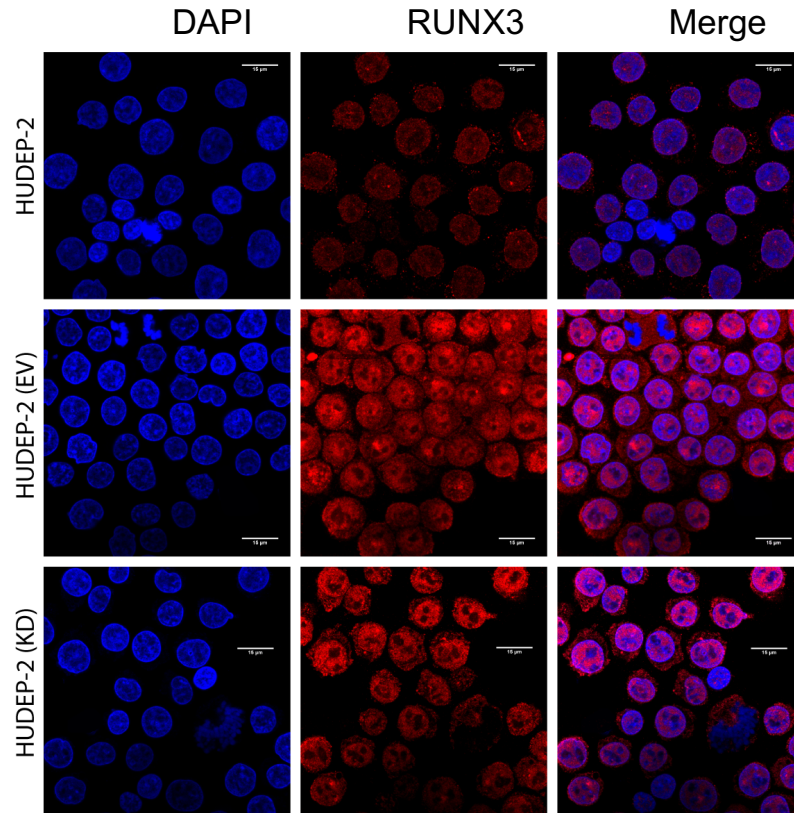


Figure 3.4. Cellular localization of RUNX3 in HUDEP-2 cell line

Immunofluorescent detection of RUNX3 in untransduced, empty vector transduced, and RUNX3 sh4 transduced HUDEP-2 erythroblastic progenitor cell line.

Progenitor Deficiency of RUNX3 Alters the Balance of Lineage Output

To analyze in greater detail the effects of RUNX3 deficiency on progenitor fates, mass cytometry (CyTOF) was employed for comprehensive single cell profiling of cells in HSPC expansion culture, and cells in erythroid, megakaryocyte, or granulocyte culture conditions for 48 hours. Cells from each culture condition were clustered into populations defined by surface marker staining, followed by construction of minimum spanning tree (MST) plots describing average fold changes in population abundance associated with RUNX3 knock-down [Figure 4.1A and Figure 4.2 A-B]. These populations segregated into two main branches: a lower erythro-megakaryocytic compartment (Ery/Mk: red oval) defined by CD36 and/or CD41 positivity, and an upper compartment (Myeloid: blue oval) lacking both markers [Figure 4.2C-D]. As expected from results in Figure 3, RUNX3 knock-down selectively diminished cell populations within the Ery/Mk compartment in lineage culture conditions, but not in HSPC expansion conditions [Figure 4.1A and Figure 4.2A]. This contraction was associated with impaired proliferation, as reflected by decreased Ki-67 expression, but with no evidence of increased apoptosis based on lack of cleaved Caspase-3 [Figure 4.1 B-C].

Notably, populations in the myeloid compartment (blue oval) were augmented in RUNX3-deficient progenitors grown in erythroid medium but not in other culture conditions. Analysis of these populations revealed a myeloid-skewed shift in HSPC distribution, similar to what has been described in aged bone marrow. These populations displayed a GMP (granulocyte-monocyte progenitor) phenotype, based on expression of CD34, CD38, CD123, and CD45RA in various combinations

[Table 1]. Strikingly, RUNX3-deficient populations in the Ery/Mk compartment (red oval) exhibited aberrant retention of CD123, as well as global upregulation the GMP marker CD45RA and the myeloid differentiation antigen CD11b [Figure 4.1D-F].

The CyTOF panel permitted assessment of the frequencies of cells with marker profiles of megakaryocyte-erythroid progenitors (MEP), common myeloid progenitors (CMP), and granulocyte monocyte progenitors (GMP)³¹. This analysis showed RUNX3 deficiency to decrease MEP frequency and increase CMP and GMP frequencies [Figure 4.1G and Figure 4.2E]. Within the CMP and MEP compartments, knockdown of RUNX3 was associated with diminished expression of erythroid markers CD36 and CD235a, but enhanced expression of the myeloid marker CD11b [Figure 4.1 H-I and Figure 4.1F].

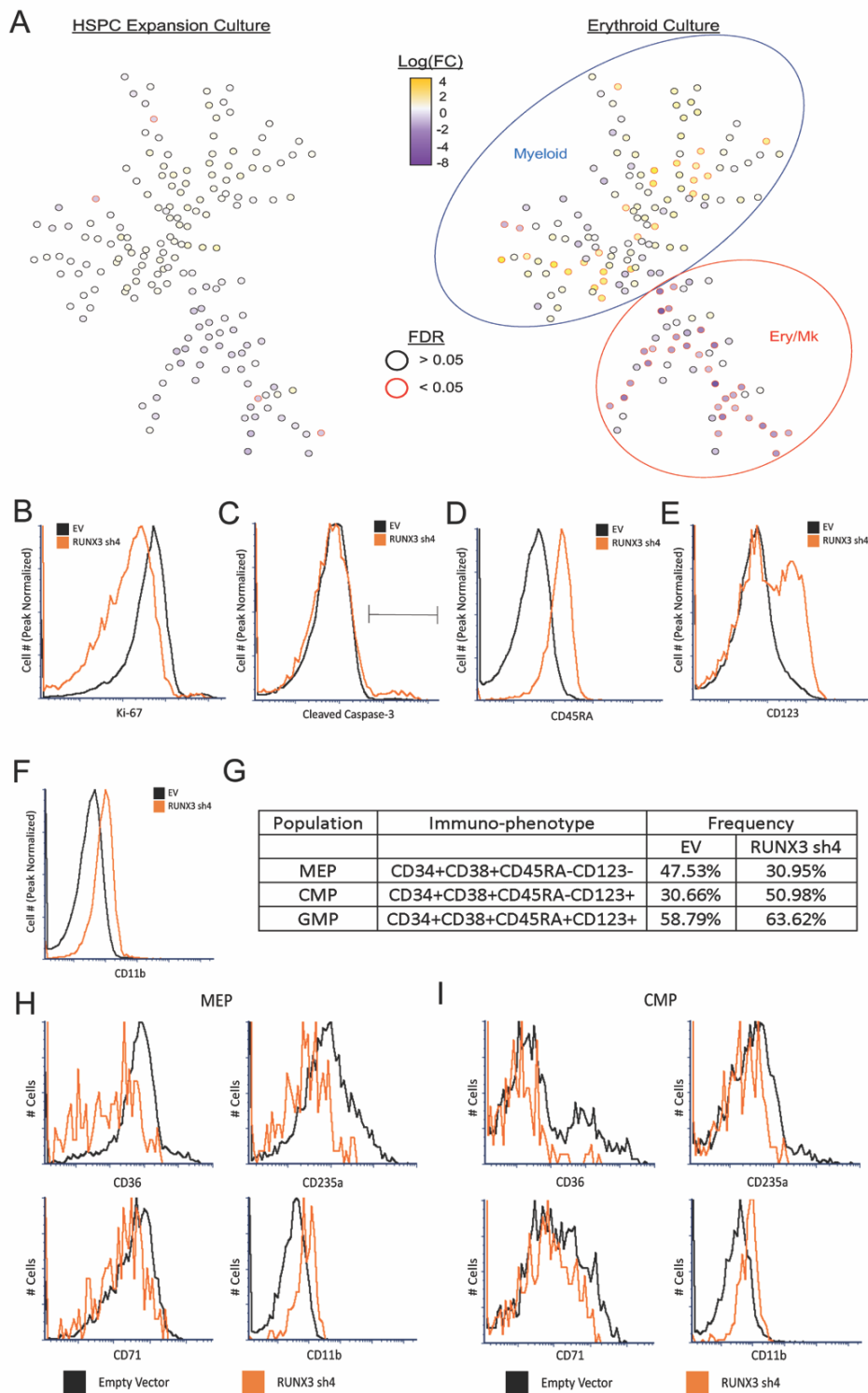


Figure 4.1. RUNX3 Levels Influence Progenitor Lineage Output Balance

(A) Minimum spanning tree plots depicting cell population-nodes identified by CyTOF on indicated cultures of transduced CD34+ progenitors. Heatmap coloration of nodes reflects \log_2 (fold changes) in their frequency associated with RUNX3 knock-down. Erythroid-megakaryocytic (Ery/Mk) and myeloid compartments are indicated by red and blue ovals

respectively. (B-C) CyTOF histogram overlays from transduced progenitors cultured in erythroid medium, comparing expression of Ki-67 and cleaved caspase-3 between control (EV, black) and RUNX3-deficient (RUNX3 sh4, orange) populations in the Ery/Mk compartment. (D-F) CyTOF histogram overlays from transduced progenitors cultured in erythroid medium, comparing expression of CD123, CD45RA, and CD11b between control (EV, black) and RUNX3-deficient (RUNX3 sh4, orange) populations in the Ery/Mk compartment. (G) Frequencies of MEP, CMP, and GMP populations calculated from all cells cultured in erythroid medium. (H-I) Histogram overlays comparing CD36, CD235a, CD71, and CD11b expression between control (EV, black) and RUNX3-deficient (RUNX3 sh4, orange) MEP and CMP.

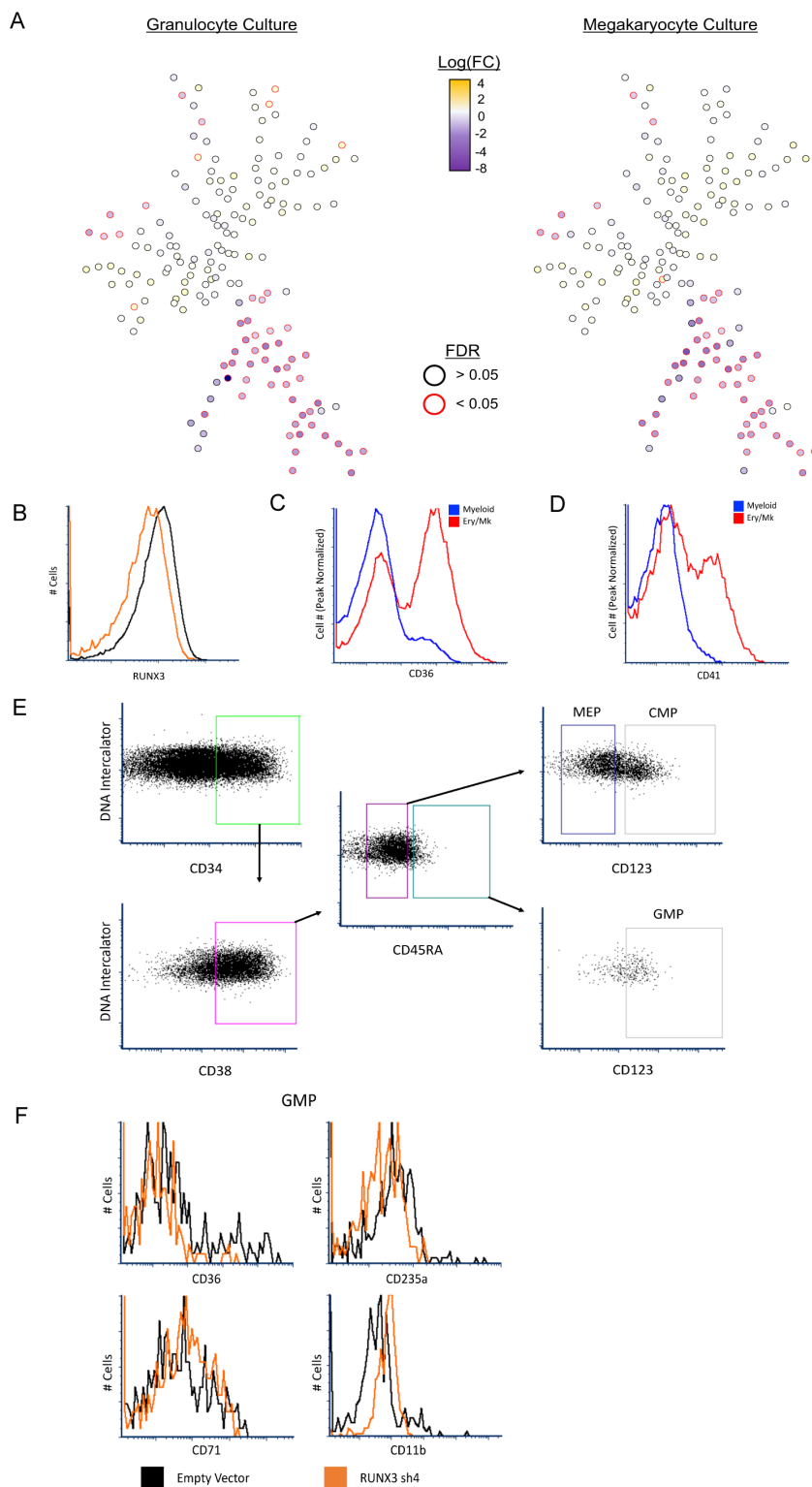


Figure 4.2. RUNX3 Levels Influence Progenitor Lineage Output Balance

(A) Minimum spanning tree plots depicting cell population-nodes identified by CyTOF on indicated cultures of transduced CD34+ progenitors. Heatmap coloration of nodes reflects \log_2 (fold changes) in their frequency associated with RUNX3 knock-down. (B) Histogram

overlay comparing RUNX3 levels in cells transduced with empty vector (black) or RUNX3 sh4 construct (orange). (C-D) CyTOF histogram overlays from control EV-transduced progenitors cultured in erythroid medium, comparing expression of CD36 and CD41 between myeloid (blue) and erythro-megakaryocytic (Ery/Mk, red) compartments as depicted in Figure 4A. (E) Gating strategy used to determine CMP, MEP, and GMP population frequencies. (F) Histogram overlay comparing CD36, CD235a, CD71, and CD11b expression between control (EV, black) and RUNX3-deficient (RUNX3 sh4, orange) GMP.

RUNX3 Deficiency Causes Perturbations in Erythroid Transcriptional Program

To identify the genes affected by RUNX3 knockdown, we performed mRNA sequencing on undifferentiated CD34⁺ cells and cells in erythroid culture for 24 hours, before cell viability was impacted by RUNX3 deficiency. In line with our other data, few changes were found between control and RUNX3-deficient undifferentiated cells (<70 genes with differential expression). However, among the down-regulated genes were key erythroid transcription factors including *KLF1*, *GATA1*, and *GFI1B* [Figure 5A]. Several globin- and erythroid blood group antigen-encoding genes were decreased as well (data not shown). Notably, *Klf1*, *Gata1*, and downstream erythroid target genes *Gypa* and *Epore* also underwent downregulation in aged versus young murine HSC [Figure 5B]. When comparing control and RUNX3-deficient progenitors in erythroid culture, ~1,100 genes showed differential expression. These included many of the same genes affected in the undifferentiated cells as well as additional erythroid genes such as *CD36* and *EPOR* [Figure 5A]. In addition, several granulocytic transcription factors were aberrantly up-regulated, including *GFI1*, *JUN*, and *FOS* [Figure 5A]. Gene ontology (GO) analysis of genes differentially expressed in control versus RUNX3-deficient undifferentiated progenitors revealed only two significant functional categories, oxygen transport (i.e. erythroid; >100 fold enrichment; FDR 1.22E-6) and blood coagulation (i.e. megakaryocytic; 15.08 fold enrichment; FDR 1.91E-3), both of which showed downregulation. GO analysis of progenitors in erythroid culture yielded similar results but also included genes related to mitochondrial protein synthesis/transport and ribosomal biogenesis [Figure 5C].

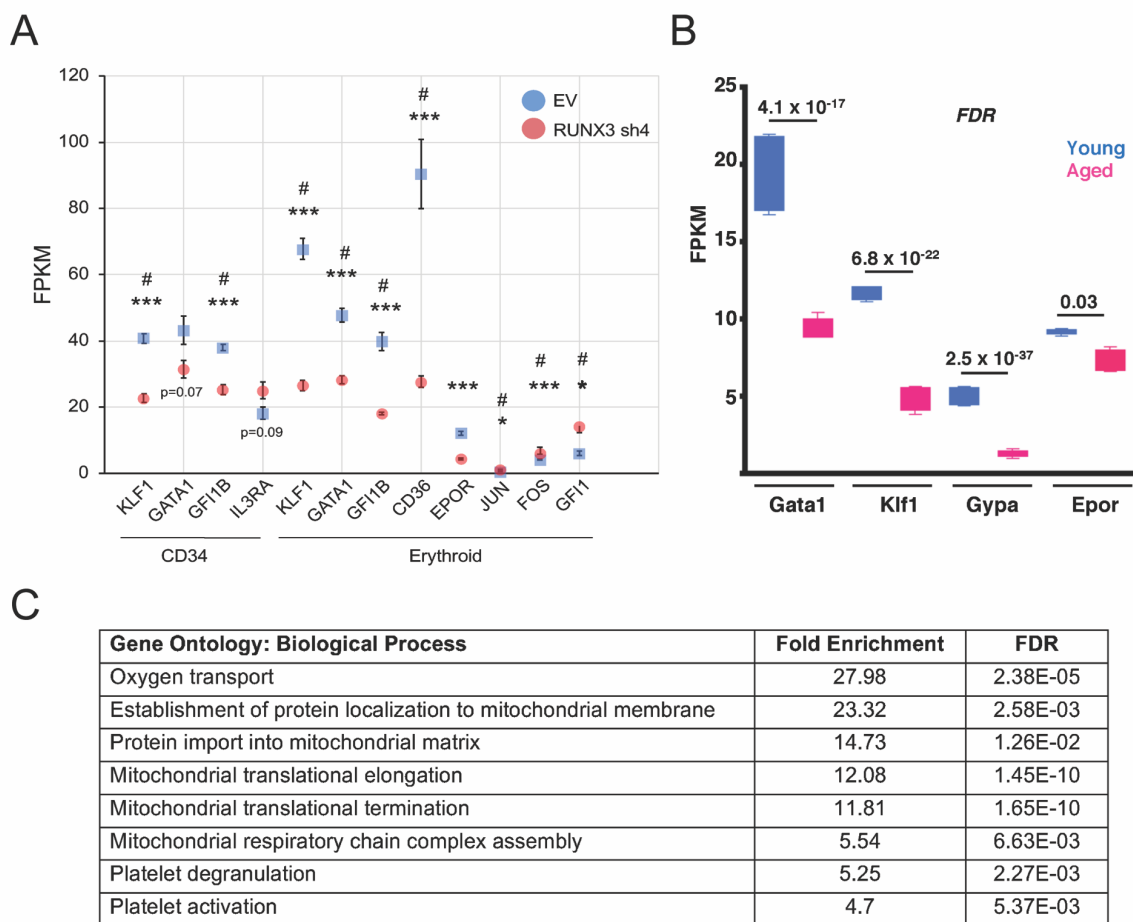


Figure 5. RUNX3 Deficiency Causes Perturbations in Erythroid Transcriptional Program
 (A) FPKM read counts of relevant genes in transduced progenitors cultured in expansion or erythroid medium, N = 3. (B) FPKM read counts of key erythroid genes in young and aged murine HSC as in Figure 2.1B (GSE47819; Sun et al., 2014). (C) Gene Ontology classification by biological process of gene sets significantly downregulated in association with RUNX3 deficiency in cells undergoing erythroid culture, N = 3. All statistics False Discovery Rate (denoted by '#' in A, DESeq2), plus two-tailed Student t test for FPKM values denoted by asterisks in A, * $P \leq 0.05$, ** $P \leq 0.01$, *** $P \leq 0.005$. Error bars: +/- SEM.

HSPC RUNX3 Deficiency Occurs in Human Anemias Associated with Aging

Because RUNX3 expression levels strongly influence human erythroid differentiation, its downregulation could potentially contribute to anemias associated with aging. To address this possibility, we analyzed highly purified marrow progenitors from the following subjects: normal non-anemic young (20-35 years old), non-anemic aged (>65 years old), and aged (>65 years old) with unexplained anemia of the elderly (UAE). The diagnosis of UAE was made by ruling out all other potential causes of anemia, as per the criteria of Goodnough and Schrier¹⁵⁷. Gene expression profiling by microarray confirmed *RUNX3* downregulation in UAE versus aged HSC⁴⁰ (GSE32719) [Figure 6A]. Functional studies revealed intrinsic differences in lineage output between UAE and non-anemic old progenitors. UAE HSC yielded fewer erythroid colonies (BFU-E) but similar numbers of myeloid colonies (CFU-GM) [Figure 6B]. These findings resemble the effects of RUNX3 knockdown on colony formation by CD34+ progenitors, as shown in Figure 3.1B. Furthermore, UAE MEP also showed poor TGF β responsiveness in erythroid colony (CFU-E) enhancement [Figure 6C], a finding notable given the known influences of HSC aging and RUNX3 expression on this pathway^{68,158}.

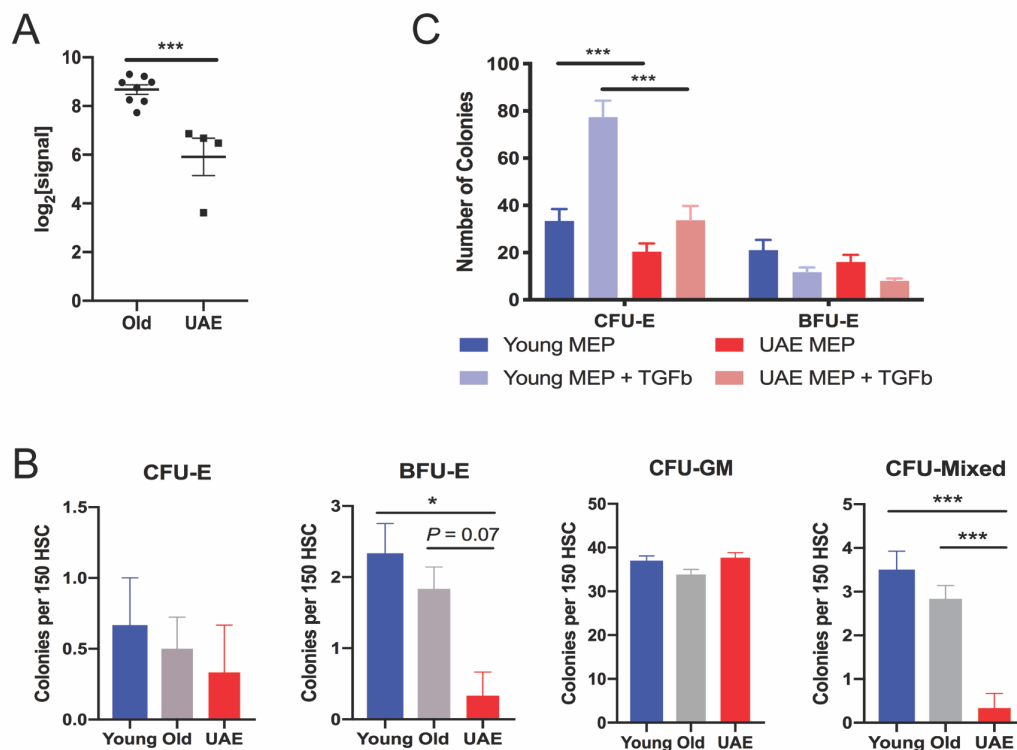


Figure 6. Decreased *RUNX3* Expression and Impaired Erythropoiesis in Unexplained Anemia of the Elderly

(A) Log₂[signal] derived from microarray analysis of *RUNX3* mRNA levels in purified human marrow HSC and CMP from normal old and UAE subjects. N = 4-8/group (B) Summary of colony formation assays on 150 HSC from normal young, normal old, and UAE subjects, N = 3-6/group. (C) Summary of erythroid colony formation assays +/- TGFβ on 150 MEP from normal young versus UAE subjects. A: two-tailed Student t test. B: one-way ANOVA with Tukey's Test. C: two-way ANOVA with Bonferroni's test. **P* ≤ 0.05, ***P* ≤ 0.01, ****P* ≤ 0.005. Error bars: +/- SEM.

D. Discussion

HSC alterations with aging are complex, result from cell-autonomous and micro-environmental mechanisms, and involve transcriptional changes in numerous genes. Interestingly, several of the transcriptional programs affected have been previously linked to *RUNX3* function, including quiescence, DNA-damage responsiveness, and TGF β signaling^{85,105,128,158}. Decreased *RUNX3* in aged tissues has been previously reported but was analyzed in heterogeneous mixtures of mature cell types^{138–140,149}. Our results derive from purified, long-lived stem cells and reveal conservation between mice and humans. The repressive mechanism likely relates to the aging-associated epigenetic changes identified. Beerman et al. have shown that murine HSC aging and proliferative stress reconfigure the DNA methylation landscape, with key erythroid and lymphoid regions targeted for hypermethylation and repression⁶⁷. The increased *Runx3* P2 promoter methylation we identified in aged murine HSC has also been found in aging of other tissues and cancers^{136,137,149}. The aging associated decreases in H3K27ac that we identified at the human *RUNX3* promoter and upstream super-enhancer may contribute to its repression in human HSC.

A feature of HSC aging conserved from mice to humans consists of myeloid skewing characterized by augmented marrow production of neutrophils and monocytes at the expense of erythroid and lymphoid cells^{68,142,143}. This propensity likely contributes to aging-associated pathologies such as generalized inflammation, risk for myeloid malignancies, and anemia. Exaggerated myeloid skewing occurs during aging of mice with hematopoietic knock-out of *Runx3*¹³⁵. These animals also

experience an expansion of LSK+ HSPC, and are more sensitive to G-CSF-stimulated mobilization of the marrow progenitors. Thus RUNX3 loss in young HSC elicits some features of aging and in old HSC augments the process of myeloid skewing. Combined marrow knock-out of *Runx3* with *Runx1* has demonstrated synthetic lethality with rapid development of multilineage failure including anemia and thrombocytopenia, suggesting that Runx1 compensation in young mice may mask phenotypic consequences of Runx3 loss in HSPC¹⁰⁵. Additional studies have implicated RUNX3 in non-lymphoid hematopoietic development. In human CD34+ cell erythroid cultures, RUNX3 was predicted by Cytoscape MiMI analysis of gene expression profiles to be a “parent protein,” i.e. a central node, in an erythroid transcription factor network¹³⁴. In zebrafish, morpholino knock-down of *runx3* during embryogenesis resulted in severe anemia¹³³.

Our results define a novel role for RUNX3 in the erythropoietic program, governing the expression of lineage-specific transcription factors such as *KLF1*, *GATA1*, and *GFI1B*. Notably, *Klf1* and *Gata1* displayed downregulation in aged murine HSC. We further show that RUNX3 deficiency produces perturbations at multiple developmental stages including MEP and committed erythroid progenitors. The decreased proliferation seen in RUNX3-deficient progenitors may contribute to differentiation impairment. However, the retained capacity for myeloid differentiation and the aberrant retention of GMP markers such as CD123 and CD45RA on RUNX3 deficient cells suggests an additional role in lineage resolution. Taken together, the current findings implicate RUNX3 in the maintenance of bone

marrow lineage balance and identify its decline in aged HSPC as a likely contributory factor in aging-associated anemias.

Table 1. Populations in erythroid culture identified by CyTOF to be significantly affected by RUNX3 deficiency.

Population Phenotype (diminished frequency)	log(fold change abundance)	FDR
CD117- CD235a+ CD34+ CD36hi CD71+	-3.719262064	0.020801921
CD117- CD34+ CD36hi	-2.93570212	0.020801921
CD117- CD34+	-2.927367589	0.020801921
CD36hi	-2.026476318	0.020801921
CD235a+ CD36hi	-1.962454631	0.020801921
CD117+ CD36hi	-1.94043204	0.020801921
CD36hi CD71+	-1.924672676	0.020801921
CD117+ CD235a+ CD36hi	-1.906223603	0.020801921
CD235a+ CD36hi CD71+	-1.87934004	0.020801921
CD34+ CD36hi CD45RA- CD71+	-5.527807648	0.021172785
CD36hi CD38-	-3.20231726	0.021172785
CD117+ CD123- CD235a+ CD36hi CD71+	-2.324952873	0.021172785
CD123- CD36hi	-2.295056993	0.021172785
CD34+ CD36hi	-2.272313596	0.021172785
CD34+ CD36hi CD71+	-2.169146303	0.021172785
CD117+ CD235a+ CD34- CD71+	-2.112339189	0.021172785
CD117+ CD235a+ CD36hi CD71+	-1.821118771	0.021172785
CD117+ CD235a+ CD71+	-1.623566908	0.021172785
CD235a+ CD71+	-1.336391726	0.021172785
CD117+ CD71+	-1.068179401	0.021172785
CD117+ CD123- CD235a+ CD34- CD71+	-4.221637154	0.02181571
CD123+ CD235a+ CD34+ CD36hi CD45RA+ CD71+	-2.424672903	0.02181571
CD117+ CD34+ CD36hi	-2.183237624	0.02181571
CD235a+ CD34+ CD36hi CD71+	-1.911194053	0.021826715
CD117+ CD235a+ CD34-	-1.741000304	0.021826715
CD117+ CD34- CD71+	-1.546220087	0.021826715
CD117+ CD123- CD71+	-1.37695306	0.021826715
CD117+ CD38- CD71+	-2.62508303	0.022251608
CD117+ CD235a+ CD34+ CD36hi CD45RA+	-2.464415391	0.022251608
CD235a+ CD34+ CD36hi CD45RA+	-2.378683681	0.022251608
CD235a+ CD34+ CD36hi	-2.154723865	0.022251608
CD235a+ CD34+ CD36hi CD45RA+ CD71+	-2.044416618	0.022251608
CD117+ CD123- CD235a+ CD71+	-1.505742441	0.022251608
CD117+ CD123-	-1.289467248	0.022251608
CD117+ CD235a+	-1.064811503	0.022251608

CD71+	-0.7540356	0.022251608
CD34- CD36hi	-1.839183625	0.022768574
CD117+ CD235a+ CD34+ CD45RA- CD71+	-4.18452121	0.023049541
CD235a+	-0.919235293	0.024478996
CD235a+ CD36hi CD45RA+	-1.687778826	0.025456838
CD123- CD71+	-1.231364348	0.025456838
CD123- CD34- CD71+	-3.149913022	0.026118862
CD117+ CD235a+ CD34+ CD36hi	-2.011961177	0.026152719
CD36hi CD45RA- CD71+	-5.575943728	0.027394542
CD117+ CD235a+ CD36hi CD45RA+	-1.633671867	0.027394542
CD117+ CD235a+ CD36hi CD45RA- CD71+	-5.334345011	0.027678568
CD36hi CD45RA+	-1.578658274	0.027777726
CD34- CD71+	-1.477818478	0.028036592
CD117+ CD235a+ CD34+ CD36hi CD45RA+ CD71+	-1.932433149	0.030212605
CD36hi CD71-	-2.038562279	0.030255547
CD123- CD34+ CD36hi	-1.506923466	0.034311297
CD235a- CD34+ CD36hi	-1.880093946	0.034318267
CD117+ CD235a+ CD45RA- CD71+	-5.034412802	0.03624554
CD117+ CD235a+ CD34+ CD36hi CD71+	-1.495710107	0.03624554
CD235a+ CD36hi CD45RA+ CD71+	-1.475378789	0.039628627
CD117+ CD235a+ CD34- CD36hi CD71+	-1.655453922	0.041382437
CD117+ CD235a+ CD36hi CD45RA+ CD71+	-1.447625685	0.041382437
CD117+ CD34+ CD45RA- CD71+	-4.390262537	0.045572809
CD117+ CD34-	-1.054308414	0.045705551
CD123- CD34+	-1.274233859	0.047666676
Population Phenotype (increased frequency)	log(fold change abundance)	FDR
CD45RA+	0.961620903	0.021172785
CD36lo CD45RA+	1.949999308	0.021172785
CD117+ CD36lo CD45RA+	2.0199171	0.021172785
CD123+ CD36lo CD45RA+	2.079819864	0.021172785
CD123+ CD38+ CD45RA+	2.093917809	0.021172785
CD117+ CD123+ CD36lo CD45RA+	2.170353906	0.021172785
CD117- CD38+ CD45RA+	2.35114823	0.021172785
CD117+ CD123+ CD38+ CD45RA+	2.370327689	0.021172785
CD123+ CD36lo CD38+ CD45RA+	2.52321586	0.021172785
CD117+ CD123+ CD36lo CD38+ CD45RA+	3.168493405	0.021172785
CD117+ CD123+ CD36lo CD38+ CD45RA+ CD71-	3.486666794	0.021172785

CD123+ CD45RA+	1.690158574	0.021176596
CD36lo CD38+ CD45RA+	2.272647679	0.021176596
CD117+ CD123+ CD34+ CD36lo CD45RA+	2.283017298	0.021176596
CD117- CD123+ CD38+ CD45RA+	2.353692155	0.021176596
CD117+ CD36lo CD38+ CD45RA+ CD71+	2.535769836	0.021176596
CD117+ CD36lo CD38+ CD45RA+	2.600259996	0.021176596
CD117+ CD123+ CD36lo CD45RA+ CD71-	2.680126994	0.021176596
CD117+ CD123+ CD235a- CD45RA+ CD71+	2.687459827	0.021176596
CD45RA+ CD71-	2.016784542	0.021268162
CD117+ CD36- CD45RA+ CD71+	2.299899769	0.021268162
CD117+ CD123+ CD34+ CD45RA+	1.704345953	0.02181571
CD117+ CD45RA+ CD71-	1.986693782	0.02181571
CD117+ CD36lo	1.620452606	0.021826715
CD38+ CD45RA+	1.644879664	0.021826715
CD117+ CD123+ CD45RA+	1.671525396	0.021826715
CD123+ CD34+ CD45RA+	1.684655878	0.021826715
CD117+ CD123+ CD36lo CD71-	1.966847719	0.021826715
CD117+ CD123+ CD45RA+ CD71+	1.97001232	0.021826715
CD36lo CD38+ CD45RA+ CD71+	1.975230993	0.021826715
CD117+ CD36- CD38+ CD45RA+ CD71+	2.134898349	0.021826715
CD117+ CD123+ CD34+ CD36- CD45RA+ CD71+	2.186756531	0.021826715
CD117+ CD123+ CD45RA+ CD71-	2.192298028	0.021826715
CD117+ CD123+ CD34+ CD45RA+ CD71-	2.277775625	0.021826715
CD117+ CD123+ CD235a- CD36lo CD38+ CD45RA+ CD71+	2.649605266	0.021826715
CD117+ CD123+ CD235a- CD34+ CD36- CD45RA+ CD71+	2.734785211	0.021826715
CD117+ CD123+ CD34+ CD36lo CD45RA+ CD71-	2.839704884	0.021826715
CD117+ CD45RA+	0.820382787	0.022251608
CD117+ CD123+ CD34+ CD36lo	1.57550775	0.022251608
CD117+ CD123+ CD36lo	1.578013625	0.022251608
CD117+ CD71-	1.601521438	0.022251608
CD123+ CD45RA+ CD71+	1.70375139	0.022251608
CD117+ CD123+ CD71-	1.753618176	0.022251608
CD123+ CD38+ CD45RA+ CD71+	1.780140967	0.022251608
CD123+ CD36lo CD38+ CD45RA+ CD71+	1.827312586	0.022251608
CD235a- CD45RA+	1.905278528	0.022251608
CD117+ CD235a- CD45RA+	1.92979801	0.022251608
CD117+ CD123+ CD38+	2.058814479	0.022251608
CD117+ CD235a- CD38+ CD45RA+	2.109723532	0.022251608
CD235a- CD36lo CD45RA+	2.141941418	0.022251608

CD117+ CD123+ CD235a- CD34+ CD36- CD45RA+	2.184052312	0.022251608
CD117+ CD36lo CD38+	2.24701988	0.022251608
CD117+ CD235a- CD36lo CD45RA+	2.270590293	0.022251608
CD117+ CD235a+ CD36lo CD38+ CD45RA+ CD71+	2.36368958	0.022251608
CD117+ CD123+ CD36lo CD38+	2.517235551	0.022251608
CD117+ CD34- CD36- CD38+ CD45RA+ CD71+	2.74466792	0.022251608
CD117+ CD123+	1.395585034	0.022509853
CD117+ CD123+ CD34+	1.425052707	0.022694075
CD235a- CD36lo	1.940196737	0.022768574
CD117+ CD38+ CD45RA+	1.503418954	0.025427647
CD117+ CD123+ CD38+ CD45RA+ CD71+	1.744456412	0.025427647
CD117- CD123- CD36lo CD71-	2.374625197	0.025456838
CD34- CD45RA+ CD71-	2.235289254	0.025725544
CD34- CD36- CD71+	2.557835468	0.025956549
CD36- CD45RA+ CD71+	1.931527814	0.026118862
CD123+ CD34+ CD36lo	1.477841918	0.026152719
CD117+ CD123+ CD34+ CD36lo CD71-	1.77349216	0.026355272
CD123+ CD34+	1.332506425	0.026857217
CD34+ CD36lo	1.415031769	0.027394542
CD34- CD45RA+	1.971837004	0.027394542
CD117+ CD123+ CD34+ CD45RA+ CD71+	1.710120145	0.027678568
CD34- CD36- CD45RA+	2.515739011	0.027678568
CD123+ CD235a+ CD38+ CD45RA+ CD71+	1.610692758	0.028659103
CD117+ CD36- CD38+ CD45RA+	1.747189368	0.028659103
CD117- CD34- CD36lo	2.228242427	0.028659103
CD38+ CD45RA+ CD71+	1.439757948	0.028790802
CD117+ CD123+ CD34+ CD71-	1.615420271	0.028790802
CD123+ CD34+ CD45RA+ CD71+	1.644404536	0.028790802
CD117- CD38+	1.684508468	0.028790802
CD123+ CD235a+ CD34+ CD38+ CD45RA+ CD71+	1.741804463	0.028790802
CD123+ CD235a- CD36lo CD71+	1.737054092	0.031330165
CD235a+ CD36lo CD38+ CD45RA+ CD71+	1.632398539	0.03159593
CD123+ CD38+	1.46944081	0.031910071
CD117+ CD235a-	1.446718275	0.032742922
CD117- CD123+ CD38+	1.667976719	0.03293287
CD117+ CD123+ CD235a- CD36lo CD45RA+	1.942988443	0.034318267
CD117+ CD123+ CD34+ CD71+	1.506950682	0.034606909
CD117+ CD38+	1.367833291	0.03624554
CD34- CD36- CD38+	2.217660354	0.03624554

CD117+ CD36lo CD38+ CD71+	1.882729378	0.036964803
CD123+ CD36lo CD71-	1.306104029	0.038056128
CD117+ CD235a- CD36- CD45RA+	1.727856868	0.038056128
CD123+	1.01407299	0.038141191
CD36lo	1.088420266	0.039628627
CD117+ CD38+ CD45RA+ CD71+	1.296671901	0.041382437
CD34+ CD71-	1.29931619	0.041382437
CD123+ CD235a+ CD45RA+ CD71+	1.368995023	0.041382437
CD117+ CD123+ CD71+	1.468879417	0.041382437
CD36- CD38+ CD45RA+ CD71+	1.731075573	0.041382437
CD117+ CD34- CD45RA+	1.855595825	0.041382437
CD123+ CD71-	1.249028359	0.041539258
CD71-	1.130962136	0.042454287
CD117+ CD123+ CD235a+ CD34+ CD36- CD38+ CD45RA+ CD71+	1.578437851	0.042454287
CD34- CD38+ CD71+	2.490096029	0.043667741
CD38+	1.277308649	0.043784112
CD123+ CD36lo CD38+	1.578960511	0.043823071
CD235a-	1.219792524	0.044528442
CD117+ CD123+ CD235a- CD45RA+	1.654594197	0.044528442
CD123+ CD235a+ CD34+ CD45RA+ CD71+	1.428613685	0.044983013
CD123+ CD235a+ CD34+ CD45RA+	1.232751363	0.045322654
CD117+ CD235a+ CD36- CD38+ CD45RA+ CD71+	1.592963585	0.045572809
CD123+ CD34+ CD36- CD45RA+ CD71+	1.669095408	0.045572809
CD117- CD235a+ CD36- CD38+ CD45RA+ CD71+	1.836492088	0.045572809
CD123+ CD36lo	0.977073229	0.045705551
CD36lo CD71-	1.230438919	0.045705551
CD123+ CD235a- CD71+	1.624765909	0.045705551
CD123+ CD235a+ CD45RA+	1.137180858	0.047381762
CD117+ CD36- CD45RA+	1.286272205	0.047381762
CD34- CD38+	2.047977524	0.049929175

E. Methods

Cell Culture

Cryopreserved primary human adult G-CSF-mobilized CD34+ cells were purchased from Fred Hutchinson Cancer Research Center. Cells were thawed and expanded 2-3 days in medium composed of IMDM (GIBCO BRL) supplemented with BIT 9500 (Stem Cell Technologies), and the following cytokines: 100 ng/ml each of rhTPO, rhSCF, and rhFlt3-l, plus 10 ng/ml rhIL-3 (all from PeproTech). After expansion, cells were moved into unilineage media, and cultured from 1-8 days. Erythroid medium is composed of IMDM supplemented with BIT 9500, and the following cytokines: 4.5 U/ml rhEPO (Procrit, Janssen) and 25 ng/ml rhSCF (PeproTech). Megakaryocyte medium is composed of IMDM supplemented with BIT 9500, and the following cytokines: 40 ng/ml rhTPO, 25 ng/ml rhSCF, and 20 ng/ml rhSDF1-alpha (PeproTech). Megakaryocyte cultures utilized fibronectin-coated plates, which were prepared by incubating plates at room temperature for one hour with IMDM containing 20 µg/ml fibronectin (Becton Dickinson). Granulocyte medium is composed of IMDM supplemented with BIT 9500, and the following cytokines: 25 ng/ml rhSCF, 10 ng/ml rhIL-3, and 20 ng/ml rhG-CSF (PeproTech). For colony formation assays, 3,000 undifferentiated CD34+ cells were seeded into MethoCult SF H4236 (Stem Cell Technologies) supplemented with the following cytokines: 50 ng/ml rhSCF, 10 ng/ml rhIL-3, 20 ng/ml rhIL-6 (PeproTech), 3 U/ml rhEPO, 20 ng/ml rhG-CSF, and 10 ng/ml rhGM-CSF. Cells were cultured for 10 days, followed by colony scoring and counting.

HUDEP-2 cells (Kurita, et al. 2013) were maintained in expansion medium composed of StemSpan (Stem Cell Technologies) supplemented with 50 ng/ml rhSCF, 3 U/ml rhEPO, 1 μ M dexamethasone (Sigma-Aldrich), and 1 μ g/ml doxycycline (Sigma-Aldrich). HUDEP-2 differentiation induction was achieved by culturing the cells for 48 hours in doxycycline-free medium. HEK293T cells (ATCC) were grown in DMEM (GIBCO BRL) supplemented with 2 mM L-glutamine, antibiotic-antimycotic (Thermo Fisher Scientific), and 10% FBS (GIBCO BRL).

Transfection and Transduction

For production of lentivirus, pCMV-dR8.74 (GAG POL TAT REV) and pMD2.G (VSV-G) were co-transfected into HEK293T with pLKO.1 shRNA vectors at a 3:1:4 mass ratio using the Clontech CalPhos mammalian transfection kit (Clontech 631312). pLKO.1 shRNA plasmids were purchased from GE Dharmacon. After 12-16 hours, the transfection medium was replaced with Opti-MEM I (Thermo Fisher Scientific), and viral supernatant was collected 36 hours later, passed through a 0.45 μ m filter, and stored at -80°C. HUDEP-2 cells were transduced via incubation for 24 hours in a 1:1 mixture of viral supernatant and StemSpan, supplemented with 50 ng/ml rhSCF, 3 U/ml rhEPO, 1 μ M dexamethasone, and 1 μ g/ml doxycycline. Transduced cells were selected by adding 2 μ g/ml puromycin (Sigma Aldrich) for 72 hours. CD34⁺ cells, pre-expanded for 2 days, were transduced over two additional days in a 1:1 combination of viral supernatant and IMDM, supplemented with 100 ng/ml each of rhTPO, rhSCF, and rhFlt3-l, plus 10 ng/ml rhIL-3. These cultures were seeded onto retronectin-coated plates, prepared by pre-treatment with 40

$\mu\text{g/ml}$ retronectin (Takara) in PBS at room temperature for 2 hours, followed by incubation with 2% Fraction V BSA (Sigma Aldrich) in PBS, and then a wash with 2.5% wt/wt HEPES in HBSS (GIBCO BRL). The transduction cultures were incubated at 37°C for 2 hours, spun at 500 rcf for 90 minutes at room temperature, then incubated at 37°C overnight. The spin procedure was repeated the following day with fresh viral medium. Cells were selected on the third day with 2 $\mu\text{g/ml}$ puromycin until we observed total cell death in un-transduced control cells (a minimum of 24 hours), followed by unilineage cultures as described above.

Fluorescence Cytometry

Cells were washed once with PBS, followed by staining for 30 minutes on ice with PBS containing 1:500 Zombie Violet viability dye (BioLegend), and 3 μl fluorochrome-conjugated antibody per sample. After staining, cells were washed once with PBS, followed by fixation for 20 minutes on ice using IC Fixation Buffer (eBioscience). After fixation, cells were washed once with PBS with 1% FBS, and re-suspended in PBS with 1% FBS. Cells were analyzed on a BD FACSCalibur, and data was analyzed using FlowJo version 8.8.7. For cell sorting, cells were stained as described above, re-suspended in 1% Fraction V BSA in PBS, and sorted into the serum-free expansion medium using a BD FACSAria Fusion. The PKH26 membrane staining was performed according to the manufacturer's protocol, and cells were cultured for 3 days before analysis.

Table of antibodies used in fluorescence cytometry

Reagent	Source	Identifier
CD235a (FITC)	Invitrogen	11-9987-82
CD235a (PE)	BD Pharmingen	555570
CD41a (APC)	BD Pharmingen	559777
CD15 (FITC)	BioLegend	301903
CD36 (APC)	BD Biosciences	561822
CD71 (APC)	BD Pharmingen	551374

Immunoblot

For lysis, cells were washed once with PBS, followed by resuspension in Laemmli buffer (60 mM Tris-HCl, pH 6.8, 2% SDS, 100 μ M dithiothreitol, 10% glycerol, and 0.01% bromophenol blue) supplemented with cOmplete protease inhibitor cocktail (Roche Diagnostics 11836170001) and PhosSTOP phosphatase inhibitor cocktail (Roche Diagnostics 04906845001). Samples were passed through 27G needles to shear DNA, followed by 5-10 minutes incubation at 95°C. After SDS-polyacrylamide gel electrophoresis and Western transfer, nitrocellulose or PVDF membranes were blocked with 5% non-fat dried milk in Tris-buffered saline (50 mM Tris and 150 mM NaCl) with 0.1% Tween-20. For protein detection, primary antibodies (Cell Signaling Technologies; RUNX1 – 4334S; RUNX2 – 12556S; RUNX3 – 9647S) were applied overnight at a dilution of 1:1000 at 4°C with shaking. HRP-conjugated secondary antibodies were applied for one hour at a dilution of 1:10,000 at room temperature with shaking. All antibodies were diluted in TBS with Tween-20 and 1% non-fat dried milk. HRP substrates consisted of Super Signal West Pico and Super Signal West Femto (Thermo Fisher Scientific). Immunoblot signal quantitation was performed using a BioRad GS-800 scanning densitometer.

Immunofluorescence

10^5 cells were cytopun onto glass slides, fixed for 15 minutes at room temperature with 4% paraformaldehyde, and permeabilized for one hour at room temperature with PBS containing 2% FBS, 2% BSA, and 0.03% Triton X-100. Mouse anti-human RUNX3 primary antibody (R&D Systems) was applied overnight at 20 $\mu\text{g}/\text{ml}$ in staining buffer (PBS with 2% FBS, 2% BSA, and 0.03% Triton X-100) at 4°C. Goat anti-mouse Alexa Fluor 546 secondary antibody (Thermo Fisher) was applied at 1:300 in staining buffer at room temperature for one hour. The slides were washed three times with staining buffer and once with PBS before mounting coverslips with Vectashield medium (Vector Laboratories H-1000). Images were obtained with a Zeiss LSM-700 confocal microscope using the 63x objective, and image processing was performed with Fiji ImageJ v2 (National Institutes of Health).

Immunohistochemistry

Immunohistochemistry was performed using a robotic platform (Ventana discover Ultra Staining Module, Ventana Co., Tucson, AZ, USA) on paraffin-embedded bone marrow clots of young (<10 years old) and aged (60-70 years old) subjects obtained according to IRB-reviewed protocols. A heat-induced antigen retrieval protocol was carried out using a TRIS–ethylenediamine tetracetic acid (EDTA)–boric acid pH 8.4 buffer (Cell Conditioner 1), with a 64 minute setting. Endogenous peroxidases were blocked with peroxidase inhibitor (CM1) for 8 min before incubating the tissues with RUNX3 antibody (Abcam, Cat # Ab 135248) at a 1:800 dilution for 60 min at room temperature. Antigen-antibody complex was then

detected using DISCOVERY anti-mouse HQ HRP detection system and DISCOVERY ChromoMap DAB Kit (Ventana Co.). All the slides were counterstained with hematoxylin subsequently; they were dehydrated, cleared and mounted for the assessment. Slides were imaged using a NonoZoomer S360 (Hamamatsu Corporation) and the final images were prepared using NDP.view2 Plus Image viewing software U12388-02.

Mass Cytometry

Cells were washed once with PBS, then stained for 60 seconds with 100 μ M cisplatin (Sigma Aldrich P4394) in PBS. 1% FBS in PBS was promptly added to quench the staining. After washing, cells were fixed with 0.2 μ m filtered 1.6% paraformaldehyde in PBS for 10 minutes at room temperature. 1% FBS in PBS was promptly added to quench fixing, and after washing, cells were stored at -80°C. Upon thawing, each sample was washed once with cell staining medium consisting of 0.5% Fraction V BSA (Sigma Aldrich), and 0.02% w/v sodium azide (Sigma Aldrich S2002) in PBS. Subsequently, cells were washed twice with 0.02% w/v saponin (Sigma Aldrich S7900) and 0.02% w/v sodium azide in PBS to transiently permeabilize them. Each sample was then separately stained with a unique barcoding combination of palladium isotopes, shaking at room temperature for 15 minutes followed by washing three times with cell staining medium. The barcoded samples were pooled and simultaneously stained for surface antigens for 30 minutes at room temperature with shaking. Antibodies to CD45RA, CD11b, CD117, CD36, and CD71 were used at a dilution of 1:800. Antibodies to CD34, CD38, CD123,

CD41, and CD235a were used at 1:400. Cells were washed twice with cell staining medium, then permeabilized in -20°C methanol for 10 minutes on ice with intermittent shaking. Cells were washed once with cell staining medium, followed by intracellular staining for 1 hour at room temperature with shaking. The Ki-67 antibody was used at 1:400, and antibodies to RUNX3 and cleaved Caspase-3 were used at $0.25\ \mu\text{g}/\text{ml}$. After staining, cells were washed twice with cell staining medium, then incubated for at least 15 minutes at room temperature in intercalator buffer consisting of $0.2\ \mu\text{m}$ filtered PBS/1.6% paraformaldehyde with a 1:5,000 dilution of CellID Ir-Intercalator (Fluidigm 201192A). Cells were washed once with cell staining medium, once with 0.05% Tween-20 (Sigma Aldrich) in water, and finally re-suspended in water. The sample volume was adjusted with water and normalization beads (Fluidigm 201078) to achieve a cell concentration of approximately $0.5 \times 10^6/\text{mL}$. Data acquired using the Fluidigm CyTOF 2 was bead-normalized and underwent barcode deconvolution using the debarcoding tool MATLAB standalone executable from Zunder et al. Nature Protocols 2015.

Data was inverse hyperbolic sine-transformed using a cofactor of 0.25. FlowSOM (Van Gassen et al. 2017) was used to construct a self-organizing map with a number of grid points equal to the square of the number of lineage markers. Each cell was assigned a phenocode for every lineage marker using flowType (Aghaeepour et al. 2014). Each grid point was then immunophenotyped using the aggregated phenocodes of the cells assigned to the grid point. For any given grid point to be assigned an immunophenotype for a particular marker (i.e. CD45RA+), 75 percent of the cells assigned to the gridpoint had to be labelled with

the same phenocode for the particular marker. For each immunophenotype observed, number of cells were tabulated to form a hierarchical count table. Every level of the hierarchy was tested for differential abundance between conditions using edgeR (Robinson et al. 2010; McCarthy et al. 2012) with a quasi-likelihood framework as specified by the cydar™ package (Lun 2017).

Table of antibodies used for mass cytometry

CD41a (89 Yb)	Fluidigm	3089004B
CD117 (143 Nd)	Fluidigm	3143001B
CD123 (151 Eu)	Fluidigm	3151001B
CD45RA (153 Eu)	Fluidigm	3153001B
CD36 (155 Gd)	Fluidigm	3155012B
Ki-67 (162 Dy)	Fluidigm	3162012B
CD235a (163 Dy)	Fluidigm	3163008B
CD34 (166 Er)	Fluidigm	3166012B
CD38 (172 Yb)	Fluidigm	3172007B
CD71 (175 Lu)	Fluidigm	3175011B
CD11b (209 Bi)	Fluidigm	3209003B
RUNX3 (148 Nd)	This study	R&D Systems RUNX3 antibody (MAB3765); Fluidigm Maxpar X8 antibody labeling kit (201148)
Cleaved Caspase-3 (173 Yb)	This study	BD Biosciences cleaved Caspase-3 antibody (559565); Fluidigm Maxpar X8 antibody labeling kit (201173)

RNA-sequencing

Cells were washed with PBS, followed by RNA extraction using the QIAgen RNeasy Plus Mini Kit (QIAgen 74134), with added DNA digestion. Briefly, cells were lysed using buffer RLT supplemented with beta-mercaptoethanol, and lysates were applied to the gDNA eliminator column. The flow-through was applied to the RNeasy spin column, and the column was washed once with buffer RW1. Freshly

prepared DNase solution (QIAGEN 79254) was applied to the column and incubated at room temperature for 10 minutes. The column was washed once with buffer RW1, and twice with buffer RPE. RNA was eluted with nuclease-free water, and the eluate was re-applied to the column for a second spin to ensure complete elution of the RNA. RNA yield was assessed using a NanoDrop spectrophotometer (Thermo Fisher Scientific). Samples were sequenced by the Genomic Services Laboratory at HudsonAlpha Institute for Biotechnology using ribosomal reduction, 100bp, paired-end, and 50 million read-depth parameters on an Illumina HiSeq 2500 machine.

Raw fastq.gz data files were merged (fastq Merger; gsl.hudsonalpha.org) and uploaded to usegalaxy.org. Trimmomatic was used to eliminate low quality sequences from the reads, followed by alignment to the hg19 human reference genome using HISAT2. RmDup was used to eliminate PCR duplicates from the resulting bam files. Differential gene expression was determined with DESeq2 applied to data converted by featureCounts. The data was also processed using Cufflinks to estimate FPKM for each sample, followed by Student's t-test to assess statistical significance for specific transcripts. The Synergizer tool was used to convert UCSC gene identifiers into hgnc gene symbols.

Unexplained Anemia of the Elderly Studies

Normal young, normal elderly, and UAE human bone marrow samples were obtained according to IRB-approved protocols. Mononuclear cells were prepared using Ficoll-Paque Plus (GE Healthcare), and stained with the appropriate antibodies and analyzed and sorted using a FACSAriaII cytometer (BD Biosciences).

Cell types were defined as follows: HSC, Lin-CD34+CD38-CD90+ CD45RA-; MEP, Lin-CD34+CD38+CD123-CD45RA-; CMP, Lin-CD34+CD38+CD123+CD45RA-.

Methylcellulose colony formation was assayed by sorting cells into individual wells of a 6-well plate, each containing 3 ml of complete methylcellulose (Methocult GF+H4435, Stemcell Technologies). Plates were incubated for 12-14 days at 37°C, and colonies then scored based on morphology.

For microarray analysis, total RNA was extracted using TRIzol (Invitrogen) or Ambion RNA Isolation Kit (Applied Biosystems by Life Technologies) according to the manufacturer's protocols and treated with DNase I (Qiagen). All RNA samples were quantified with the RiboGreen RNA Quantitation Kit (Molecular Probes), subjected to reverse transcription, two consecutive rounds of linear amplification, and production and fragmentation of biotinylated cRNA (Affymetrix). Fifteen micrograms of cRNA from each sample was hybridized to Affymetrix HG U133 Plus 2.0 microarrays. Hybridization and scanning were performed according to the manufacturer's instructions (Affymetrix). Data was analyzed using the gene expression commons platform (Seita J, Sahoo D, Rossi DJ, Bhattacharya D, Serwold T, Inlay MA, Ehrlich LI, Fathman JW, Dill DL, Weissman IL. *PLoS One*. 2012;7(7):e40321. doi: 10.1371/journal.pone.0040321. PMID: 22815738).

Data Availability

RNA-sequencing accession numbers: GSE119264, GSE104406. Microarray accession number: GSE123991.

III. Discussion and Future Directions

A. Discrepancies between *in vivo* and *in vitro* models of RUNX3 deficiency

The murine model of RUNX3 deficiency described by Wang *et al.*¹³⁵ caused diminished bone marrow erythroid content that failed to translate into diminished red cell counts in the circulation, yet the *in vitro* approach described in this study elicited a robust blockade in erythropoiesis even with an incomplete knock-down. This raises questions as to the mechanisms by which RUNX3 mediates erythropoiesis and whether differences between the models could color the interpretation of the results. Wang *et al.* used the Mx1-Cre system to target RUNX3 in the bone marrow. In this system, poly I:C is injected into the animals to invoke a strong inflammatory response leading to interferon-dependent activation of an Mx1 promoter upstream of the Cre recombinase gene in a transgenic locus¹⁵⁹. The caveats to this system are that 1) the Mx1 promoter is active in the whole bone marrow niche, not just the hematopoietic stem cells, 2) baseline inflammation can cause leaky expression of Cre recombinase, and 3) poly I:C can imbue long lasting effects on the proliferative state of hematopoietic stem cells^{160,161}. These issues can be partially circumvented by purifying cell types of interest from the Mx1-cre knock-out animals and transplanting them into wild type recipients that have a relatively unperturbed bone marrow niche.

In the Wang *et al.* study, most of the data reported were measurements from the primary mice at young and old time-points after injection with poly I:C.

Relevant findings included 1) diminished frequency of erythroid cells in the bone marrow, but no change in peripheral red blood cells, 2) increased frequency of LSK progenitors, and 3) increased mobilization of LSK progenitors after treatment with

G-CSF. The analysis of bone marrow transplant recipients consisted only of measuring the engraftment of myeloid, B-cells, and T-cells using the percent of peripheral blood cell types contributed by donor CD45 isoform-positive marrow cells. An analysis of the aged bone marrow composition including erythroid progenitors and their contribution to circulating red blood cells was not included in the Wang *et al.* study. Thus, it remains unclear to what degree the Mx1-Cre system affected the phenotypes observed in primary mice and what the effect of RUNX3 deficiency is on erythropoiesis *in vivo*.

To determine the effect of Mx-Cre-mediated RUNX3 knock-out on erythropoiesis, specific subsets of donor marrow (such as LSKs) need to be evaluated after transplantation. In such an experiment, equal number of LSKs should be sorted from aged Mx1-Cre/RUNX3-floxed animals that were treated with or without poly I:C when young. These cells should be transplanted into lethally irradiated wild type animals along with equal numbers of wild type competitor bone marrow cells. After recovery, the recipient bone marrow and peripheral blood composition can be assessed. Engraftment efficiency can be defined by the percentage of donor CD45 isoform-positive cells in the bone marrow relative to total bone marrow, or in circulation relative to total peripheral blood. Biological changes in the bone marrow compartment that are due to RUNX3 deficiency could be measured by taking the percent of a donor cell type (such as MEP) relative to total donor cells in the marrow or peripheral blood. Erythroid perturbations that would validate our *in vitro* knock-down data might include diminished erythroid

progenitors and increased myeloid progenitors in the bone marrow, as well as fewer red blood cells and more myeloid cells in the peripheral blood.

In some instances, such as aging studies, the SCL-Cre system may be a better alternative to Mx1-Cre because SCL promoter activity is more restricted to early hematopoietic progenitors in the bone marrow than Mx1-Cre¹⁶². While Mx1-Cre induces pan-hematopoietic recombination, SCL-Cre specifically targets LT-HSCs (defined as LSK, Flk-2-) at greater than 90% efficiency, which accounts for roughly 20% of LSK cells¹⁶². In primary animals, the high specificity for LT-HSCs offers another added benefit over Mx-Cre in that the incorporation of a fluorescent reporter cassette allows one to observe the native contribution of LT-HSCs to the bone marrow progenitor pool.

In this study, mass cytometry was employed to evaluate how the distribution of the HSPC subtypes was affected by RUNX3 deficiency. The frequency of CMPs were found to be increased at the expense of MEPs, with minimal effect on GMPs. But, because all CD34+ cells simultaneously underwent knock-down in that experiment, it was impossible to discern whether the change in distribution of CMPs and MEPs was due to a defect in one or both of those subsets. In other words, RUNX3 deficiency could have conceivably blocked the differentiation of CMPs into MEPs, but it could have also affected the proliferation or viability of one or both subpopulations. Both outcomes could explain the phenotype observed, but the SCL-Cre system with lineage tracing capability may shed additional light on whether HSC differentiation is in fact blocked at specific subsets of cells in the hematopoietic hierarchy.

However, the SCL-Cre system also relies on inducible signaling that has potentially confounding effects on HSCs. In this system, the transgenic SCL promoter drives the expression of a Cre recombinase that is fused to a part of the estrogen receptor (Cre-ER). Cre-ER remains in the cytosol until the synthetic estrogen receptor agonist, tamoxifen, is administered. Binding of tamoxifen to Cre-ER induces its nuclear translocation and subsequent Cre-mediated recombination of the target site¹⁶³. But, in addition to inducing Cre translocation, tamoxifen will also bind to the endogenous estrogen receptors expressed in HSPCs and modulate the cells' biology. Specifically, tamoxifen induces rapid apoptosis of ST-HSCs and MPPs while inducing the proliferation of LT-HSCs. While these changes appear to be reversible by withdrawal of tamoxifen, the total bone marrow cellularity does not change after the initial treatment, suggesting that HSPCs may experience accelerated differentiation¹⁶⁴. These effects may represent long lasting changes in HSPC biology that may affect our interpretation of data collected from these experiments.

The *in vitro* system used in the current study differs from the murine system in several substantial ways. First, RUNX3 was only partially knocked down compared to the more robust knock-out described in the Wang *et al.* study, which may lead to “dosing” effects as previously described for some RUNX family transcription factors^{119,165}. Second, CD34+ HSPC are a similar, but not fully matched cell population to the KSLs that were scrutinized in the murine system. Third, cell culture of hematopoietic cells has known effects on the biology and differentiation potential of HSPCs, especially considering the lack of supporting niche or stromal

cells, as well as the non-physiological cytokine milieu present in the culture media^{30,166}. Lastly, the time it takes to transduce, culture, and analyze cells *in vitro* is significantly shorter than the workflow required for a well-controlled *in vivo* experiment.

To best address some of these discrepancies between systems, human CD34+ HSPCs transduced with either control or RUNX3-targeting vectors with a fluorescent reporter could be transplanted into NOD/SCID immunodeficient animals and monitored for progenitor and multi-lineage engraftment. This strategy may offer a more accurate comparison to what is happening when murine HSPC are transplanted into recipient animals. While it is unclear whether this approach is suitable for aging studies, it may reveal effects of the bone marrow niche as well as the extended kinetics of engraftment on the lineage potential of the donor progenitors. Similarly, *ex vivo* erythroid cell culture of mouse HSPC subjected to Cre-mediated deletion of RUNX3 could also reveal potential effects of the bone marrow niche on lineage potential.

One conceivable weakness of cell culture-based and inducible Cre systems is the potential to impart lasting effects on HSC behavior due to off-target cell cycle alterations. Previous reports have described cell-intrinsic alterations in HSPC potency after repeated rounds of cell division^{25,75,76}. One such study postulates that stem cell aging is directly correlated with the number of cell divisions that any given cell undergoes, requiring as few as four cell divisions to render the cell dormant¹⁶⁷. After Cre induction, cells of interest experience additional cell cycle-related stress inherent to transplantation, as small numbers of donor cells and inefficient

engraftment elicit enhanced cell cycle entry of HSCs. The use of appropriate controls within any given system does account for these changes, and does allow for meaningful comparisons to be made; however, it remains incompletely understood to what degree these systems impact normal biology.

A prospective strategy for studying HSC biology in the most native manner possible is *in vivo* transduction. This approach uses G-CSF to mobilize HSPCs followed by infusion of a lentivirus with targeting and selection constructs into the circulation. Once the HSPCs re-enter the bone marrow, a selection drug can be administered to eliminate un-transduced cells from the bone marrow. There are several advantages to this approach over *ex vivo* or Cre-based systems. First, recent studies have shown that treatment with G-CSF mobilizes a long-lived subset of quiescent HSPCs that do not become stimulated to proliferate, in contrast to the general increase in proliferation observed in the bone marrow as has been previously described¹⁶⁷. Second, lentiviral transduction does not significantly alter the biology of HSPCs even after sustained engraftment¹⁶⁸. Third, the need for transplantation is potentially eliminated as the system can be engineered to target cells with some degree of specificity to surface antigens, such as for CD46 which is highly expressed in HSCs¹⁶⁹. The current efficiency of this system is modest, but workable with fluorescent labeling of target cells. Use of this approach in standard mouse models currently yields approximately 50% efficiency in LSKs and 70% efficiency in Ter-119-positive erythrocytes.

B. Potential RUNX factor compensation

The RUNX family proteins all carry out their function by binding to chromatin. Each of the three RUNX proteins heterodimerize with their cognate binding partner, CBF β . This causes a change in the conformation of the RUNX protein which makes DNA-binding more favorable^{103,104}. For RUNX1, it has been demonstrated that the wild type protein without CBF β and the Runt domain N109A mutant that is unable to bind CBF β both have greatly reduced affinity for RUNX DNA binding motif-containing oligonucleotides in biochemical assays¹⁰¹. Extrapolating from this finding, it is thought that all RUNX proteins should be able to bind any given RUNX DNA binding motif across the chromatin. This begs the question of whether or not RUNX factors are able to compensate for the loss of other RUNX factors, especially between RUNX1 and RUNX3 which are co-expressed in hematopoietic tissues.

Indeed, ectopic expression of RUNX2 or RUNX3 in RUNX1-deficient murine embryonic para-aortic splanchnopleural cells restores the cells' normal hematopoietic function¹⁷⁰. Knock-down of RUNX3 in zebrafish embryos phenocopies RUNX1 deficiency which is characterized by severe anemia as a consequence of a failure to establish definitive hematopoiesis¹³³. In mice, loss of RUNX3 elicits a synthetic phenotype in conjunction with the loss of RUNX1. Specifically, the double knock-out has a more severe bone marrow failure phenotype than RUNX1 single knock-out, as well as severe anemia which is not observed in either RUNX1 or RUNX3 single knock-out. Interestingly, this model also provided evidence that RUNX1 and RUNX3 have non-overlapping roles as well. A

subset of the double knock-out mice developed myeloproliferative disorder as was observed in the RUNX3 single knock-out, but not the RUNX1 single knock-out. RUNX1 and RUNX3 are also both required in a double-stranded DNA damage repair pathway¹⁰⁵. Furthermore, RUNX1 has been reported to suppress erythroid differentiation, while data in the current study show RUNX3 to promote it¹⁵⁶. Thus, it is unlikely that RUNX1 can fully compensate for the loss of RUNX3.

To determine to what degree RUNX1 can compensate for RUNX3 deficiency in HSPCs, the chromatin binding profiles of RUNX1 and RUNX3 must be determined via chromatin immuno-precipitation followed by DNA sequencing (ChIP-seq). First, the binding profiles of RUNX1 and RUNX3 in control cells could be compared to define peaks that are unique to RUNX3. The peaks that are unique to RUNX3 can then be compared to RUNX1 peaks observed in RUNX3-deficient cells to determine the extent to which RUNX1 is re-localized to sites previously occupied by RUNX3. The expression of genes associated with RUNX1 peaks that were gained after loss of RUNX3 should be evaluated in order to discern whether RUNX1 binding elicits similar function as RUNX3 binding.

The degree to which RUNX1 could compensate for RUNX3 deficiency should be the same *in vitro* and *in vivo*, and would not explain the differences in the data between the two models. However, the kinetics of RUNX1 redistribution after loss of RUNX3 may differ between the two systems. Cytokine signaling and cell proliferation critically influence transcription factor occupancy across the chromatin, and both are substantially different between the two models. The current study utilized a cell culture system in which HSPC expansion, transduction,

selection, and differentiation were performed over just 8-9 days. By contrast, typical inducible Cre-based systems require 1-2 weeks for the administration of the reagents and up to one month for the recovery of animals. Primary animals can be studied at this point, but transplantation and aging studies tend to add up to two years to the experimental design. Thus, it is possible that accelerated cell proliferation alters the kinetics of RUNX1 redistribution in the cell culture system as compared to the animal model.

To test whether the temporal differences between models could explain the differences in data, the CHIP-seq experiment should be performed on young mice as close to RUNX3 deletion as possible, as well as aged mice. If there are differences in the kinetics of RUNX1 distribution between the *in vitro* and *in vivo* systems, then the binding profile of RUNX1 in young animals would differ from the aged animals and the cell culture system. An alternative strategy could be to rapidly degrade RUNX1 by way of the dTAG protein degradation system, and determine any immediate changes in RUNX3 chromatin occupancy that may be induced as a result of RUNX1 deficiency¹⁷¹. For *in vivo* studies, a bone marrow population of interest, such as LSK, would be subjected to CRISPR-mediated knock-in of the FKPBF^{F36V} fusion fragment, which would generate RUNX1 fusion proteins that can be degraded upon treatment with the dTAG reagent. These cells can then be transplanted into recipient mice, and after engraftment treated with the dTAG reagent to induce rapid loss of RUNX1 *in vivo*.

C. Identification of direct RUNX3 targets

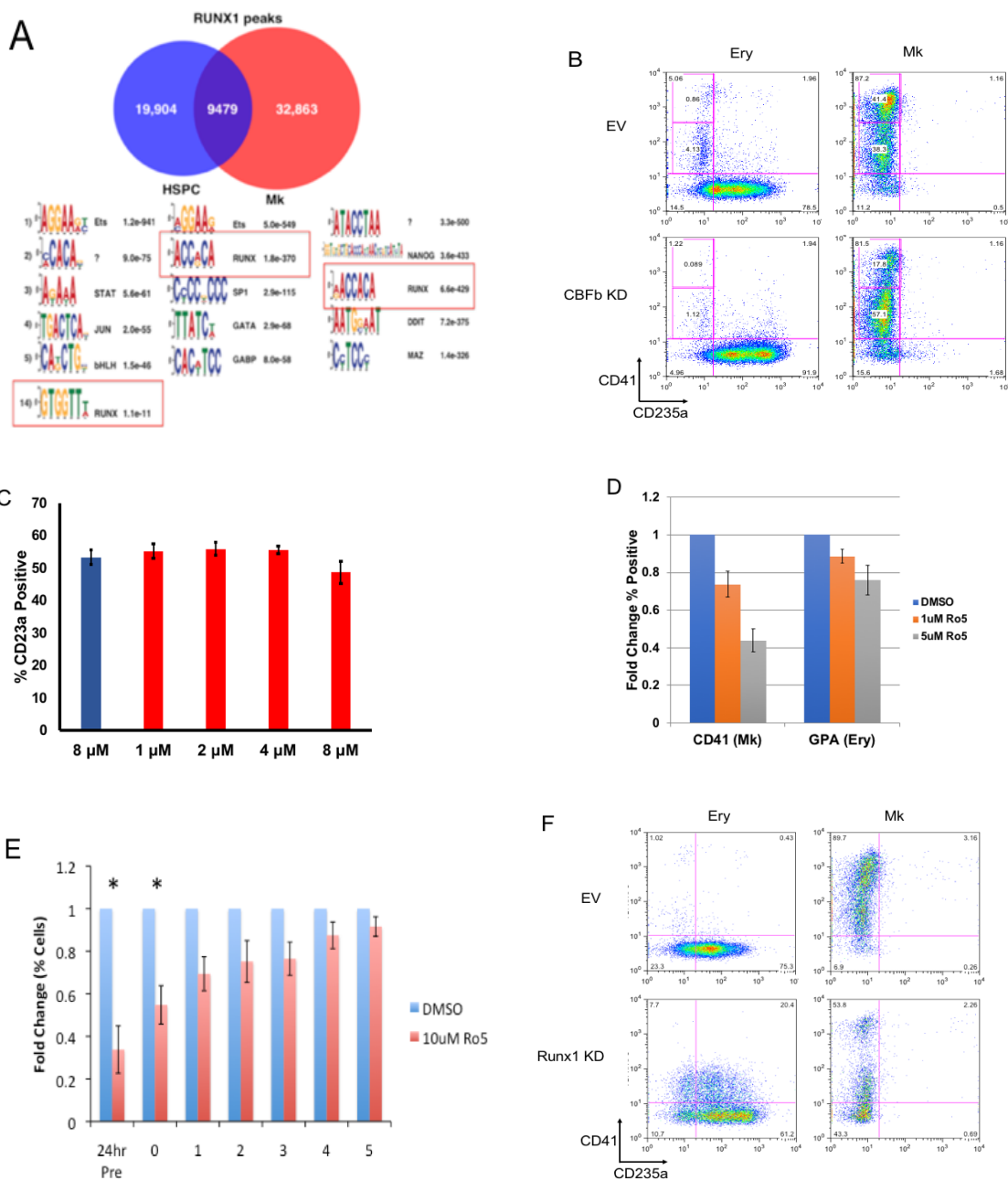
The RNA sequencing data described in the current study shows global gene expression changes in the context of RUNX3 deficiency. However, this dataset does not discriminate between genes that are directly regulated by RUNX3, and those that are regulated by its downstream targets. Because RUNX proteins are thought to carry out their function through chromatin binding, ChIP-seq can be used to identify RUNX3 targets. This strategy has been used in other studies to determine the global chromatin binding profile of RUNX1 in human CD34+ HSPCs. Interestingly, our analysis of those data revealed an unexpected distribution of motif enrichment among RUNX1 peaks in undifferentiated CD34+ HSPCs. In these cells, RUNX1 binds with highest frequency to the Ets family transcription factor DNA motif, while the RUNX motif is only the fourteenth most represented binding site [Supplementary Figure 1A]. This implies that the vast majority of RUNX1 function is not carried out according to RUNX dogma – the assumption that RUNX proteins function by binding their own cognate DNA motif. Although it is not known if all of the ChIP-seq peaks represent sites where RUNX1 is actually functional, prior studies have shown that RUNX1 and RUNX3 carry out DNA repair functions in a CBF β -independent manner¹⁰⁵. This indicates that RUNX localization, including that of RUNX3, to alternate DNA binding motifs could occur indirectly through binding to other factors and may be functional.

What remains to be shown is whether RUNX proteins always require their canonical DNA-binding partner CBF β to regulate gene expression, or if they can be localized to target sites by binding to other factors alone. In the context of

erythropoiesis, the role of CBF β is further obfuscated by the fact that it is rapidly down-regulated during early differentiation¹⁷². To address this concern, CBF β was knocked down in undifferentiated CD34+ HSPCs and induced to differentiate down the erythroid lineage. As expected based on the lack of CBF β expression in the erythroblasts, erythroid differentiation was not blocked in the context of CBF β deficiency [Supplementary Figure 1B]. Additionally, cells treated with small molecule inhibitors of CBF β and RUNX1 showed minimal perturbation of erythropoiesis^{123,124} [Supplementary Figure 1C-D]. But, because RUNX3 deficiency does block erythropoiesis, these results indicate that the erythroid-specific function of RUNX3 does not utilize CBF β .

ChIP-seq could be performed on undifferentiated CD34+ HSPCs and early erythroblasts for both RUNX3 and CBF β to identify putative targets that are regulated by either RUNX3 alone or the two factors together. To determine whether CBF β is required for RUNX3 binding to loci harboring both RUNX3 and CBF β peaks, one could perform ChIP-seq on cells expressing either wild type RUNX3 or a RUNX3 mutant with the N109A substitution that was previously shown to disallow RUNX1/CBF β dimerization¹⁰¹. With respect to the binding profile of the RUNX3 mutant, peaks that are lost from the set of genes bound by both wild type RUNX3 and CBF β would presumably require CBF β /RUNX3 dimerization for binding to a RUNX3 DNA motif. To test this hypothesis, the sequences obtained from the various RUNX3 ChIP-seq experiments can be analyzed using motif-discovery algorithms to identify DNA motifs associated with any given RUNX3 binding site.

In this study, we also showed that loss of RUNX3 blocks megakaryocyte differentiation. RUNX3-deficient cells in erythroid medium experienced down-regulation of several megakaryocyte-specific genes, suggesting a partial overlap in RUNX3-dependent erythroid and megakaryocyte lineage programming. Interestingly, manipulation of the RUNX factors elicits different results in megakaryocytes than it does in erythroblasts. While RUNX1 is dispensable for erythropoiesis, it is required for megakaryopoiesis, which we validated using our own cell culture system¹⁷³⁻¹⁷⁵ [Supplementary Figure 1B]. Similarly, while CBF β is not required for erythropoiesis, we found it to be required for megakaryopoiesis although knock-down of CBF β blocked maturation while treatment with the RUNX1 inhibitor Ro5-3335 appeared to block differentiation [Supplementary Figure 1 B, D-E]. This suggests that RUNX1 may not require CBF β to carry out functions related to lineage commitment, but that the two factors must cooperate during maturation. Further, these findings indicate that the erythroid and megakaryocyte lineages have different requirements for CBF β . Thus, identifying target genes in megakaryocytes using the above ChIP-seq strategy could reveal how lineage-specific programming is achieved between erythroblasts and megakaryocytes.



Supplementary Figure 1. Megakaryocyte and erythroid phenotypes with CBF β and RUNX1 inhibition

(A) RUNX1 ChIP-seq peaks in CD34+ HSPCs and megakaryocytes. DNA binding motifs are listed for those shared between undifferentiated HSPC and megakaryocytes (center column) and those unique to HSPC (left) or megakaryocyte (right); (B) Knock-down of CBF β permits erythroid differentiation and inhibits terminal megakaryocyte maturation; (C) Inhibition of CBF β permits erythroid differentiation (blue: control molecule AI-4-88, red: AI-14-91); (D) Inhibition of RUNX1 with Ro5-3335 inhibitor selectively impairs megakaryocyte differentiation; (E) RUNX1 inhibition preferentially impairs early megakaryocyte commitment; (F) Knock-down of RUNX1 impairs megakaryocyte differentiation, but has no effect on erythropoiesis.

D. Mechanism and implication of RUNX3's sub-cellular localization

In this study, we observed by immunofluorescent microscopy that undifferentiated HSPCs in expansion medium had RUNX3 distributed between the cytoplasm and in the nucleus, while cells cultured in erythroid medium for three days had predominantly nuclear staining. Erythroid medium contains erythropoietin (EPO) which binds the EPO receptor and requires JAK2 and STAT5 to propagate its signals¹⁷⁶. RUNX3 and STAT5 have been shown to interact in the cytoplasm where they each inhibit the activity of the other until a cell surface receptor ligand induces their translocation to the nucleus¹⁰⁸. In our system, the translocation of RUNX3 to the nucleus in cells added to erythroid medium might be induced by EPO.

To test whether the localization of RUNX3 is affected by EPO, cells can be treated with EPO and RUNX3 can be monitored via immunofluorescent imaging. Subsequently, cells can be deprived of EPO to determine whether RUNX3 translocation is reversible. Further, pharmacological inhibition of JAK2 or STAT5 when EPO is present could help determine whether RUNX3 localization is indeed dependent on those factors. To validate those findings, co-immunoprecipitation of RUNX3 and STAT5 under the various conditions should be performed on the cytoplasmic and nuclear cell lysate fractions to confirm their physical association.

RUNX3 translocation may be induced in a similar fashion by TPO, G-CSF, or IL-3 in cells cultured in megakaryocyte and granulocyte media, as those cytokines also require JAK2 and STAT5 for signaling¹⁷⁶. If this is true, the implication is that granulocytes may require STAT5 but not RUNX3 during differentiation, while

erythroblasts and megakaryocytes require the inverse. Indeed, myeloid differentiation is known to be hindered with loss or mutation of STAT5, and highly exaggerated in a STAT5 gain-of-function model¹⁷⁷⁻¹⁷⁹. In the context of erythropoiesis, STAT5 deficiency during embryogenesis results in severe anemia due to a survival defect; however, adult animals do not show any signs of defective erythropoiesis with single or double isoform knock-outs¹⁸⁰. Furthermore, EPO-dependent STAT5 target genes do not include any canonical erythroid genes¹⁸¹.

RNA-seq after stimulus with the relevant cytokines followed by gene ontology analysis may also shed light on whether STAT5 and RUNX3 target genes required for differentiation of the different lineages. In this study, RNA-seq was performed on cells transferred to erythroid medium (EPO stimulation) and loss of RUNX3 was shown to down-regulate many critical erythroid genes. As a follow-up to this experiment, STAT5 could be knocked down in an otherwise similar experimental design, and the genes affected by knock-down could be interrogated for erythroid-specific targets. Given that STAT5 deficiency does not block erythropoiesis as RUNX3 does, if there is minimal overlap between the RUNX3- and STAT5-affected genes, the data would support the hypothesis that EPO stimulation relies predominantly on the activation of RUNX3 to drive the expression of erythroid genes. These experiments could also be performed on cells induced for granulocyte differentiation (G-CSF and/or IL-3 stimulation) to determine whether STAT5 or RUNX3 targets are relevant.

E. Regulation of RUNX3 Expression

The mechanisms of RUNX3 gene expression via transcription factors remain poorly understood. Three putative regulatory elements have been identified at the RUNX3 locus as well as two promoters that feature Sp1, Egr-1, Ikaros, CREB, and Ets binding sites, two RUNX binding sites at the 5' UTR, as well as an upstream enhancer^{153,182}. Manipulation of some of these sequences can perturb RUNX3 expression; however, there are few clear examples of transcription factors interacting with their corresponding binding sites at the RUNX3 locus. Brn3a, miR-130a, and miR-495 have been implicated in the control of RUNX3 expression, although these may act through epigenetic means¹⁸³⁻¹⁸⁵. Indeed, changes in RUNX3 expression are mostly linked to epigenetic changes, specifically DNA methylation of the P2 promoter, although most of those observations have been made in diseased tissues rather than healthy tissues. For example, RUNX3 hypermethylation has been observed in leukemias, many solid tumors, and neuronal cells in the context of Alzheimer's disease¹³⁶⁻¹⁴¹. Intriguingly, the strongest correlation to RUNX3 promoter methylation is age.

In this study, we observed hypermethylation of the P2 promoter in mouse HSCs and loss of H3K27Ac at the P2 promoter and enhancer in human HSPCs, but we did not test whether these modifications affected RUNX3 expression. To test whether DNA methylation or H3K27ac at the RUNX3 promoter affects its expression, the dCas system could be employed to modulate these epigenetic marks in a site-specific manner¹⁸⁶. This system utilizes a mutant Cas protein that is enzymatically inactive, but is fused to a protein of interest that acts as bait to recruit

other factors. Using a guide-RNA complementary to a sequence found in the RUNX3 locus, it is possible to localize epigenetic factors to that region and modulate DNA methylation and H3K27ac. In an alternative approach, a methylated reporter plasmid harboring the RUNX3 promoter or a non-methylated plasmid of identical sequence could be introduced into cells. Comparing quantities of the plasmid product transcripts may shed light on whether methylation of the promoter impacts RUNX3 expression. Because plasmids are devoid of histones, the use of reporter plasmids will not be useful in gleaning interactions between multiple epigenetic modifications. To this end, pharmacological inhibition of DNA methyltransferases via azacytidine or decitabine will be a useful alternative strategy to compare with the reporter plasmid approach. Similarly, global inhibition of HATs and HDACs may shed light on whether H3K27Ac contributes to the control of RUNX3 expression.

Intriguingly, bivalent chromatin harboring both H3K27Ac and DNA methylation has recently been described at enhancer regions and at promoters regions at a significantly lower frequency. Pharmacological manipulation of either mark altered the other, with a preference for DNA methylation maintaining H3K27Ac. Bivalent promoters were correlated with diminished transcription factor binding and active gene expression¹⁸⁷. Because the control of RUNX3 appears to be somewhat uncoupled from transcription factor mediated regulation, it would be of particular interest to determine whether the promoter and enhancer regions are differentially regulated with aging. In other words, diminished DNA methylation at the enhancer and increased promoter methylation may be the basis for reduced RUNX3 expression.

Another intriguing line of investigation would be to determine whether the RUNX3 promoter and enhancer are physically associated via chromatin looping and whether the looping is dependent on H3K27Ac. Young and aged human HSPCs could be subjected to Hi-C analysis to determine chromatin interactions, and the comparison of samples could establish a correlation between looping and H3K27Ac. If looping occurs, young cells could be treated with HAT inhibitors to diminish H3K27Ac levels and aged cells could be treated with HDAC inhibitors to augment H3K27Ac levels. Modulation of chromatin looping and RUNX3 expression in accordance with H3K27Ac levels and would support a model wherein RUNX3 expression is controlled by promoter-enhancer interaction.

F. Does RUNX3 deficiency drive aging?

Few specific targets have been identified as drivers of aging in otherwise healthy cells. As such, stem cell aging studies have primarily employed large-scale unbiased screening strategies to identify global changes such as gene expression. Most processes that have been interrogated such as cell metabolism, maintenance of the epigenetic landscape, gene expression, DNA repair pathways, and bone marrow niche interactions undergo changes with aging. The targets implicated by these findings are generally master regulators of the aforementioned processes, such as DNMT factors that mediate global DNA methylation.

As discussed previously, age-associated decline in RUNX3 expression has been shown to be dependent on promoter methylation in various disease states including hematological malignancies¹⁴¹. If RUNX3 deficiency alone could generate

a myeloid skewing phenotype, it would have likely been identified as a high-frequency target in some hematological malignancies. Thus, the prospect of RUNX3 being one of many down-stream targets that are dysregulated due to mutation of factors such as DNMTs is rather intriguing. DNMT mutations are frequently found in age-associated hematological malignancies where aging phenotypes such as myeloid skewing are often exacerbated, supporting the hypothesis that RUNX3 perturbations could arise as a secondary hit.

Intriguingly, DNMTs are among the most frequently mutated targets in healthy aged individuals, and in this study we show diminished RUNX3 expression in healthy aged individuals¹⁸⁸. What remains incompletely understood is to what degree the functions of these proteins is altered under these conditions and what the threshold is for loss of function to yield an overt phenotype. Also of interest is what the overall mutational burden in healthy aged individuals is compared to those with hematological malignancies, and if the critical difference is mutation of specific targets, number of mutations, or a combination of the two.

IV. References

1. Lacaud G, Kouskoff V. Hemangioblast, hemogenic endothelium, and primitive versus definitive hematopoiesis. *Experimental Hematology* 2017;49:19–24.
2. Dzierzak E, Bigas A. Blood Development: Hematopoietic Stem Cell Dependence and Independence. *Cell Stem Cell* 2018;22(5):639–651.
3. Yamane T. Mouse Yolk Sac Hematopoiesis. *Front Cell Dev Biol* 2018;61–8.
4. Golub R, Cumano A. Embryonic hematopoiesis. *Blood Cells, Mol Dis* 2013;51(4):226–231.
5. Palis J. Hematopoietic stem cell-independent hematopoiesis: emergence of erythroid, megakaryocyte, and myeloid potential in the mammalian embryo. *FEBS Lett* 2016;590(22):3965–3974.
6. Jagannathan-Bogdan M, Zon LI. Hematopoiesis. *Development* 2013;140:2463–2467.
7. Ivanovs A, Rybtsov S, Ng ES, Stanley EG, Elefanty AG, Medvinsky A. Human haematopoietic stem cell development: from the embryo to the dish. *Development* 2017;144(13):2323–2337.
8. Kauts ML, Vink CS, Dzierzak E. Hematopoietic (stem) cell development — how divergent are the roads taken? *FEBS Lett* 2016;590(22):3975–3986.
9. Tavian M, Biasch K, Sinka L, Vallet J, Péault B. Embryonic origin of human hematopoiesis. *Int J Dev Biol* 2010;54:1061–1065.
10. Ng AP, Alexander WS. Haematopoietic stem cells: Past, present and future. *Cell Death Discov* 2017;3:17002.

11. Becker AJ, McCulloch EA, Till JE. Cytological demonstration of the clonal nature of spleen colonies derived from transplanted mouse marrow cells. *Nature*. 1963. 197:452-454. *Nature* 1963;197:452-454.
12. Wu AM, Till JE, Siminovitch L, McCulloch EA. A cytological study of the capacity for differentiation of normal hemopoietic colony-forming cells. *J Cell Physiol* 1967;69(2):177-184.
13. Wu AM, Till JE, Siminovitch L, McCulloch EA. Cytological evidence for a relationship between normal hematopoietic colony-forming cells and cells of the lymphoid system. *J Exp Med* 1968;127(3):455-64.
14. Hodgson GS, Bradley TR. Properties of Haematopoietic stem cells surviving 5-Fluorouracil treatment: Evidence for a pre-CFU-S cell? *Nature* 1979;281(5730):381-382.
15. Nakahata T, Ogawa M. Identification in culture of a class of hemopoietic colony-forming units with extensive capability to self-renew and generate multipotential hemopoietic colonies. *Proc Natl Acad Sci* 1982;79(12):3843-3847.
16. McNiece IK, Stewart FM, Deacon DM, et al. Detection of a human CFC with a high proliferative potential. *Blood* 1989;74(2):609-612.
17. Bock TA. Assay systems for hematopoietic stem and progenitor cells. *Stem Cells* 1997;15:185-195.
18. Dexter TM, Allen TD, Lajtha LG. Conditions controlling the proliferation of haemopoietic stem cells in vitro. *J Cell Physiol* 1977;91(3):335-344.

19. Roder JC, Duwe A. The beige mutation in the mouse selectively impairs natural killer cell function. *Nature* 1979;278:451–453.
20. Pantelouris EM. Observations on the immunobiology of 'nude' mice. *Immunology* 1971;20:247–252.
21. Scher BYI, Steinberg AD, Berning AK, Paul WE. X-linked B-lymphocyte immune defect in CBA/N mice. II. Studies of the mechanisms underlying the immune defect. *J Exp Med* 1975;142:637–650.
22. Malynn BA, Blackwell TK, Fulop GM, et al. The scid defect affects the final step of the immunoglobulin VDJ recombination mechanism. *Cell* 1988;54(4):453–460.
23. Shultz LD, Schweitzer PA, Christianson SW, et al. Multiple defects in innate and adaptive immunologic function in NOD/LtSz-scid mice. *J Immunol* 1995;154:180–91.
24. Sun J, Ramos A, Chapman B, et al. Clonal dynamics of native haematopoiesis. *Nature* 2014;514(7522):322–327.
25. Busch K, Klapproth K, Barile M, et al. Fundamental properties of unperturbed haematopoiesis from stem cells in vivo. *Nature* 2015;518(7540):542–546.
26. Attar A. Changes in the Cell Surface Markers During Normal Hematopoiesis: A Guide to Cell Isolation Armin. *Glob J Hematol Blood Transfus* 2014;1:20–28.
27. Doulatov S, Notta F, Laurenti E, Dick JE. Hematopoiesis: A human perspective. *Cell Stem Cell* 2012;10(2):120–136.

28. Notta F, Zandi S, Takayama N, et al. Distinct routes of lineage development reshape the human blood hierarchy across ontogeny. *Science* (80-) 2016;351aab2116.
29. Mayle A, Luo M, Jeong M, Goodell MA. Flow cytometry analysis of murine hematopoietic stem cells. *Cytometry Part A* 2013;83 A(1):27–37.
30. Kita K, Xiu F, Jeschke MG. Ex vivo expansion of hematopoietic stem and progenitor cells: Recent advances. *World J Hematol* 2014;3(2):18–28.
31. Bagger FO, Kinalis S, Rapin N. BloodSpot: a database of healthy and malignant haematopoiesis updated with purified and single cell mRNA sequencing profiles. *Nucleic Acids Res* 2019;47(D1):D881–D885.
32. Sanada C, Xavier-Ferrucio J, Lu YC, et al. Adult human megakaryocyte-erythroid progenitors are in the CD34+CD38mid fraction. *Blood* 2016;128(7):923–933.
33. Sumide K, Matsuoka Y, Kawamura H, et al. A revised road map for the commitment of human cord blood CD34-negative hematopoietic stem cells. *Nat Commun*;9(1):.
34. Ghaedi M, Steer CA, Martinez-Gonzalez I, Halim TYF, Abraham N, Takei F. Common-Lymphoid-Progenitor-Independent Pathways of Innate and T Lymphocyte Development. *Cell Rep* 2016;15(3):471–480.
35. Buenrostro JD, Corces MR, Lareau CA, et al. Integrated Single-Cell Analysis Maps the Continuous Regulatory Landscape of Human Hematopoietic Differentiation. *Cell* 2018;173(6):1535-1548.e16.

36. Karamitros D, Stoilova B, Aboukhalil Z, et al. Single-cell analysis reveals the continuum of human lympho-myeloid progenitor cells article. *Nat Immunol* 2018;19(1):85–97.
37. Lee J, Breton G, Oliveira TYK, et al. Restricted dendritic cell and monocyte progenitors in human cord blood and bone marrow. *J Exp Med* 2015;212(3):385–99.
38. Woolthuis CM, Park CY. Hematopoietic stem/progenitor cell commitment to the megakaryocyte lineage. *Blood* 2016;127(10):1242–1248.
39. Renoux VM, Zriwil A, Peitzsch C, et al. Identification of a Human Natural Killer Cell Lineage-Restricted Progenitor in Fetal and Adult Tissues. *Immunity* 2015;43(2):394–407.
40. Pang WW, Price E a, Sahoo D, et al. Human bone marrow hematopoietic stem cells are increased in frequency and myeloid-biased with age. *Proc Natl Acad Sci* 2011;108(50):20012–20017.
41. Sudo K, Ema H, Morita Y, Nakauchi H. Age-Associated Characteristics of Murine Hematopoietic Stem Cells. *J Exp Med* 2000;192(9):1273–1280.
42. Kuranda K, Vargaftig J, de la Rochere P, et al. Age-related changes in human hematopoietic stem/progenitor cells. *Aging Cell* 2011;10(3):542–546.
43. Rossi DJ, Bryder D, Zahn JM, et al. Cell intrinsic alterations underlie hematopoietic stem cell aging. *Proc Natl Acad Sci* 2005;102(26):9194–9199.
44. Benz C, Copley MR, Kent DG, et al. Hematopoietic stem cell subtypes expand differentially during development and display distinct lymphopoietic programs. *Cell Stem Cell* 2012;10(3):273–283.

45. Dykstra B, Olthof S, Schreuder J, Ritsema M, de Haan G. Clonal analysis reveals multiple functional defects of aged murine hematopoietic stem cells. *J Exp Med* 2011;208(13):2691–2703.
46. Röhrig G, Becker I, Pappas K, Polidori MC, Schulz RJ. Analysis of cytopenia in geriatric inpatients. *Z Gerontol Geriatr* 2018;51(2):231–236.
47. Liang Y, Zant G Van, Szilvassy SJ. Effects of aging on the homing and engraftment of murine hematopoietic stem and progenitor cells. *Blood* 2005;106:1479–1487.
48. Noda S, Ichikawa H, Miyoshi H. Hematopoietic stem cell aging is associated with functional decline and delayed cell cycle progression. *Biochem Biophys Res Commun* 2009;383(2):210–215.
49. Qiu J, Papatsenko D, Niu X, Schaniel C, Moore K. Divisional history and hematopoietic stem cell function during homeostasis. *Stem Cell Reports* 2014;2(4):473–490.
50. Xing Z, Ryan MA, Daria D, et al. Increased hematopoietic stem cell mobilization in aged mice. *Blood* 2006;108(7):2190–2197.
51. Bernitz JM, Daniel MG, Fstchyan YS, Moore K. Granulocyte colony-stimulating factor mobilizes dormant hematopoietic stem cells without proliferation in mice. *Blood* 2017;129(14):1901–1912.
52. Rube CE, Fricke A, Widmann TA, et al. Accumulation of DNA damage in hematopoietic stem and progenitor cells during human aging. *PLoS One* 2011;6(3):e17487.

53. Allsopp RC, Morin GB, DePinho R, Harley CB, Weissman IL. Telomerase is required to slow telomere shortening and extend replicative lifespan of HSCs during serial transplantation. *Blood* 2003;102(2):517–520.
54. Lee H-W, Blasco MA, Gottlieb GJ, Horner II JW, Greider CW, DePinho RA. Essential role of mouse telomerase in highly proliferative organs. *Nature* 1998;392(6676):569–574.
55. Sekulovic S, Gylfadottir V, Vulto I, et al. Prolonged self-renewal activity unmasks telomerase control of telomere homeostasis and function of mouse hematopoietic stem cells. *Blood* 2011;118(7):1766–1773.
56. Raval A, Behbehani GK, Nguyen LXT, et al. Reversibility of defective hematopoiesis caused by telomere shortening in telomerase knockout mice. *PLoS One* 2015;10(7):1–20.
57. Wang JCY, Warner JK, Erdmann N, Lansdorp PM, Harrington L, Dick JE. Dissociation of telomerase activity and telomere length maintenance in primitive human hematopoietic cells. *Proc Natl Acad Sci* 2005;102(40):14398–14403.
58. Zimmermann S, Glaser S, Ketteler R, Waller CF, Klingmuller U, Martens UM. Effects of telomerase modulation in human hematopoietic progenitor cells. *Stem Cells* 2004;22:741–749.
59. Ju Z, Jiang H, Jaworski M, et al. Telomere dysfunction induces environmental alterations limiting hematopoietic stem cell function and engraftment. *Nat Med* 2007;13(6):742–747.

60. Beerman I, Seita J, Inlay MA, Weissman IL, Rossi DJ. Quiescent hematopoietic stem cells accumulate DNA damage during aging that is required upon entry into cell cycle. *Cell Stem Cell* 2014;15(1):37–50.
61. Flach J, Bakker ST, Mohrin M, et al. Replication stress is a potent driver of functional decline in ageing haematopoietic stem cells. *Nature* 2014;512(7513):198–202.
62. Mohrin M, Bourke E, Alexander D, et al. Hematopoietic stem cell quiescence promotes error-prone DNA repair and mutagenesis. *Cell Stem Cell* 2010;7(2):174–185.
63. Moehrle BM, Nattamai K, Brown A, et al. Stem cell-specific mechanisms ensure genomic fidelity within HSCs and upon aging of HSCs. *Cell Rep* 2015;13(11):2412–2424.
64. Wahlestedt M, Norddahl GL, Sten G, et al. An epigenetic component of hematopoietic stem cell aging amenable to reprogramming into a young state. *Blood* 2013;121(21):4257–4264.
65. Beerman I, Rossi DJ. Epigenetic regulation of hematopoietic stem cell aging. *Exp Cell Res* 2014;329(2):192–199.
66. Kramer A, Challen GA. The Epigenetic Basis of Hematopoietic Stem Cell Aging Functional and Molecular Manifestations of HSC Aging. *Semin Hematol* 2017;54(1):19–24.
67. Beerman I, Bock C, Garrison BS, et al. Proliferation-dependent alterations of the DNA methylation landscape underlie hematopoietic stem cell aging. *Cell Stem Cell* 2013;12(4):413–425.

68. Sun D, Luo M, Jeong M, et al. Epigenomic profiling of young and aged HSCs reveals concerted changes during aging that reinforce self-renewal. *Cell Stem Cell* 2014;14(5):673–688.
69. Moran-Crusio K, Reavie L, Shih A, et al. Tet2 Loss Leads to Increased Hematopoietic Stem Cell Self-Renewal and Myeloid Transformation. *Cancer Cell* 2011;20(1):11–24.
70. Attema JL, Papathanasiou P, Forsberg EC, Xu J, Smale ST, Weissman IL. Epigenetic characterization of hematopoietic stem cell differentiation using miniChIP and bisulfite sequencing analysis. *Proc Natl Acad Sci* 2007;104(30):12371–12376.
71. Orford K, Kharchenko P, Lai W, et al. Differential H3K4 Methylation Identifies Developmentally Poised Hematopoietic Genes. *Dev Cell* 2008;14(5):798–809.
72. Schultz MB, Sinclair DA. When stem cells grow old: phenotypes and mechanisms of stem cell aging. *Development* 2016;143(1):3–14.
73. Latchney SE, Calvi LM. The aging hematopoietic stem cell niche: Phenotypic and functional changes and mechanisms that contribute to hematopoietic aging. *Semin Hematol* 2017;54(1):25–32.
74. Challen GA, Boles NC, Chambers SM, Goodell MA. Distinct Hematopoietic Stem Cell Subtypes Are Differentially Regulated by TGF- β 1. *Cell Stem Cell* 2010;6(3):265–278.
75. Kowalczyk MS, Tirosh I, Heckl D, et al. Single-cell RNA-seq reveals changes in cell cycle and differentiation programs upon aging of hematopoietic stem cells. *Genome Res* 2015;25(12):1860–1872.

76. Kirschner K, Chandra T, Kiselev V, et al. Proliferation Drives Aging-Related Functional Decline in a Subpopulation of the Hematopoietic Stem Cell Compartment. *Cell Rep* 2017;19(8):1503–1511.
77. Grover A, Sanjuan-Pla A, Thongjuea S, et al. Single-cell RNA sequencing reveals molecular and functional platelet bias of aged haematopoietic stem cells. *Nat Commun*;7.
78. Mann M, Mehta A, de Boer CG, et al. Heterogeneous Responses of Hematopoietic Stem Cells to Inflammatory Stimuli Are Altered with Age. *Cell Rep* 2018;25(11):2992-3005.e5.
79. Tothova Z, Kollipara R, Huntly BJ, et al. FoxOs Are Critical Mediators of Hematopoietic Stem Cell Resistance to Physiologic Oxidative Stress. *Cell* 2007;128:325–339.
80. Ito K, Hirao A, Arai F, et al. Regulation of oxidative stress by ATM is required for self-renewal of haematopoietic stem cells. *Nature* 2004;431(7011):997–1002.
81. Ito K, Hirao A, Arai F, et al. Reactive oxygen species act through p38 MAPK to limit the lifespan of hematopoietic stem cells. *Nat Med* 2006;12(4):446–451.
82. Jang YY, Sharkis SJ. A low level of reactive oxygen species selects for primitive hematopoietic stem cells that may reside in the low-oxygenic niche. *Blood* 2007;110(8):3056–3063.
83. Ho TT, Warr MR, Adelman ER, et al. Autophagy maintains the metabolism and function of young and old stem cells. *Nature* 2017;543(7644):205–210.

84. Mohrin M, Shin J, Liu Y, et al. A mitochondrial UPR-mediated metabolic checkpoint regulates hematopoietic stem cell aging. *Science* (80-) 2015;347(6228):1374–1377.
85. Mendelson A, Frenette PS. Hematopoietic stem cell niche maintenance during homeostasis and regeneration. *Nat Med* 2014;20(8):833–846.
86. Naveiras O, Nardi V, Wenzel P, Fahey F, Daley GQ. Bone marrow adipocytes as negative regulators of the hematopoietic microenvironment. *Nature* 2009;460:259–263.
87. Siclari VA, Zhu J, Akiyama K, et al. Mesenchymal progenitors residing close to the bone surface are functionally distinct from those in the central bone marrow. *Bone* 2013;53(2):575–586.
88. Kohler A, Schmithorst V, Filippi MD, et al. Altered cellular dynamics and endosteal location of aged early hematopoietic progenitor cells revealed by time-lapse intravital imaging in long bones. *Blood* 2009;114(2):290–298.
89. Pinho S, Marchand T, Yang E, Wei Q, Nerlov C, Frenette PS. Lineage-Biased Hematopoietic Stem Cells Are Regulated by Distinct Niches. *Dev Cell* 2018;44(5):634-641.e4.
90. Ergen A V., Boles NC, Goodell MA. Rantes/Ccl5 influences hematopoietic stem cell subtypes and causes myeloid skewing. *Blood* 2012;119(11):2500–2509.
91. Tuljapurkar SR, McGuire TR, Brusnahan SK, et al. Changes in human bone marrow fat content associated with changes in hematopoietic stem cell numbers and cytokine levels with aging. *J Anat* 2011;219(5):574–581.

92. Zhu J, Emerson SG. Hematopoietic cytokines, transcription factors and lineage commitment. *Oncogene* 2002;213295–3313.
93. Wilson NK, Calero-Nieto FJ, Ferreira R, Göttgens B. Transcriptional regulation of haematopoietic transcription factors. *Stem Cell Res Ther* 2011;2(6):1–8.
94. Sive JI, Göttgens B. Transcriptional network control of normal and leukaemic haematopoiesis. *Exp Cell Res* 2014;329(2):255–264.
95. Yokomizo T, Hasegawa K, Ishitobi H, et al. Runx1 is involved in primitive erythropoiesis in the mouse. *Blood* 2008;111(8):4075–4080.
96. Eliades A, Wareing S, Marinopoulou E, et al. The Hemogenic Competence of Endothelial Progenitors Is Restricted by Runx1 Silencing during Embryonic Development. *Cell Rep* 2016;15(10):2185–2199.
97. Swiers G, de Bruijn M, Speck NA. Hematopoietic stem cell emergence in the conceptus and the role of Runx1. *Int J Dev Biol* 2010;541151–1163.
98. Lichtinger M, Ingram R, Hannah R, et al. RUNX1 reshapes the epigenetic landscape at the onset of haematopoiesis. *EMBO J* 2012;31(22):4318–4333.
99. Chuang LSH, Ito K, Ito Y. RUNX family: Regulation and diversification of roles through interacting proteins. *Int J Cancer* 2013;132(6):1260–1271.
100. Melnikova IN, Crute BE, Wang S, Speck NA. Sequence Specificity of the Core-Binding Factor. *J Virology* 1993;67(4):2408–2411.
101. Zhang L, Li Z, Yan J, et al. Mutagenesis of the runt domain defines two energetic hot spots for heterodimerization with the core binding factor β subunit. *J Biol Chem* 2003;278(35):33097–33104.

102. Bowers SR, Calero-Nieto FJ, Valeaux S, Fernandez-Fuentes N, Cockerill PN. Runx1 binds as a dimeric complex to overlapping Runx1 sites within a palindromic element in the human GM-CSF enhancer. *Nucleic Acids Res* 2010;38(18):6124–6134.
103. Yan J, Liu Y, Lukasik SM, Speck NA, Bushweller JH. CBF β allosterically regulates the Runx1 Runt domain via a dynamic conformational equilibrium. *Nat Struct Mol Biol* 2004;11(9):901–906.
104. Li Z, Lukasik SM, Liu Y, et al. A Mutation in the S-switch Region of the Runt Domain Alters the Dynamics of an Allosteric Network Responsible for CBF β Regulation. *J Mol Biol* 2006;364(5):1073–1083.
105. Wang CQ, Krishnan V, Tay LS, et al. Disruption of Runx1 and Runx3 leads to bone marrow failure and leukemia predisposition due to transcriptional and DNA repair defects. *Cell Rep* 2014;8(3):767–782.
106. Bae SC, Lee YH. Phosphorylation, acetylation and ubiquitination: The molecular basis of RUNX regulation. *Gene* 2006;366(1):58–66.
107. Qin X, Jiang Q, Matsuo Y, et al. Cbfb regulates bone development by stabilizing Runx family proteins. *J Bone Miner Res* 2015;30(4):706–714.
108. Ogawa S, Satake M, Ikuta K. Physical and functional interactions between STAT5 and Runx transcription factors. *J Biochem* 2008;143(5):695–709.
109. Miyazono K, Maeda S, Imamura T. Coordinate regulation of cell growth and differentiation by TGF- β superfamily and Runx proteins. *Oncogene* 2004;23(24):4232–4237.

110. Ito Y, Miyazono K. RUNX transcription factors as key targets of TGF- β superfamily signaling. *Current Opinion in Genetics and Development* 2003;13(1):43–47.
111. Komori T, Yagi H, Nomura S, et al. Targeted Disruption of Cbfa1 Results in a Complete Lack of Bone Formation owing to Maturation Arrest of Osteoblasts. *Cell* 1997;89(5):755–764.
112. Otto F, Thornell AP, Crompton T, et al. Cbfa1, a candidate gene for cleidocranial dysplasia syndrome, is essential for osteoblast differentiation and bone development. *Cell* 1997;89(5):765–771.
113. Levanon D, Bettoun D, Harris-Cerruti C, et al. The Runx3 transcription factor regulates development and survival of TrkC dorsal root ganglia neurons. *EMBO J* 2002;21(13):3454–3463.
114. Li Q, Ito K, Sakakura C, et al. Causal Relationship between the Loss of RUNX3 Expression and Gastric Cancer Summary. *Cell* 2002;109:113–124.
115. Niki M, Okada H, Takano H, et al. Hematopoiesis in the fetal liver is impaired by targeted mutagenesis of a gene encoding a non-DNA binding subunit of the transcription factor, polyomavirus enhancer binding protein 2/core binding factor. *Proc Natl Acad Sci* 1997;94:5697–5702.
116. Chen MJ, Yokomizo T, Zeigler BM, Dzierzak E, Speck NA. Runx1 is required for the endothelial to haematopoietic cell transition but not thereafter. *Nature* 2009;457:887–891.

117. de Bruijn M, Dzierzak E. Runx transcription factors in the development and function of the definitive hematopoietic system. *Blood* 2017;129(15):2061–2069.
118. Cai X, Gaudet JJ, Mangan JK, et al. Runx1 loss minimally impacts long-term hematopoietic stem cells. *PLoS One* 2011;6(12):1–14.
119. Sun W, Downing JR, Dc W. Haploinsufficiency of AML1 results in a decrease in the number of LTR-HSCs while simultaneously inducing an increase in more mature progenitors. *Blood* 2004;104(12):3565–3572.
120. Erickson P, Gao J, Chang KS, et al. Identification of Breakpoints in t (8;21) Acute Myelogenous Leukemia and Isolation of a Fusion Transcript, AML1/ETO, With Similarity to Drosophila Segmentation Gene, runt. *Blood* 1992;80(7):1825–1832.
121. Deltcheva E, Nimmo R. RUNX transcription factors at the interface of stem cells and cancer. *Biochem J* 2017;474(11):1755–1768.
122. Osato M. Point mutations in the RUNX1/AML1 gene: Another actor in RUNX leukemia. *Oncogene* 2004;23(24):4284–4296.
123. Cunningham L, Finckbeiner S, Hyde RK, et al. Identification of benzodiazepine Ro5-3335 as an inhibitor of CBF leukemia through quantitative high throughput screen against RUNX1-CBF interaction. *Proc Natl Acad Sci* 2012;109(36):14592–14597.
124. Illendula A, Gilmour J, Grembecka J, et al. Small Molecule Inhibitor of CBF β -RUNX Binding for RUNX Transcription Factor Driven Cancers. *EBioMedicine* 2016;8:117–131.

125. Oo ZM, Illendula A, Grembecka J, et al. A tool compound targeting the core binding factor Runt domain to disrupt binding to CBF β . *Leuk Lymphoma* 2018;59(9):2188–2200.
126. Landry J, Kinston S, Knezevic K, et al. Runx genes are direct targets of Scl / Tal1 in the yolk sac and fetal liver. *Blood* 2008;111(6):3005–3014.
127. Shi M-J, Stavnezer J. b. CBF α 3 (AML2) is induced by TGF- β 1 to bind and activate the mouse germline Ig α promoter. *J Immunol* 1998;161(12):6751–6760.
128. Fainaru O, Woolf E, Lotem J, et al. Runx3 regulates mouse TGF- β -mediated dendritic cell function and its absence results in airway inflammation. *EMBO J* 2004;23(4):969–979.
129. Borkowski TA, Letterio JJ, Farr AG, Udey MC. A Role for Endogenous Transforming Growth Factor beta 1 in Langerhans Cell Biology: The Skin of Transforming Growth Factor beta 1 Null Mice Is Devoid of Epidermal Langerhans Cells. *J Exp Med* 1996;184(6):2417–2422.
130. Voon DCC, Hor YT, Ito Y. The RUNX complex: Reaching beyond haematopoiesis into immunity. *Immunology* 2015;146(4):523–536.
131. Woolf E, Xiao C, Fainaru O, et al. Runx3 and Runx1 are required for CD8 T cell development during thymopoiesis. *Proc Natl Acad Sci* 2003;100(13):7731–7736.
132. Inoue KI, Shiga T, Ito Y. Runx transcription factors in neuronal development. *Neural Dev* 2008;3(1):1–7.

133. Kalev-Zylinska ML, Horsfield JA, Flores MVC, et al. Runx3 Is Required for Hematopoietic Development in Zebrafish. *Dev Dyn* 2003;228(3):323–336.
134. Li B, Ding L, Yang C, et al. Characterization of transcription factor networks involved in umbilical cord blood CD34+ stem cells-derived erythropoiesis. *PLoS One* 2014;9(9):e107133.
135. Wang CQ, Motoda L, Satake M, et al. Runx3 deficiency results in myeloproliferative disorder in aged mice. *Blood* 2013;122(4):562–567.
136. Waki T, Tamura G, Sato M, Motoyama T. Age-related methylation of tumor suppressor and tumor-related genes: An analysis of autopsy samples. *Oncogene* 2003;22(26):4128–4133.
137. Waki T, Tamura G, Sato M, Terashima M, Nishizuka S, Motoyama T. Promoter methylation status of DAP-kinase and RUNX3 genes in neoplastic and non-neoplastic gastric epithelia. *Cancer Sci* 2003;94(4):360–364.
138. Meng G, Zhong X, Mei H. A systematic investigation into Aging Related Genes in Brain and Their Relationship with Alzheimer's Disease. *PLoS One* 2016;11(3):1–17.
139. Wolff EM, Liang G, Cortez CC, et al. RUNX3 methylation reveals that bladder tumors are older in patients with a history of smoking. *Cancer Res* 2008;68(15):6208–6214.
140. Tserel L, Kolde R, Limbach M, et al. Age-related profiling of DNA methylation in CD8+ T cells reveals changes in immune response and transcriptional regulator genes. *Sci Rep* 2015;5(August):1–11.

141. Estécio MRH, Maddipoti S, Bueso-Ramos C, et al. RUNX3 promoter hypermethylation is frequent in leukaemia cell lines and associated with acute myeloid leukaemia inv(16) subtype. *Br J Haematol* 2015;169(3):344–351.
142. Choudry FA, Frontini M. Epigenetic Control of Haematopoietic Stem Cell Aging and Its Clinical Implications. *Stem Cells Int*;2016.
143. Akunuru S, Geiger H. Aging, Clonality and Rejuvenation of Hematopoietic Stem Cells. *Trends Mol Med* 2016;22(8):701–712.
144. Yamamoto R, Wilkinson AC, Ooehara J, et al. Large-Scale Clonal Analysis Resolves Aging of the Mouse Hematopoietic Stem Cell Compartment. *Cell Stem Cell* 2018;22(4):600-607.e4.
145. Maryanovich M, Zahalka AH, Pierce H, et al. Adrenergic nerve degeneration in bone marrow drives aging of the hematopoietic stem cell niche. *Nat Med* 2018;24(6):782–791.
146. Chi XZ, Lee JW, Lee YS, Park IY, Ito Y, Bae SC. Runx3 plays a critical role in restriction-point and defense against cellular transformation. *Oncogene* 2017;36(50):6884–6894.
147. Krishnan V, Chong YL, Tan TZ, et al. TGF β promotes genomic instability after loss of RUNX3. *Cancer Res* 2018;78(1):88–102.
148. Ebihara T, Song C, Ryu SH, et al. Runx3 specifies lineage commitment of innate lymphoid cells. *Nat Immunol* 2015;16(11):1124–1133.

149. So K, Tamura G, Honda T, et al. Multiple tumor suppressor genes are increasingly methylated with age in non-neoplastic gastric epithelia. *Cancer Sci* 2006;97(11):1155–1158.
150. Xing Z, Ryan MA, Daria D, et al. Increased hematopoietic stem cell mobilization in aged mice. *Blood* 2012;108(7):2190–2197.
151. Tusi BK, Wolock SL, Weinreb C, et al. Population snapshots predict early haematopoietic and erythroid hierarchies. *Nature* 2018;555(7694):54–60.
152. Ren R, Ocampo A, Liu GH, Izpisua Belmonte JC. Regulation of Stem Cell Aging by Metabolism and Epigenetics. *Cell Metab* 2017;26(3):460–474.
153. Gunnell A, Webb HM, Wood CD, et al. RUNX super-enhancer control through the Notch pathway by Epstein-Barr virus transcription factors regulates B cell growth. *Nucleic Acids Res* 2016;44(10):4636–4650.
154. Mabuchi M, Kataoka H, Miura Y, et al. Tumor suppressor, AT motif binding factor 1 (ATBF1), translocates to the nucleus with runt domain transcription factor 3 (RUNX3) in response to TGF- β signal transduction. *Biochem Biophys Res Commun* 2010;398(2):321–325.
155. Torquati A, O'Rear L, Longobardi L, Spagnoli A, Richards WO, Daniel Beauchamp R. RUNX3 inhibits cell proliferation and induces apoptosis by reinstating transforming growth factor beta responsiveness in esophageal adenocarcinoma cells. *Surgery* 2004;136(2):310–316.
156. Kuvardina ON, Herglotz J, Kolodziej S, et al. RUNX1 represses the erythroid gene expression program during megakaryocytic differentiation. *Blood* 2015;125(23):3570–3579.

157. Goodnough LT, Schrier SL. Evaluation and Management of Anemia in the Elderly. *Am J Hematol* 2014;89(1):88–96.
158. Krishnan V, Ito Y. RUNX3 loss turns on the dark side of TGF-beta signaling. 2017;4(November):156–157.
159. Velasco-Hernandez T, Säwén P, Bryder D, Cammenga J. Potential Pitfalls of the Mx1-Cre System: Implications for Experimental Modeling of Normal and Malignant Hematopoiesis. *Stem Cell Reports* 2016;7(1):11–18.
160. Frelin C, Herrington R, Janmohamed S, et al. GATA-3 regulates the self-renewal of long-term hematopoietic stem cells. *Nat Immunol* 2013;14(10):1037–1044.
161. Kemp R, Ireland H, Clayton E, Houghton C, Howard L, Winton DJ. Elimination of background recombination: somatic induction of Cre by combined transcriptional regulation and hormone binding affinity. *Nucleic Acids Res* 2004;32(11):1–7.
162. Gothert JR, Gustin SE, Hall MA, et al. In vivo fate-tracing studies using the Scl stem cell enhancer: embryonic hematopoietic stem cells significantly contribute to adult hematopoiesis. *Blood* 2005;105(7):2724–2732.
163. Feil R, Brocard J, Mascrez B, LeMeur M, Metzger D, Chambon P. Ligand-activated site-specific recombination in mice. *Proc Natl Acad Sci U S A* 1996;93(20):10887–90.

164. Sánchez-Aguilera A, Arranz L, Martín-Pérez D, et al. Estrogen signaling selectively induces apoptosis of hematopoietic progenitors and myeloid neoplasms without harming steady-state hematopoiesis. *Cell Stem Cell* 2014;15(6):791–804.
165. Talebian L, Li Z, Guo Y, et al. T-lymphoid , megakaryocyte , and granulocyte development are sensitive to decreases in CBFb dosage. *Blood* 2007;109:11–21.
166. Yagi M, Ritchie KA, Sitnicka E, Storey C, Roth GJ, Bartelmez S. Sustained ex vivo expansion of hematopoietic stem cells mediated by thrombopoietin. *Proc Natl Acad Sci* 2002;96(14):8126–8131.
167. Bernitz JM, Kim HS, MacArthur B, Sieburg H, Moore K. Hematopoietic Stem Cells Count and Remember Self-Renewal Divisions. *Cell* 2016;167(5):1296–1309.e10.
168. Sellers SE, Dumitriu B, Morgan MJ, et al. No Impact of lentiviral transduction on hematopoietic stem/progenitor cell telomere length or gene expression in the rhesus macaque model. *Mol Ther* 2014;22(1):52–58.
169. Wang H, Richter M, Psatha N, et al. A Combined In Vivo HSC Transduction/Selection Approach Results in Efficient and Stable Gene Expression in Peripheral Blood Cells in Mice. *Mol Ther - Methods Clin Dev* 2018;8(March):52–64.
170. Goyama S, Yamaguchi Y, Imai Y, et al. The transcriptionally active form of AML1 is required for hematopoietic rescue of the. *Blood* 2004;104(12):3558–3564.

171. Nabet B, Roberts JM, Buckley DL, et al. The dTAG system for immediate and target-specific protein degradation. *Nat Chem Biol* 2018;14(5):431–441.
172. Kundu M, Liu PP. Cbfb is involved in maturation of all lineages of hematopoietic cells during embryogenesis except erythroid. *Blood Cells, Mol Dis* 2003;30(2):164–169.
173. Rao AK. Spotlight on FLI1, RUNX1, and platelet dysfunction. *Blood* 2013;122(25):4004–4006.
174. Elagib KE, Racke FK, Mogass M, Khetawat R, Delehanty LL, Goldfarb AN. RUNX1 and GATA-1 coexpression and cooperation in megakaryocytic differentiation. *Blood* 2003;101(11):4333–4341.
175. Pencovich N, Jaschek R, Dicken J, et al. Cell-Autonomous Function of Runx1 Transcriptionally Regulates Mouse Megakaryocytic Maturation. *PLoS One* 2013;8(5):1–11.
176. Shea JJO, Schwartz DM, Villarino A V, Gadina M, Iain B, Laurence A. The JAK/STAT pathway: impact on human disease and therapeutic intervention. *Annu Rev Med* 2015;66:311–328.
177. Lin WC, Schmidt JW, Creamer BA, Triplett AA, Wagner KU. Gain-of-Function of Stat5 Leads to Excessive Granulopoiesis and Lethal Extravasation of Granulocytes to the Lung. *PLoS One* 2013;8(4):e60902.
178. Robert B, Jr LI, Hawley RG, Etten RA Van. Dominant Negative Mutants Implicate STAT5 in Myeloid Cell Proliferation and Neutrophil Differentiation. *Blood* 1999;93(12):4154–4166.

179. Feldman GM, Rosenthal LA, Liu X, et al. STAT5A-deficient mice demonstrate a defect in granulocyte-macrophage colony-stimulating factor-induced proliferation and gene expression. *Blood* 1997;90(5):1768–76.
180. Socolovsky M, Fallon AE, Wang S, Brugnara C, Lodish HF. Fetal Anemia and Apoptosis of Red Cell Progenitors in Stat5a^{-/-}5b^{-/-} Mice: a direct role for Stat5 in Bcl-XL induction. *Cell* 1999;98(2):181–191.
181. Gillinder KR, Tuckey H, Bell CC, et al. Direct targets of pStat5 signalling in erythropoiesis. *PLoS One* 2017;12(7):1–20.
182. Bangsow C, Rubins N, Glusman G, et al. The RUNX3 gene - Sequence, structure and regulated expression. *Gene* 2001;279(2):221–232.
183. Appel E, Weissmann S, Salzberg Y, et al. An ensemble of regulatory elements controls Runx3 spatiotemporal expression in subsets of dorsal root ganglia proprioceptive neurons. *Genes Dev* 2016;30(23):2607–2622.
184. Paudel D, Zhou W, Ouyang Y, et al. MicroRNA-130b functions as a tumor suppressor by regulating RUNX3 in epithelial ovarian cancer. *Gene* 2016;586(1):48–55.
185. Lee SH, Jung YD, Choi YS, Lee YM. Targeting of RUNX3 by miR-130a and miR-495 cooperatively increases cell proliferation and tumor angiogenesis in gastric cancer cells. *Oncotarget* 2015;6(32):33269–33278.
186. O’Geen H, Ren C, Nicolet CM, et al. DCas9-based epigenome editing suggests acquisition of histone methylation is not sufficient for target gene repression. *Nucleic Acids Res* 2017;45(17):9901–9916.

187. Charlet J, Duymich CE, Lay FD, et al. Bivalent Regions of Cytosine Methylation and H3K27 Acetylation Suggest an Active Role for DNA Methylation at Enhancers. *Mol Cell* 2016;62(3):422–431.
188. Zink F, Stacey SN, Norddahl GL, et al. Clonal hematopoiesis, with and without candidate driver mutations, is common in the elderly. *Blood* 2017;130(6):742–752.